Dissertations, Theses, and Masters Projects   Theses, Dissertations, & Master Projects

1994

Collisions of atomic hydrogen with oxygen, sulfur, sodium and halogen anions at low energies

James Anthony Fedchak

College of William & Mary - Arts & Sciences

Recommended Citation

INFORMATION TO USERS

This manuscript has been reproduced from the microfilm master. UMI films the text directly from the original or copy submitted. Thus, some thesis and dissertation copies are in typewriter face, while others may be from any type of computer printer.

The quality of this reproduction is dependent upon the quality of the copy submitted. Broken or indistinct print, colored or poor quality illustrations and photographs, print bleedthrough, substandard margins, and improper alignment can adversely affect reproduction.

In the unlikely event that the author did not send UMI a complete manuscript and there are missing pages, these will be noted. Also, if unauthorized copyright material had to be removed, a note will indicate the deletion.

Oversize materials (e.g., maps, drawings, charts) are reproduced by sectioning the original, beginning at the upper left-hand corner and continuing from left to right in equal sections with small overlaps. Each original is also photographed in one exposure and is included in reduced form at the back of the book.

Photographs included in the original manuscript have been reproduced xerographically in this copy. Higher quality 6" x 9" black and white photographic prints are available for any photographs or illustrations appearing in this copy for an additional charge. Contact UMI directly to order.

Collisions of atomic hydrogen with O^-, S^-, Na^- and halogen anions at low energies

Fedchak, James Anthony, Ph.D.

The College of William and Mary, 1994

COLLISIONS OF ATOMIC HYDROGEN WITH O⁻, S⁻, Na⁻

AND HALOGEN ANIONS AT LOW ENERGIES

A Dissertation

Presented to

The Faculty of the Department of Physics

The College of William and Mary in Virginia

In Partial Fulfillment

Of the Requirements for the Degree of

Doctor of Philosophy

---

by
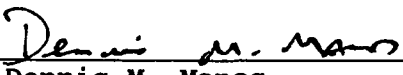
James A. Fedchak

1994

APPROVAL SHEET

This dissertation is submitted in partial fulfillment of
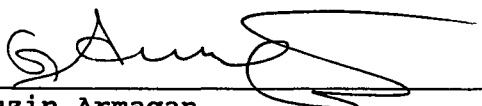
the requirements for the degree of

Doctor of Philosophy

James A. Fedchak

James A. Fedchak

Approved, June 1994

Roy L. Champion

Dennis M. Manos

Guzin Armagan

Harlan E. Schone

Stephen K. Knudson
(Department of Chemistry)

COLLISIONS OF ATOMIC HYDROGEN WITH O⁻, S⁻, Na⁻

AND HALOGEN ANIONS AT LOW ENERGIES

ABSTRACT

Total electron detachment and charge transfer cross
sections, $\sigma_e(E)$ and $\sigma_{ct}(E)$, have been measured for collisions
of the negative ions O⁻, S⁻, F⁻, Cl⁻, Br⁻, I⁻,
Na⁻, and K⁻ with atomic hydrogen for laboratory energies
ranging from 2 to 500 eV. For the systems F⁻, Cl⁻, Br⁻, O⁻,
and S⁻ + H, $\sigma_e(E)$ displays no barrier for associative
detachment; the results are found to be adequately described
by simple curve-crossing models based upon available
intermolecular potentials, or by classical orbiting models
which assume that the anion interacts with the H atom via an
attractive potential of the form $1/R^4$. Analysis of $\sigma_e(E)$
for the system S⁻ + H required the cross section for S⁻ + H_2
→ e + ... to be experimentally determined, and these results
resolved an apparent discrepancy in previous measurements.
The measured detachment cross section for the Cl⁻ + H is
also found to be in agreement with a calculation for that
system based on the effective range potential model. Unlike
the other halogen anion-hydrogen systems, $\sigma_e(E)$ for I⁻ + H
is found to increase with increasing energy over the higher
collision energies investigated.

The cross section for charge transfer in collisions of

O^-, S^-, F^-, Cl^-, Br^- and I^- with atomic hydrogen is found to be less than 1 Å² over the entire range of laboratory energies investigated. A reasonable extrapolation of $\sigma_{ct}(E)$ for collisions of $O^- + H$ is found to agree with a previous measurement at a higher collision energy.

For the collision systems K^- and $Na^- + H$, $\sigma_{ct}(E)$ is found to be much smaller than $\sigma_d(E)$. The measured detachment cross section for $Na^- + H$ is described using available potential energy curves and by assigning the anion state an average lifetime in the unstable region. A perturbed stationary state calculation of $\sigma_{ct}(E)$ for the reactant Na^- is performed, and this calculation underestimates the observed cross section for charge transfer at low collision energies.

JAMES A. FEDCHAK

DEPARTMENT OF PHYSICS

THE COLLEGE OF WILLIAM AND MARY IN VIRGINIA

In memory of my lost creativity

and also in dedication

to all the loss the world has incurred

so that the West could be reasonable.

At least one is recoverable.

TABLE OF CONTENTS

ACKNOWLEDGEMENTS

Before proper credit is given to those individuals who have made significant contributions to this work, I would like to briefly reflect on what has been accomplished. My primary goal in pursuing a Ph. D. degree was to obtain a higher degree of EDUCATION; that is to say, to gain both a broader and deeper perspective on life. Therefore, my goal in receiving an education at The College of William & Mary transcended the particular subject I studied. Perspective is often painful, and this experience was no exception to painful trials; nevertheless, I believe my goal was achieved and I will forever benefit from the wisdom I gained. Many people have made positive contributions to this experience, and I would now like to point out and thank a few special individuals who have made the experience worth it.

I have not forgotten the excellent training in physics that I have received at The College of William Mary, which will be an important factor either in terms of a career, or, at least, the language which I use to gain insight and understanding of the physical world. For this I thank the many fine teachers I have had at the Department of Physics, and especially my advisors Lynn Doverspike and Roy Champion, who let me know, a few days before my thesis defense, that my all my research was really just an investigation of Beers Law. I would also like to thank Dr. Doverspike for teaching me to drive a stick.

For being a friend at a time when I thought I had none, Michael Huels will forever have a special place in my heart. However, I must also blame Michael for all the money I will blow and have blown on fine wine.

For listening to me whine and for all the great conversations on physics and otherwise, I thank my friend co-worker Doug Baker, who can always go to 11.

What would life in the 'Burg have been like without the likes of Jay Larson? Jay taught me that life MUST be an adventure (even bus trips), and will always be counted among my friends. So will Paul Rutt; I'll let you press the green button when the time comes. I haven't forgotten my friends April Baugher, whose tireless pursuit of culture (if not activity) in the mire is admirable, and Melanie Liddle, who has never read a bad book (or, at least, has never recommended one), and always seemed to rise above the boredom of the 'Burg. Speaking of attempts to make the place interesting, I would also like to thank the members of my incoming class, especially Benny Bach, the likes of which

LIST OF TABLES

LIST OF FIGURES

x

ABSTRACT

Total electron detachment and charge transfer cross sections, $\sigma_e(E)$ and $\sigma_{ct}(E)$, have been measured for collisions of the negative ions O^-, S^-, F^-, Cl^-, Br^-, I^-, Na^-, and K^- with atomic hydrogen for laboratory energies ranging from 2 to 500 eV. For the systems F^-, Cl^-, Br^-, O^-, and $S^- + H$, $\sigma_e(E)$ displays no barrier for associative detachment; the results are found to be adequately described by simple curve-crossing models based upon available intermolecular potentials, or by classical orbiting models which assume that the anion interacts with the H atom via an attractive potential of the form $1/R^4$. Analysis of $\sigma_e(E)$ for the system $S^- + H$ required the cross section for $S^- + H_2 \rightarrow e + \ldots$ to be experimentally determined, and these results resolved an apparent discrepancy in previous measurements. The measured detachment cross section for the $Cl^- + H$ is also found to be in agreement with a calculation for that system based on the effective range potential model. Unlike the other halogen anion-hydrogen systems, $\sigma_e(E)$ for $I^- + H$ is found to increase with increasing energy over the higher collision energies investigated.

The cross section for charge transfer in collisions of O^-, S^-, F^-, Cl^-, Br^- and I^- with atomic hydrogen is found to be less than 1 $Å^2$ over the entire range of laboratory energies investigated. A reasonable extrapolation of $\sigma_{ct}(E)$ for collisions of $O^- + H$ is found to agree with a previous measurement at a higher collision energy.

For the collision systems K^- and $Na^- + H$, $\sigma_{ct}(E)$ is found to be much smaller than $\sigma_e(E)$. The measured detachment cross section for $Na^- + H$ is described using available potential energy curves and by assigning the anion state an average lifetime in the unstable region. A perturbed stationary state calculation of $\sigma_{ct}(E)$ for the reactant Na^- is performed, and this calculation underestimates the observed cross section for charge transfer at low collision energies.

COLLISIONS OF ATOMIC HYDROGEN

WITH O$^-$, S$^-$, Na$^-$, AND HALOGEN ANIONS AT LOW ENERGIES

CHAPTER I

INTRODUCTION

The hydrogen atom, consisting of only one electron and
one proton, exhibits a rich spectrum which served as a
prototype for the development of quantum mechanics. When
the complexity of the electron-proton system is increased by
adding another electron, the resultant negative ion reveals
structure which is unprecedented in the H atom and cannot be
described using the lexicon of independent particles so
common to the description of simple atomic systems. The
stability of H^-, for example, is only understood when
exchange correlation between the two electrons is taken into
account; furthermore, unlike hydrogen or any other neutral
atom, H^- exhibits no excited states which are stable with
respect to autodetachment. While the electronic structure
of other atomic anions is not as easily ascertained by basic
approximation methods as is H^-, the property of possessing a
single stable bound state, and the necessity of including
correlation effects in the electronic wave function, is
shared by all atomic anions [1]. Consequently, when an
electron detaches from an atomic negative ion, as in a
collision of the anion with an atom, the detachment process

is governed by a single bound state coupled to a continuum of states; this is contrasted to the ionization of an atom, where the ionization process may be accompanied by electronic excitation of the atom [2]. Hence atomic anion-atom collisions are ideal for studying bound-free transitions, and are inherently different from reactions involving positive ions and neutrals.

Not all atoms form stable negative ions. Only those atoms for which the total ground state energy lies above the total energy of the respective anion form a stable negative ion. The difference between these two energies is defined as the electron affinity (EA) of the atom, so that a positive EA implies a stable negative ion [3]. Many molecules also form negative ions, and these may exist (as stable negative ions) in excited rotational or vibrational states. All negative ions, atomic or molecular, are characterized by electron affinities which are small compared to ionization potentials of atoms (for example, the largest atomic EA is 3.61 eV for Cl whereas the smallest ionization potential for an atom is 3.8 eV for Cs; Table I.1 lists the EA for a few atoms). This property makes negative ions rather reactive, and low energy collisions of anions with atoms typically results in the neutralization of the ion via electron detachment or charge transfer. If the collision is sufficiently slow, then the collision system X^- + Y can be regarded as temporarily forming the molecular anion XY^-, so that electron detachment can be viewed as

Electron Affinities and Polarizabilities

of a Few Elements

Element	EA (eV)	Polarizability ($\text{\AA}^3$)
H (Z=1)	0.754	0.667
Li (3)	0.6	24.3
Na (11)	0.546	23.6
K (19)	0.5	22.8
Rb (37)	0.486	47.3
Cs (55)	0.472	59.6
O (8)	1.46	0.80
S (16)	2.08	2.9
F (9)	3.40	0.56
Cl (17)	3.61	2.18
Br (35)	3.36	3.05
I (53)	3.059	4.7

Table I.1: The electron affinities [3] and polarizabilities [4] for a few elements relevant to the present study.

coupling between states of the neutral molecule XY and the anion XY^-. Additionally, charge transfer reactions,

$$X^- + Y \rightarrow X + Y^-,$$
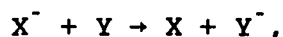
can be viewed as electronic states of XY^- corresponding to $X^- + Y$ at infinite internuclear separation, coupling to those corresponding to $X + Y^-$. In this way, it is seen that collisions of negative ions with atoms may also be used as a probe of the potential curves of the XY^- anion. Collisions of negative ions with atomic hydrogen are among the most fundamental examples of anion-atom collision systems; indeed slow collisions of negative ions with atomic hydrogen will be the topic of this thesis. Before this subject is presented in detail, it will be of interest to first consider other research areas in which negative ion reactions are prevalent.

Collisions of negative ions with neutrals are more than a theoretical curiosity; since negative ions exist with some natural abundance, they participate in the chemistry of many naturally occurring physical phenomenon. Nowhere is this more apparent than in the chemistry of the Earth's atmosphere. Negative ion chemistry is particularly complex in the D-region (<80 km) of the atmosphere, where reactions involving negative ions are an important factor governing the electron density in the ionosphere [5]. This has been of importance to physicists, since radio-wave propagation is controlled by the ionospheric electron density [5,6]. The

primary anion in the D-region is O_2^-, which is mainly

produced by the three body process

$$O_2 + e + M \rightarrow O_2^- + M,$$
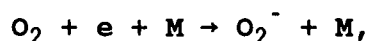
but O^- produced via the reaction

$$e + O_3 \rightarrow O^- + O_2$$

is also of some abundance [5]. In the D-region, negative

ion chemistry proceeds along paths which lead to the

terminal ions CO_3^-, HCO_3^-, Cl^-, $NO_3^-(H_2O)_n$, and $CO_3^-(H_2O)_n$

[5,6,7,8] which are characterized by their relatively

large EA and long atmospheric lifetimes, as compared to

other anions in the ionosphere. Reaction paths leading to

the terminal ions mainly involve the ions O_4^-, CO_4^-, NO_4^-, and

$NO_3^- * (O_2^-$, NO) and the neutrals H_2, O, O_2, O_3, CH_4, NO, NO_2,

HCl, and H_2O [5,6,7,8,9,10]. The anion concentration is

sensitive to temperature as well as the abundance of the

minor atmospheric species O, O_3, NO, and H [6,10].

Ion formation in the atmosphere is not regarded as an

important source or sink of atmospheric neutrals [5,8].

This has been discussed in the context of compounds which

catalytically destroy ozone [11,12], such as

chloroflourocarbons (CFCs) and other halogenated compounds

like CF_2Cl_2 (freon-12), $CFCl_3$ (freon-11), carbon

tetrachloride (CCl_4), methyl chloroform (CH_3CCl_3), and

methylbromide (CH_3Br), to name only a few. However,

negative ions may be produced in the lower D-region and

troposphere by reactions such as [4]:

$$e + CF_2Cl_2 \rightarrow Cl^- + CF_2Cl$$

$$\rightarrow F^- + CFCl_2,$$
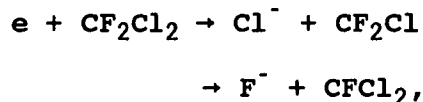
thus producing halogen anions which are not likely to be very reactive with ozone [13,14]. This observation has been the basis of schemes to remove ozone-destroying halogen atoms from the atmosphere by artificially creating anions from the halogen atoms [15,16,17]. In any case, halogen anions such as Cl^-, for example, may be destroyed by an associative detachment process:

$$Cl^- + H \rightarrow HCl + e,$$
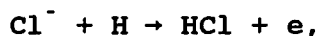
for which the rate constant is known to be high [18,19]. Thus the role of halogens in the ozone cycle may be complicated since free electrons resulting from the destruction of negative ions may react with ozone or other halogen containing compounds.

Negative ions have also been observed in hydrocarbon flames and also in flames which contain trace amounts of hydrocarbons or alkali metals added as a chloride [20,21,22,23]. In the latter case, the predominant negative ions are O_2^-, OH^-, and Cl^- produced by three body electron attachment [24]. It has been suggested that associative detachment with atomic hydrogen may be an important loss mechanism for Cl^- [22]; moreover, in alkali containing hydrogen flames, the concentration of electrons may be raised by

$$X + Y \rightarrow X^- + Y^+$$

and
$$X^- + H \rightarrow XH + e,$$
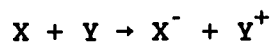
where X represents a halogen and Y an alkali [20,24]. In halocarbon-containing flames, the main anions are those which contain carbon, such as C_2^- or C_2H^-. Although the negative ion concentration is very different for flames which contain hydrocarbons than for those which do not, it is interesting to note that, in both cases, the negative ion concentration reaches its greatest value outside the flame front [20].

The presence of negative ions in the interstellar medium and in stellar atmospheres has also been confirmed. Perhaps the best-known case is that of the continuous absorption spectrum of the sun. In order to explain the absorption spectrum, atoms with low ionization potentials, i.e. metals, were supposed to be present in the solar atmosphere in sufficient quantity to account for the absorption. However, such a quantity of metals would produce stronger absorption lines than observed, and also give rise to a number of absorption edges. It was then suggested that H^- should be present in sufficient quantity in the stellar atmosphere to explain the spectrum [25]; this hypothesis was subsequently confirmed [26]. The production of molecules in interstellar gases containing mainly H_2 via negative ion reactions has been discussed by Dalgarno and McCray [27] and by Takayamagi [28]. The

molecules OH and H_2O, for example, may be produced by

$$O^- + H \rightarrow OH + e,$$

$$H^- + O \rightarrow OH + e,$$

$$O^- + H_2 \rightarrow H_2O + e,$$

and $\qquad\qquad H^- + H_2 \rightarrow H_2O + e.$
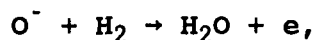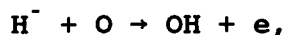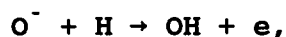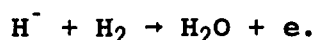
Prior to the present study, no rate constants or cross sections have been measured for low energy collisions of O^- + H; consequently the importance of OH produced in O^- + H $\rightarrow$ OH + e could not be determined. Finally, recent reports indicate the presence of O^-, OH^-, C^-, CH^-, and CN^- in the inner coma of comet Halley [29], but the exact origin of these anions could not be identified.

In gas lasers, the formation of negative ions is important in regard to both laser stability and the creation of a population inversion. In CO_2 lasers, for example, dissociative attachment,

$$e + CO_2 \rightarrow O^- + CO,$$
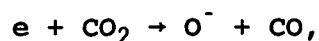
is an important electron loss mechanism, but the product O^- and CO may recombine via associative attachment,

$$O^- + CO \rightarrow e + CO_2,$$

and give rise to local plasma instabilities [30]. This process may also be important in excimer lasers, such as the XeCl laser, where HCl is used as a halogen donor: Cl^- formed via dissociative attachment, e + HCl^*, recombines with Xe^+ to form the lasing molecule XeCl [31]; therefore,

associative detachment,

$$Cl^- + H \rightarrow HCl + e,$$

may also be an important mechanism for the formation of free electrons and the destruction of halogen anions in excimer lasers.

Another important research area involving negative ions has been in the development of neutral beam injectors for use in accelerator and fusion reactor (i.e. Tokamak) applications. This is the subject of ongoing research because the next generation of fusion devices will require high intensity neutral beams with kinetic energies on the order of 1 MeV [32,33,34]. For these applications, neutral beams are formed via the neutralization of ion beams. To this end, negative ion beams are preferred over positive ion beams since the neutralization efficiency of negative ions in a gas cell remains relatively constant for beam energies ranging from 100 keV to greater than 1 MeV, whereas the neutralization efficiency for positive ions decreases greatly with beam energy for energies larger than a few tens of electron volts [33]. This has lead to the development of surface-plasma sources (SPS) and plasma-discharge "volume" sources for the production of intense H^- beams [34]. In both cases, it has been observed that the addition of alkali metal greatly enhances the production of H^- [34,35,36,37]. Although this is mainly due to the increase of negative ion formation on the alkali-coated

surfaces, the gas-phase processes

$$H^- + X \rightarrow e + \ldots \, ,$$

$$H^- + X \rightarrow H + X^- \, ,$$

$$X^- + H \rightarrow e + \ldots \, ,$$

and

$$X^- + H \rightarrow X + H^- \, ,$$
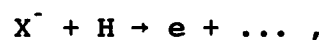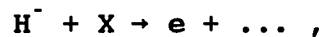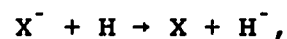
where X represents an alkali atom, may be important mechanisms governing the intensity of H^- extracted from the source. The latter processes are among the systems investigated in this thesis.

From the above discussion, it is clear that studies concerning anion-atom collisions in the gas-phase are relevant to a variety of applications. Moreover, many of the principles developed to understand the mechanisms governing gas-phase collision processes can be applied, with certain limitations, to an understanding of the more complicated process of negative ion desorbtion from surfaces [38].

In low energy collisions of atomic anions, X, with hydrogen atoms, there are three distinct reactions which involve electron loss:
direct detachment (DD),

$$X^- + H \rightarrow X + H + e, \qquad (I.1)$$

associative detachment (AD),

$$X^- + H \rightarrow XH + e, \qquad (I.2)$$

and charge transfer (CT),

$$X^- + H \rightarrow X + H^-. \qquad (I.3)$$
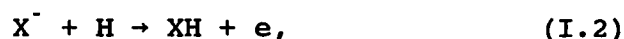
The probability for a collision to follow any of these reaction paths is governed by the cross section for that channel. In what follows, total cross section measurements for charge transfer, $\sigma_{ct}(E)$, and electron detachment, $\sigma_e(E)$, will be presented for the reactants O^-, S^-, F^-, Cl^-, Br^-, I^-, Na^-, K^-, and atomic hydrogen over the range of laboratory energies $2 < E_{lab} < 500$ eV. In the present experiments, electrons produced by direct detachment (I.1) cannot be distinguished from those produced by AD (I.2); therefore $\sigma_e(E)$ represents the sum of (I.1) and (I.2). The fundamental goal in performing these measurements is to gain an understanding of the basic mechanisms governing reactions (I.1) - (I.3). Furthermore, it is hoped and that this insight can be applied towards a more general understanding of interactions of anions with atoms. Much of the work discussed in this thesis has also been reported in the following publications:

"Electron detachment and charge transfer for collisions of O^- and S^- with H", J. A. Fedchak, M. A. Huels, L. D. Doverspike, and R. L. Champion, Phys. Rev. A **47**, 3796 (1993).

"Electron detachment in low energy collisions of halogen anions with atomic hydrogen", M. A. Huels, J. A. Fedchak, R. L. Champion, L. D. Doverspike, J. P. Gauyacq, and D. Teillet-Billy, Phys. Rev. A **49**, 255 (1994).

"Slow collisions of Na$^-$ and K$^-$ with atomic hydrogen", J. A. Fedchak, R. L. Champion, L. D. Doverspike, and Yicheng Wang, J. Phys. B **27**, XXXX (1994).

CHAPTER II

DESCRIPTION OF ELECTRON DETACHMENT

AND CHARGE TRANSFER

In this chapter a résumé of various models and theories
which have been used to describe anion-atom collisions and
to calculate the electron detachment and charge transfer
cross sections is presented. Some of the basic physical
properties of negative ions will first be discussed,
followed by a review of the adiabatic (Born-Oppenheimer)
approximation. Several theoretical frameworks for
describing anion-atom collisions will be discussed, but only
those theories and models used to interpret the experimental
results presented in Chapter IV will be described in detail.

II.A: Creation and Destruction of Negative Ions

Many atoms and molecules form stable negative ions.
The condition for stability is that the electron affinity
(EA) of an atom, defined to be the difference between the
total energy of the neutral parent atom and that of the
negative ion, is greater than zero. Molecules possess many
more degrees of freedom than atoms, and one can distinguish
between an "adiabatic" EA, defined to be the difference

between the minimum energy of the neutral molecule and that
of the anion, and a "vertical" EA, which is the difference
in energy between the neutral and anion states at a fixed
geometry. That a neutral atom can form a negative ion can
be understood in terms of classical physics: a free
electron in the vicinity of a neutral atom induces a
polarization of the atom, thus giving rise to a dipole
electric field which in turn attracts the electron. To
fully understand and calculate the EA of an atom, quantum
mechanics must be used, and the exchange correlation between
the additional electron and those which form the neutral
atom must be taken into account. The EA of atoms has been
the subject of a considerable number of publications and
will not be taken up here, the interested reader is referred
to the review article by Hotop and Lineberger [3], for
example.

Since the "extra" electron of a negative ion is weakly
bound as compared to the ionization potential of the neutral
parent (for example, the largest EA among the elements is
3.6 eV for Cl), the formation of anions in the gas phase is
generally the result of subtle collision processes. The
radiative attachment process

$$e + X \rightarrow X^- + h\nu$$
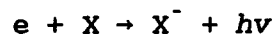
is very rare because the collision time is much less than
that required for radiation to occur. A more important
creation mechanism is the three body attachment process:

$$e + X + Y \rightarrow X^- + Y$$
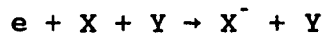
where Y is a third body, possibly a surface, which removes
the energy associated with the EA of X. In the energy range
from 0 to about 15 eV, dissociative attachment (DA),

$$e + XY \rightarrow X^- + Y,$$
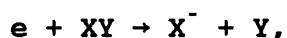
is an important mechanism for the production of negative
ions from molecular targets, and for energies exceeding 20
eV, ion-pair production must also be considered [39]:

$$e + XY \rightarrow e + X^- + Y^+$$

$$Z^+ + XY \rightarrow Z^+ + X^- + Y^+$$

$$Z^* + XY \rightarrow Z^+ + XY^-$$

$$XYZ^+ + A \rightarrow X^+ + Y^- + Z^+ + A.$$
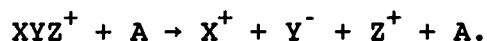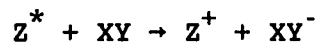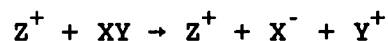
The formation of negative ions via the charge transfer (CT)
mechanism

$$X^- + Y \rightarrow X + Y^-$$
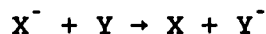
is often used in the laboratory to produce energetic neutral
atomic beams by stripping the charge from a beam of negative
ions.

All the above creation mechanisms have a counterpart
destruction mechanism, but the destruction mechanisms most
relevant to the present study are those which result in the
neutralization of the anion; such as charge transfer (CT
above), associative detachment (AD),

$$X^- + Y \rightarrow XY + e,$$

and direct detachment (DD),

$$X^- + Y \rightarrow X + Y + e.$$
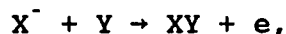
Several models have been used to describe the last three

processes and will be discussed later.

II.B: The Adiabatic (Born-Oppenheimer) Approximation

All of the anion-atom collisions considered in the
present study take place at lab energies less than $E_{lab} =$
500 eV. In collisions of $H^- + H$, for example, $E_{lab} = 500$ eV
corresponds to a relative collision velocity which is about
1/7 of typical electron velocities about the nucleus
$(H(s^1))$. By assuming that translations of the nuclei are
negligibly slow compared to the motion of the electrons, one
can obtain a good approximation which greatly simplifies a
description of the collision process; this is the basis of
the so-called "adiabatic" or "Born-Oppenheimer"
approximation and will be reviewed as follows.

Neglecting spin-orbit coupling and lesser magnetic
effects, the full Schrödinger equation for a system of atoms
is given by

$$H\Psi(r,R) = \left(\frac{p_R^2}{2M} + \frac{p_r^2}{2m_e} + V(r,R)\right)\Psi(r,R) = E\Psi(r,R) \quad (II.1)$$

where r represents the electronic coordinates and R the
nuclear coordinates. The potential V(r,R) contains the
Coulombic potential for all electron-electron, nuclei-
nuclei, and electron-nuclei interactions; it is understood
that the coordinates are summed over all the particles, e.g.

$P_r^2 = -\sum_i \hbar^2 \nabla_{r_i}^2$. It is now assumed that the wavefunction

$\Psi(r,R)$ can be written in the form:

$$\Psi(r,R) = \phi(R)\psi(r,R) . \qquad (II.2)$$

Substituting this product, known as the Born-Oppenheimer product, into the wave equation (II.1) yields

$$\left\{ \phi(R) \frac{P_R^2}{2M} \psi(r,R) + \frac{1}{M} P_R \phi(R) \, P_R \psi(r,R) \right\}$$

$$+ \psi(r,R) \frac{P_R^2}{2M} \phi(R) + \phi(R) \frac{P_r^2}{2m_e} \psi(r,R) \qquad (II.3)$$

$$+ V(r,R)\phi(r)\psi(r,R) = E\phi(r)\psi(r,R) .$$

The approximation is now made that the electrons go through many orbits before the nuclei change their positions by any appreciable amount; moreover, the electronic wavefunction is able to continually adjust to the nuclear motion, so that

$$|P_R \psi(r,R)| << |P_R \phi(R)| . \qquad (II.4)$$

If this approximation is valid, the quantities which appear in the brackets ({}) on the left hand side of Eq. (II.3) can be neglected, so that the Schrödinger equation (II.3) becomes

$$\left(\frac{\psi(r,R)}{\phi(R)}\right)\frac{P_R^2}{2M}\phi(R) \; + \; H_{el}\psi(r,R) \; = \; E\psi(r,R)$$

$$\text{where} \quad H_{el} = \frac{P_r^2}{2m_e} + V(r,R) \; . \tag{II.5}$$

The wavefunctions $\psi(r,R)$ which appear in the Born-Oppenheimer product (II.2) are carefully chosen to be the eigenfunctions of the electronic Hamiltonian:

$$H_{el}\psi(r,R) \; = \; \varepsilon(R)\psi(r,R) \; . \tag{II.6}$$

Upon substituting the eigenvalue $\varepsilon(R)$ from Eq. (II.6) into the approximated Schrödinger equation (II.5), it is seen that the energy eigenvalues depend parametrically on R. It is also worth noting that if the nuclei are held fixed in space, Eq. (II.5) reduces to the eigenvalue equation for the electronic Hamiltonian. Furthermore, we can define a "vibrational" Hamiltonian such that Eq. (II.5) can be written as

$$H_{vib}\phi(R) \; = \; E\phi(R)$$

$$\text{where} \; H_{vib} = \frac{P_R^2}{2M} + \varepsilon(R) \; , \tag{II.7}$$

so that the energy eigenvalues of the electronic Hamiltonian are treated as potentials in the vibrational Hamiltonian. The result of the adiabatic approximation has been to reduce the Schrödinger equation to two coupled differential equations defined by Eqs. (II.6) and (II.7).

Of course this approximation has applications which transcend the collision processes studied in this thesis; in

fact, the parametrically dependent energies defined by Eq. (II.6) are the adiabatic intermolecular potentials for, say, a diatomic molecule. Therefore, during a sufficiently slow collision, the reactants X^- and H can be regarded as temporarily forming the anion XH^-. Electron detachment can then be described as transitions from XH^- states to states of the XH continuum, whereas charge transfer can be regarded as transitions between XH^- states. Often the anion potential curve will cross the XH state at an internuclear separation R_c, as depicted in Fig. (II.1); in such cases the anion is regarded as unstable for $R < R_c$ and collisions which lead to internuclear separations near or less than R_c will, in most cases, result in electron detachment.

II.C: Classical Model of Electron Detachment

A simple classical model of electron detachment will now be described [40]. In this simple picture (similar to the "optical model" in nuclear physics), it is assumed that the anion trajectory is completely described by classical mechanics such that there exists a maximum impact parameter, b_{max}, below which all trajectories lead to electron detachment. This corresponds to the quantum mechanical assumption that all partial waves below some value $l_{max} \approx b_{max} m v_\infty / \hbar$ are completely absorbed by the detachment process. Once b_{max} is found, the detachment cross section
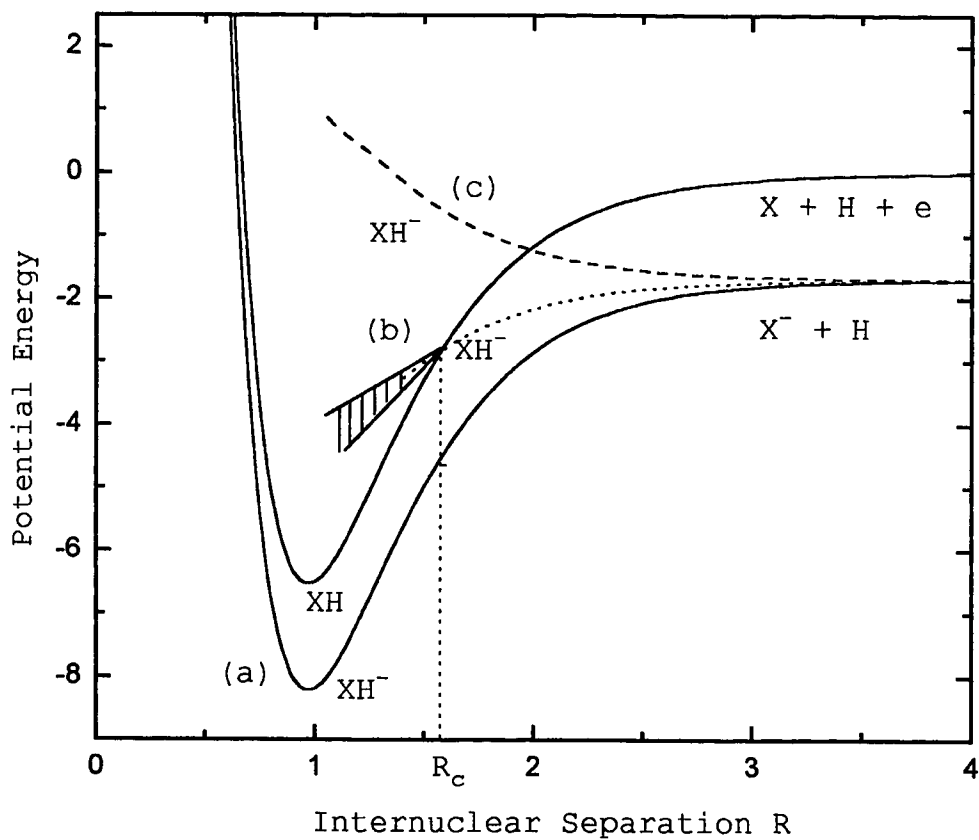
Figure II.1: Example of typical potential energy curves for an arbitrary molecule XH and an anion XH⁻. Curve (a) represents a stable molecular anion, whereas (b) and (c) represent attractive and repulsive states which cross into the XH continuum. The shaded region on (b) represents the state acquiring a "width" in the autodetaching region, as discussed in section II.D.

is simply given by $\sigma_e = \pi b_{max}^2$. While this model
oversimplifies the collision dynamics and is often not a
realistic description of the electron detachment process, it
will provide an upper limit to the cross section and, in
some cases, yield surprisingly good results.

It will first be assumed that there exists some
internuclear separation R_x such that the electron detaches
with unit probability whenever the atom and negative ion
approach to within a separation $R < R_x$. The internuclear
separation R_x is usually chosen to be the point at which the
XH⁻ potential crosses that of the continuum (R_c), as
depicted in Fig. (II.1). The trajectory with a turning
point equal to R_x is associated with an impact parameter
which will allow the two nuclei to approach within R_x. When
the conservation of energy is expressed in terms of the
impact parameter,

$$E = \frac{1}{2}\mu\dot{R}^2 + \frac{b^2 E}{R^2} + V(R),$$ (II.8)

the impact parameter corresponding to a turning point R_x,
denoted by b_x, is simply

$$b_x = R_x\sqrt{1 - \frac{V(R_x)}{E}},$$ (II.9)

where V(R) is the interaction potential between X⁻ and H.
It then follows that

$$\sigma_e(E) = \pi R_x^2 \left(1 - \frac{V(R_x)}{E}\right), \qquad (II.10)$$

so, in the limit of large relative collision energies, the cross section is simply given by πR_x^2.

If the intermolecular potential between the anion and atom is attractive, then the model can be made a little more complicated by considering that detachment could also occur for trajectories which lead to classical orbiting. The condition for classical orbiting is found by locating the extremum in the effective potential [41]:

$$\frac{d}{dR}\left[V(R) + \frac{b^2 E}{R^2}\right]_{\substack{R=R_{orb} \\ b=b_{orb}}} = 0 \quad . \qquad (II.11)$$

By combining Eq. (II.11) with Eq. (II.8), one can solve for b_{orb} as a function of E. The maximum impact parameter which leads to detachment at a given energy is then the greater of b_{orb} and b_x. It is easy to see that b_{orb} can only dominate at lower collision energies than those for which $b_{max}=b_x$.

As an illustration of this model, suppose the anion and atom interact via the polarization potential:

$$V_{pol}(R) = -\left(\frac{1}{4\pi\epsilon_o}\right)\frac{\alpha e^2}{2R^4} \qquad (II.12)$$

where α is the polarizability of the atom. From Eq. (II.11), classical orbiting occurs for impact parameter less than

$$b_{orb} = \left(\frac{1}{4\pi\epsilon_o} \cdot \frac{2\alpha e^2}{E}\right)^{\frac{1}{4}}. \qquad \text{(II.13)}$$

The resulting orbiting cross section is then πb_{orb}^2 or

$$\sigma_\theta = \sigma_L = \frac{k_L}{v} = \frac{e}{v}\sqrt{\frac{\pi\alpha}{\mu\epsilon_0}}, \qquad \text{(II.14)}$$

where k_L is the Langevin reaction rate and σ_L is known as the Langevin capture cross section. For higher collision energies this orbiting model will underestimate the cross section as it fails to account for curve-crossing which can occur for $b > b_L$. In particular for $E > E_o \equiv \alpha e^2/8\pi\epsilon_o R_c^4 = -V_{pol}(R_c)$ we have, from Eq. (II.10),

$$\sigma_\theta(E) = \pi R_c^2\left(1 + \frac{E_o}{E}\right). \qquad \text{(II.15)}$$

Thus E_o defines the "transition" energy from an orbiting to a curve-crossing dominated region.

II.D: Local Complex Potential

In this model, it is assumed that the anion state is unstable for internuclear separations $R < R_x$, and the state in this unstable region can be assigned a complex energy

$$E = V(R) - \frac{i}{2}\Gamma(R). \qquad \text{(II.16)}$$

The state then decays with a rate proportional to $\Gamma(R)$. From elementary quantum mechanics, it is easy to show that

the probability that the negative ion will survive the collision becomes:

$$P_s(b) = \exp\left(-\frac{2}{\hbar}\int_{R_o}^{\infty}\frac{\Gamma(R)}{v(R)}\,dR\right),$$ (II.17)

where R_0 is the turning point of the trajectory. An important result of this phenomenological model is the prediction of an isotope effect: the energy dependence of Eq. (II.17) is solely through v(R); therefore two isotopes, such as D^- and H^-, should have the same survival probability as a function of velocity, but, at any given energy, the heavier isotope, D^-, should have a smaller survival probability than the lighter. This theory has correctly explained such an isotope effect in collisions of H^- and D^- with He [42], but is at odds with the observed opposite isotope effect in collisions of H^- and D^- with Ne [43]. No modification of this model could force it to correspond to experimental observations; different theories were needed to explain the isotope effect in collisions of H^- and D^- with Ne.

II.E: Zero-Range Potential Model (ZRP)

A different approach to electron detachment, based on earlier work by Demkov [44], was taken by Gauyacq and used to explain the isotope effect observed in collisions of H^- and D^- with Ne [45]. In this approach, known as the zero-

range potential model (ZRP), detachment is assumed to occur when the atom and anion approach at an internuclear separation near the crossing point R_c, as shown in Fig. II.1. In this region, the binding energy of the outer electron $\varepsilon(R)$, defined to be the difference between the neutral and anion potentials for $R > R_c$, becomes very small and consequently the orbit of the electron is diffuse. Since the de Broglie wavelength of the electron will then be much larger than that of the molecule, it will be assumed that the electron can be described as being bound to the molecular core by a potential of very short range. In the region near R_c the electron will spend much of its time outside the core, where the electron wavefunction is determined by the free-particle Schrödinger equation

$$[\frac{1}{2}\hbar^2\nabla^2 - \varepsilon(R)]\psi = 0. \qquad (II.18)$$

which has solutions of the form e^{-kR}/R where $k = (2\varepsilon(R))^{1/2}$. For $R < R_c$ the problem becomes more complicated, but a boundary condition can be specified for the electronic wave function:

$$\frac{1}{\psi}\frac{\partial\psi}{\partial x}\big|_{x\to 0} = f(R(t)) \qquad (II.19)$$

In the region $R < R_c$ a linear extrapolation is often used to approximate $f(R(t))$, whereas $R(t)$ and $\varepsilon(R(t))$ are often taken from intermolecular potentials for $R > R_c$. Eq. (II.18) can be solved numerically to find $\psi(+\infty)$, and the

survival probability can be found by projecting $\psi(+\infty)$ onto the eigenfunction corresponding to the bound XY⁻ system. This model has been used to explain the inverse isotope effect observed in collisions of H⁻ and D⁻ with Ne, which could not be explained within the framework of the semi-classical local complex potential model. An extension of this model, the effective range potential model (ERP), has been used by Gauyacq and Teillet-Billy to calculate the electron detachment cross section for Cl⁻ + H; these results will be presented in section IV.B.

II.F: Perturbed Stationary State (PSS) Approximation

The formalism developed here closely follows Taylor and Delos [46] and also that reviewed by Delos [47]. The de Broglie wavelength of the nuclear motion for, say, H⁻ + H at $E_{lab} = 500$ eV, is several orders of magnitude smaller than the atomic size. Therefore, the nuclear motion can be treated classically, and the electronic wave function, $Y(r,t)$, is determined approximately by a time-dependent Schrödinger equation:

$$h(r,R(t))Y(r,t) = i\hbar\frac{\partial}{\partial t}Y(r,t). \qquad (II.20)$$

Spin-orbit couplings and lesser magnetic effects can be neglected for this problem, so the Hamiltonian $h(r,R(t))$ is just the electronic Hamiltonian H_{el} of Eq. (II.6). It is assumed that the wave function can be expanded in a complete

set of orthogonal basis functions,

$$Y(r,t) = \sum_n C_n(t)\phi_n(r,R(t)). \qquad (II.21)$$

When this expansion is substituted into the time-dependent Schrödinger equation (II.20), and both sides are multiplied by ϕ_m^* and integrated over the electron coordinates, Eq. (II.20) becomes

$$\sum_n \int dr\phi_m^*(r,R(t))\phi_n(r,R(t))\frac{dC_n(t)}{dt}$$

$$= \sum_n C_n(t)\int dr\phi_m^* h(r,R(t))\phi_n(r,R(t)) \qquad (II.22)$$

$$+ \sum_n C_n(t)\int dr\phi_m^*(r,R(t))\frac{\hbar}{i}v\cdot\nabla_R\phi_n(r,R(t)).$$

By writing the $C_n(t)$ as a column vector $\underline{C}$ and defining $P = -i\hbar\nabla_R$, Eq. (II.21) can be written in the form

$$i\hbar\frac{d}{dt}\underline{C}(t) = (\underline{h} + v\cdot\underline{P})\underline{C}(t), \qquad (II.23)$$

or, alternatively, as

$$i\hbar\frac{d}{dt}\underline{C}(t) = \underline{H}\underline{C}(t),$$

$$\underline{H} = \underline{h} + v\cdot\underline{P},$$

$$(h)_{mn} = \langle\phi_m|h(r,R(t))|\phi_n\rangle, \qquad (II.24)$$

$$(P)_{mn} = \langle\phi_m|P|\phi_n\rangle .$$

Of particular importance to this study is the two-state problem in which $\underline{C} = \begin{pmatrix} C_1(t) \\ C_2(t) \end{pmatrix}$. Charge transfer, for

example, may often be described by an anion state corresponding to X⁻ + H coupling to the state corresponding to H⁻ + X. In the two-state problem, the coupled equations (II.24) may be reduced to a more tractable form by the phase transformation

$$C_n(t) = B_n(t) \exp\left(-i \int_{-\infty}^{t} \frac{(H)_{nn}}{\hbar} dt'\right), \qquad (II.25)$$

so that the coupled equations (II.24) become

$$\frac{dB_1(t)}{dt} = \frac{B_2(t)}{i\hbar} (H)_{12} e^{-i\theta(t)},$$

$$and \quad \frac{dB_2(t)}{dt} = \frac{B_1(t)}{i\hbar} (H)_{12} e^{i\theta(t)}, \qquad (II.26)$$

$$where \quad \frac{d\theta(t)}{dt} = \frac{(H)_{22} - (H)_{11}}{\hbar}.$$

Until now, nothing has been specified concerning the basis functions $\phi_n(r,R(t))$. A convenient choice is to pick the ϕ_n to be eigenfunctions of the electronic Hamiltonian. Since these are identical to the $\psi(r,R)$ which appear in the adiabatic approximation, expressing the problem in this basis is often referred to as an "adiabatic" representation. The $\underline{h}^{(a)}$ matrix is diagonal in an adiabatic representation whereas $\mathbf{v} \cdot \underline{p}^{(a)}$ contains off-diagonal terms. Transitions between states are seen to be the results of these off-diagonal terms. It is also common to pick a "diabatic" representation $\phi_n^{(d)}$, in which the $\mathbf{v} \cdot \underline{p}^{(d)}$ matrix is zero or negligibly small compared to $\underline{h}^{(d)}$, and $\underline{h}^{(d)}$ is non-diagonal.

Often the adiabatic intermolecular potentials, $\varepsilon(R)$ of Eq. (II.6), are known and the diagonal elements of $\underline{h}^{(d)}$ can be guessed by physical reasoning. One can now derive formulas which connect the two representations, so that transition probabilities can be calculated even if the ϕ_n are not specifically known.

Since both $\phi_n^{(d)}$ and $\phi_n^{(a)}$ are assumed to form a complete and orthogonal basis set, there must exist a unitary transformation such that

$$\phi_n^{(a)}(r,R) = \sum_m U_{mn}\phi_m^{(d)}(r,R),\qquad\qquad (II.27)$$

so the matrices transform as

$$\underline{h}^{(a)} = \underline{U}^+\underline{h}^{(d)}\underline{U}$$
$$\text{and}\quad (v\cdot P)^{(a)} = \underline{U}^+(v\cdot P)^{(d)}\underline{U} - i\hbar\underline{U}^+\frac{d}{dt}\underline{U}\qquad (II.28)$$

For a two state system, $\underline{U}$ can be written as

$$\underline{U} = \begin{pmatrix} \cos\omega & \sin\omega \\ -\sin\omega & \cos\omega \end{pmatrix} \qquad\qquad (II.29)$$

with

$$\cot(2\omega) = \frac{h_{22}^{(d)} - h_{11}^{(d)}}{2h_{12}^{(d)}}. \qquad\qquad (II.30)$$

By transforming the matrices, as in Eq. (II.27), we obtain the following relations among the matrix elements:

$$h_{11}^{(a)} = \frac{1}{2}(h_{11}^{(d)} + h_{22}^{(d)}) - \frac{1}{2}\sqrt{(h_{22}^{(d)} - h_{11}^{(d)})^2 + 4(h_{12}^{(d)})^2},$$

$$h_{22}^{(a)} = \frac{1}{2}(h_{11}^{(d)} + h_{22}^{(d)}) + \frac{1}{2}\sqrt{(h_{22}^{(d)} - h_{11}^{(d)})^2 + 4(h_{12}^{(d)})^2}, \qquad \text{(II.31)}$$

so that the off-diagonal matrix element in the diabatic representation can be written as

$$h_{12}^{(d)} = \pm\frac{1}{2}\sqrt{(h_{22}^{(a)} - h_{11}^{(a)})^2 - (h_{22}^{(d)} - h_{11}^{(d)})^2}, \qquad \text{(II.32)}$$

and we also have the adiabatic element

$$\boldsymbol{v}\cdot\underline{P}^{(a)} = i\hbar\frac{d\omega}{dt}\begin{pmatrix} 0 & -1 \\ 1 & 0 \end{pmatrix}. \qquad \text{(II.33)}$$

It then follows that the off-diagonal element in the adiabatic representation becomes

$$(\boldsymbol{v}\cdot\underline{P})_{12}^{(a)} = -i\hbar v_R\frac{d\omega}{dR}$$

$$= i\hbar v_R\frac{h_{12}^{(d)}\dfrac{d\Delta}{dR} - \Delta\dfrac{d}{dR}h_{12}^{(d)}}{\Delta^2 + 4(h_{12}^{(d)})^2}, \qquad \text{(II.34)}$$

where

$$\Delta \equiv h_{22}^{(d)} - h_{11}^{(d)}. \qquad \text{(II.35)}$$

Once the off-diagonal matrix element is computed in either the adiabatic or diabatic representation via Eq. (II.34) or (II.32), the coupled equations (II.26) can be solved to find the transition probability in either representation. It must be remembered that the transition probabilities of the two representations are not equal, i.e.

$B^{(a)}(t)^2 \neq B^{(d)}(t)^2$, but are related by the unitary

transformation defined by Eqs. (II.27) and (II.29).

II.G: Close-Coupling theory of electron detachment

In a two papers by Taylor and Delos [46,48], electron

detachment is described as the coupling of a bound ion state

$V_{ion}(R(t))$ with that of the neutral continuum of states. In

a similar fashion that Eq. (II.23) was derived, they derive

an infinite set of coupled equations:

$$i\hbar \frac{dc_0(t)}{dt} = \Delta(t) c_0(t) + \int dE\rho(E) V_{0E}(t) c_E(t),$$

$$i\hbar \frac{dc_E(t)}{dt} = V_{E0} c_0(t) + E c_E(t), \qquad (II.37)$$

$$\Delta(t) = V_{ion}(R(t)) - V_{neutral}(R(t)),$$

where $V_{neutral}(R(t))$ is the lowest energy state of the

neutral continuum, and $\rho(E)$ is the density of states; the

$V_{EE'}$ term refers to a "potential" matrix (analogous to $\underline{h}$ in

Eq. (II.23)) which contains the discrete ion state, $V_{00} =$

V_{ion}, and continuum terms designated by the subscript E.

By neglecting the time dependence of $V_{E0}(R(t))$ and

approximating $\Delta(t)$ by a quadratic function of time, they

derive the survival probability for the system $H^- + He$, and,

consequently, the electron detachment cross section; these

results are in accord with experimental measurements for the

system $H^- + He$ [42]. In a later paper, Wang and Delos

[49] use the close-coupling formalism to model collisions of H⁻ and D⁻ with Ne, and their resultant detachment cross section displayed the isotope effect observed in the experiments.

II.H: Summary

For slow collisions, theoretical descriptions of electron detachment and charge transfer rely upon some knowledge of the intermolecular potential which describes+ the incoming ion X⁻ and the target H. For most of the systems in the present study, the ground state potential curve of the molecular anion XH⁻ can be adequately expressed as a Morse potential. Calculations of the XH⁻ potential energy curves for states other than the ground state also exist for many of these systems, or, in some cases, the intermolecular potential may be approximated by an induced dipole potential. The feature of the potential curves most relevant to electron detachment is the crossing or merging point of the XH⁻ potential with that of XH; the crossing point R_c will typically be in the range of 1 to 3 Å. A rough estimate of the detachment cross section can be obtained from $\sigma_e \approx \pi R_c^2$, so one would expect a cross section of a few to 10 Å^2 for low energy collisions. Charge transfer results from long range coupling between states corresponding to X⁻ + H and H⁻ + X; therefore, the energetic separation between these states, ΔE, is the feature of the

intermolecular potentials most relevant to charge transfer. At large internuclear distances, ΔE may be taken to be the difference between the EA of X and H, but, at closer internuclear distances, will depend upon the particular system being studied. Therefore, it is difficult to make a rough estimate of the charge transfer cross section; however, theoretical considerations of both charge transfer and electron detachment will be examined for particular systems in Chapter IV.2.

CHAPTER III

EXPERIMENTAL APPARATUS AND METHODS

The experiments were performed in a crossed-beam apparatus previously used to study collisions of H^- and D^- with H [50], and is shown in Fig. III.1. Following a brief description, the salient features of the apparatus will be described in detail and the methods of data analysis will be discussed.

Negative ions are extracted from a plasma-discharge by an electrostatic lens and are subsequently accelerated into a 90° magnetic mass spectrometer. After emerging from the mass spectrometer, the negative ion beam is focussed into a collision zone which lies within a truncated section of an energy analyzer. The negative ion beam passes resonantly through the analyzer, and intersects orthogonally with an atomic hydrogen beam located between the two electrodes of the collision zone. The atomic hydrogen beam is formed within a radio-frequency (rf) discharge of hydrogen gas. All slow anions and electrons formed as collision products are forced through a hole in one of the electrodes, and subsequently pass through a weak magnetic field which separates the product electrons from anions. The product

Atomic hydrogen source

z

y

x

Electrostatic lenses

Collision zone

Magnetic mass spectrometer

Faraday cup

A

A

Ion source

H⁻

e

Product magnet

Particle detectors
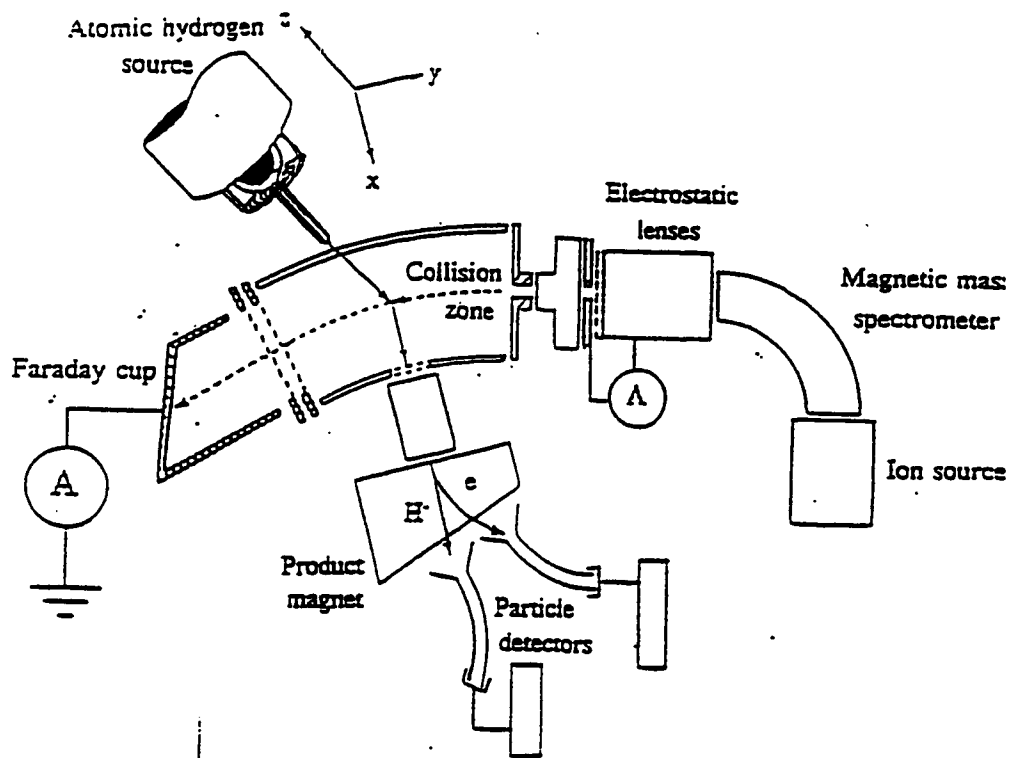
Figure III.1: Schematic diagram of the crossed-beam apparatus.

electrons and negative ions are then detected by
conventional particle multipliers, and the incident anion
beam is simultaneously monitored at a Faraday cup located at
the end of the collision zone. These three quantities, i.e.
the product ion and electron count rates along with the
incident (primary) beam current, are used to experimentally
determine the electron detachment and charge transfer cross
sections.

III.A: Ion Source

Two interchangeable plasma-discharge ion sources were
used to produce the negative ion beams required during the
experiments: a water-cooled ion source capable of producing
beams of H^-, O^-, S^-, F^-, Cl^-, Br^-, and I^-, and an alkali ion
source used to produced beams of Na^- and K^-. These two ion
sources are very similar in both construction and operation,
differing mainly in that the former has a water-cooled
discharge cell, whereas the alkali ion source lacks a
cooling system but has its discharge cell connected to an
oven in which alkali metal is heated. Beams of H^- and Cl^-
were routinely produced using the alkali ion source, but
these were less stable than those extracted from the water-
cooled ion source; stable O^- beams could not be maintained
when using the alkali ion source.

III.A.1: <u>Alkali Ion Source</u>

The alkali ion source is represented by the schematic shown in Fig. III.2. A solid piece of alkali metal is loaded into the body of a stainless-steel oven (a) with a cap of Monel alloy at one end, and narrowing to a nozzle at the other. The oven body is heated by nichrome ribbon (b), whereas the oven nozzle is separately heated by nichrome wire (c), thus allowing the nozzle to be hotter than the body to prevent its clogging. Thermocouples attached to the oven body and nozzle are used to monitor the source temperature. Typical operating temperatures are 300-320 ^{o}C for Na and 200-230 ^{o}C for K. The heated alkali vapor effuses from the furnace nozzle into a stainless-steel discharge region (d), in which a discharge is struck between a tungsten filament bent to a point (e), and an anode (f) maintained at a higher potential than the filament. The filament is mounted such that its tip lies 1.4 mm from the edge of an 1.25 mm diameter aperture in the anode, so that the tip is slightly offset from the center line of the aperture. This mounting arrangement is found to be the most effective for the extraction of negative ions. The discharge is initiated with Ar which enters the discharge region through a small inlet (g). Beams of Cl^- or H^-, used in the analysis procedures discussed below, are obtained by adding CCl_4 or H_2 to the Ar. Negative ions formed in the discharge are extracted through the small aperture in the
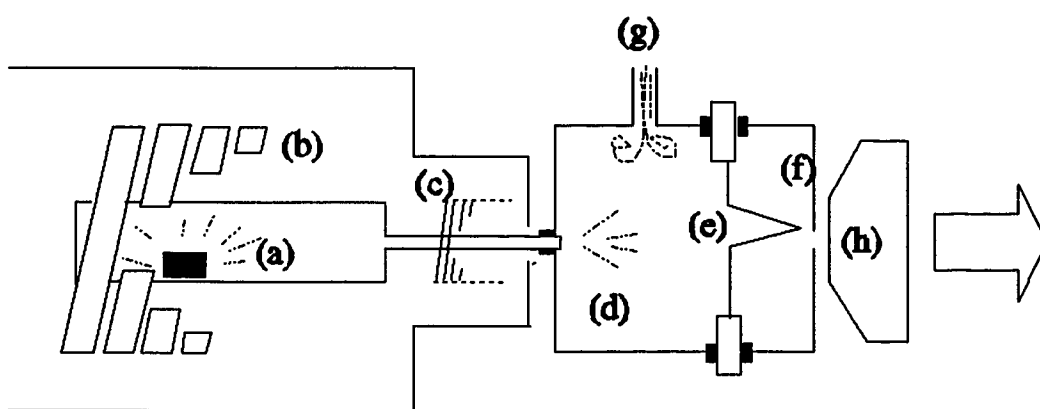
Figure III.2: Alkali ion source; oven containing alkali sample (a), resistive heating elements for the oven body (b) and nozzle (c), discharge cell (d), tungsten filament (e), anode (f), gas (Ar) inlet (g), and electrostatic extraction lens (h).

anode by an electrostatic lens (h). Typical negative alkali beam currents are measured to be between 0.1 and 0.2 nA in the collision zone.

Although obtaining a low energy beam of negative alkali ion is often considered a craft, the following method is straight forward and very successful. First, the alkali oven is baked in vacuo for about two hours at a temperature in excess of 100 $^\circ$C, but is allowed to cool before venting the system and loading the oven with alkali metal. This removes contaminants in the source and nearly eliminates the formation the alkali hydride anion in the discharge, which otherwise is the most abundantly produced negative ion within the source during the first hour of operation. Before loading into the oven body, the alkali metal is washed in petroleum ether and cut such that all surfaces are relatively clean. After the source is evacuated to a pressure of 10^{-5} - 10^{-6} torr, a discharge of about 10 mA is initiated with Ar at a pressure of about 100-125 microns. The potential between the filament and anode is set between 15 and 25 V, and the magnetic mass spectrometer is preset to the alkali mass. The temperature of the oven tip will begin to rise due to the discharge, but will reach a stable temperature of about 50 $^\circ$C. At this temperature, the current though the body heating element is set to about i_b = 0.5 A, causing a further rise in the oven temperature. As the temperature again nears stability, i_b is increased

further to about 0.75 A, but current is not sent through the nozzle heating element until the temperature of the body is to within a few degrees of the tip. At this point, the current through the nozzle heating element, i_t, may be increased slightly to maintain the nozzle between 5 and 25 °C hotter than the body. The current through the body heating element is raised further when the oven temperatures are nearly stable, and i_t is raised whenever the body temperature approaches that of the nozzle; but neither i_b nor i_t are increased by more than 0.25 A. In this way, the oven temperature is slowly raised until a body temperature of 300-320 °C (200-230 °C for K) is reached and a Na⁻ beam is attained. It is crucial that the temperature is raised very slowly since rapid vaporization of the alkali may clog the nozzle, exit aperture, or extraction lens, or may result in most of the alkali metal being removed from the oven to the discharge region, causing inefficient operation of the source or additional clogging.

Very little is known about the pathways which lead to the formation of alkali negative ions in these discharge sources, but in ion sources which produce Li⁻ from a discharge of pure lithium vapor, it is believed that Li⁻ is formed by the dissociative attachment reaction [51]

$$Li_2(v^*) + e^- \rightarrow Li + Li^-.$$
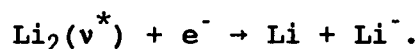
Since, in the alkali source described above, dimers are a small fraction of the sodium or potassium effusing from the

oven [51] and contribute little to the total pressure (see Fig. III.3) in the discharge region, the three body attachment process

$$Na + X + e \rightarrow Na^- + X,$$

where $X = Ar$, Li, Li_2, may be more significant in producing alkali anions. Alternatively, anions produced on the surface of the anode may also be an important mechanism for the formation of alkali negative ions in the ion source [32]. This is, of course, speculation; in any case, the chemistry which governs negative ion production in the source has no bearing on the experimental results.

III.A.2. Water-Cooled Ion Source

Since the water-cooled ion source is similar to the alkali ion source described above, a detailed description of its features will not be given. Fig. III.4 depicts the water-cooled ion source; a comparison of this picture to Fig. III.2 reveals the two most important differences between the water-cooled ion source and the alkali ion source: Fig. III.4 lacks the alkali oven shown in Fig. III.2, but has the addition of several turns of copper tubing encircling the discharge region. Water flow through the copper tubing is usually employed to cool the source, but air flow has also been used with success.

The discharge is initiated with a mixture of argon and
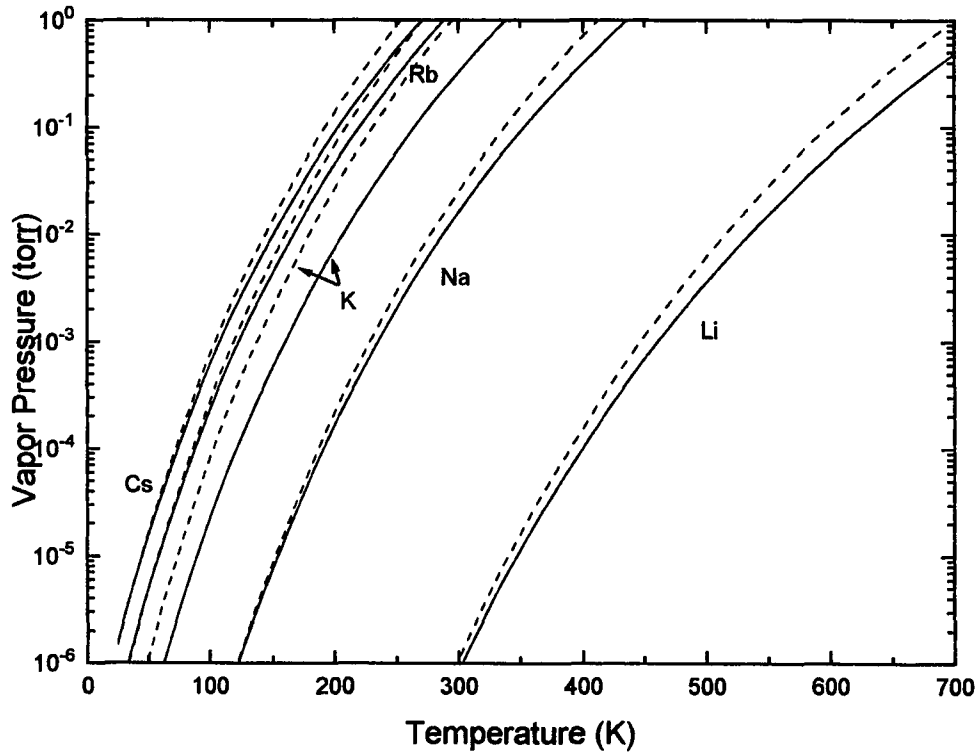
Figure III.3: Vapor pressure of the alkali metals. The solid lines represent the vapor pressure in the liquid phase while the broken lines correspond to the solid phase.
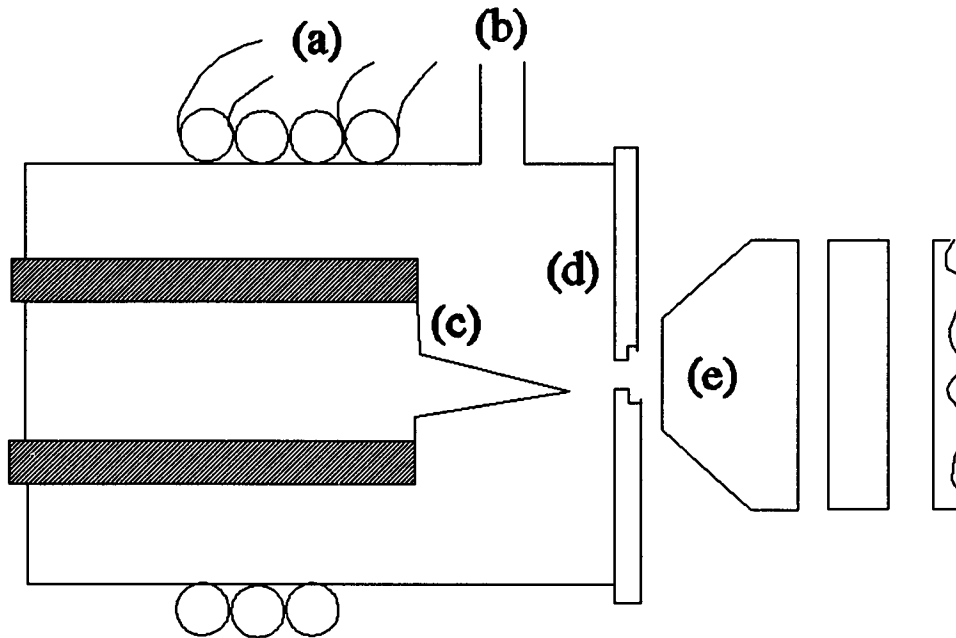
Figure III.4: Water-cooled Ion Source; water flows through copper tubes (a) encircling the discharge cell, gas flows into the cell through the gas inlet (b), a discharge is struck between a tungsten filament (c) to an anode (d), ions are extracted via an electrostatic lens (e). The diagram also demonstrates the offset of the tungsten filament form the center line of the aperture, as discussed in section III.A.1.

one or more other gases. By changing the gas mixture in thedischarge, a variety of atomic anion species can be extracted from the discharge. Each gas mixture is found to have a set of "source conditions" which will yield a stable negative ion beam with an intensity sufficient to do an experiment. These conditions are the pressure within the discharge cell, the relative densities of gases used in the discharge, the potential between the filament and anode, V_{dis}, and the corresponding discharge current, i_{dis}. The discharge current is usually controlled by increasing or decreasing the current through the filament. Beams of H^-, O^-, and S^- are produced from gas mixtures of $1(H_2):1(Ar)$, $7(Ar):1(N_2O)$, and $5(Ar):1(COS)$, respectively. For these gas mixtures, a source pressure of about 200-300 microns usually works best, along with $V_{dis} = 100$ V and i_{dis} in the range of 50 to 100 mA. Typical mass analyzed beam currents in the collision zone are about 0.1 nA for H^- and from 0.1 to 0.3 nA for O^- or S^-. Beams of Cl^- with currents in the range of 0.3 to 1.0 nA are routinely produced by gas mixtures of $30(Ar):1(CCl_4)$ or $5(Ar):1(CH_3Cl)$, and F^- beams in the range of 0.1 to 0.5 nA have been made using a 5:1 mixture of Ar to CF_4. A source pressure between 100 and 150 microns usually works best for the halogen anions. Because of certain normalization procedures discussed below, it is often desirable to extract Cl^- from the discharge as well as

another negative ion. This condition is not easily attained, but two gas mixtures which have worked are $15(Ar):7(CF_4):3(CH_3Cl)$ to extract Cl^- and F^-, and $15(Ar):3(COS):1(CH_3Cl)$ for Cl^- and S^-. Additionally, it was found that carbon tetra-chloride and argon mixed with CH_3Br produced beams of Cl^- and Br^-, but a similar mixture of CCl_4, Ar, and CH_3I produced much I^- but little Cl^-. However, once this latter mixture was evacuated from the gas handling system and replaced by a 5:1 mixture of argon to CH_3Cl, sizable beams of both Cl^- and I^- could still be extracted from the discharge. In that case, the I^- must be due to residual methyl iodide in the gas handling system. Although experiments have been performed in which beams of O^- and Cl^- were extracted from the same discharge, no source conditions could be found which made either of the beams very stable over a reasonable period of time.

III.B: Magnetic Mass Spectrometer and Beam Focusing

All electrons and negative ions extracted from the alkali ion source are subsequently accelerated through a slit of width 2 mm, or, when the water-cooled ion source is used, are accelerated through an aperture of diameter 4 mm. The negative products then pass into a $90°$ magnetic mass spectrometer with an exit slit of width 1.5 mm; quadrupole steering elements before the entrance aperture and after the exit slit correct for the magnetic fringe field. Only

negative products with a mass-to-charge ratio given by

$$\frac{m}{q}\left(\frac{a.m.u.}{a.u.}\right) = \frac{B(gauss)^2}{85.6\,V_m(volts)},\qquad\text{(III.1)}$$

where V_m is the potential difference between the anode and entrance of the spectrometer, will pass resonantly through the mass spectrometer. Since, for example, V_m is typically maintained at 150 V, H$^-$ requires a magnetic field of 110 gauss. The spectrometer is capable of resolving the isotopes of Br (masses 79 and 81) and therefore has a resolving power of at least 40.

The negative ion beam which emerges from the mass spectrometer is focussed by a series of three Einzel lenses [52] though a small aperture centered on a stainless steel plate. An electrometer can be used to measure the beam current striking the plate. From the aperture the beam passes through two retarding lenses, and is finally steered by a quadrupole through a 1.25 mm aperture into the collision region.

III.C. Collision Zone

The collision zone consists of a 30° section of an energy analyzer of radius 76 mm. This region is kept at ground potential, except, of course, for the two electrodes of the analyzer which are maintained at about ±18% of the primary beam energy w.r.t. ground. Thus the incident beam

passes resonantly through the analyzer into a faraday cup,
where the beam current is monitored by an electrometer. A
negative voltage (w.r.t. ground) can be applied to a
tungsten grid in front of the faraday cup, thus repelling
the negative ion beam as a means of measuring the energy
spread of the beam in the collision zone. The full-width at
half-the-maximum of the beams are typically found to be
about 4% of the beam energy. The atomic hydrogen beam
enters the collision zone through the top, and intersects
the incident beam orthogonally between the two electrodes of
the analyzer. A large hole, covered by a tungsten grid,
lies in the bottom of the collision zone directly below the
aperture from which the hydrogen atoms effuse. This hole
allows ultra-violet (uv) photons originating in the hydrogen
source to pass from the collision zone without hitting with
surfaces in the zone; otherwise interactions involving uv
photons with surfaces in the zone will liberate photo-
electrons which will be collected along with the desired
collision products. Slow electrons and negative ions formed
as collision products are forced by the electric field
within the analyzer though a hole in one of the electrodes.
The collision products are then focussed by an electrostatic
lens in to a small electromagnet which separates the product
electrons from negative ions, and are subsequently detected
by conventional particle multipliers (channeltrons). The
signals from the channeltrons are amplified by charge
sensitive pre-amplifiers. These are located in vacuo and

are shielded against rf noise. The pulses from the pre-amplifiers are then counted by standard scalers, and the count rates, along with primary beam intensity, are recorded by a computer over a three second time interval.

Thus the collected data consists of the count rate in either channel (electron or ion), given by $N(s^{-1})$, and the primary beam signal i_o (nA). At any given beam energy, N will only depend only on i_o since $N \sim k\sigma ln i_o$, where l is the effective target length, n is the number density of the target gas, and k is the detection efficiency of the collection system. Therefore, a normalized count rate defined by $I_o = N/i_o$ should be constant at a given beam energy. However, if, at a fixed beam energy, i_o is steadily increased, it is found that I_o does not, in fact, remain constant for count rates which exceed about 40 kHz. This is because the pre-amplifiers generate a pulse with a width of about 10 μs; thus a count rate of 40 khz begins to saturate the pre-amplifier output. Since the cross sections are expected to be less than 40 $\overset{\circ}{A}^2$, a count rate of about 10^4 s^{-1} for $\sigma = 10$ $\overset{\circ}{A}^2$ is desired. If the minimum target gas density is taken to be 10^{12} cm^{-3}, $l = 0.5$ cm, and we assume k is at least 0.1, the minimum beam current needed to do an experiment is 0.1 nA.

Experimental uncertainties associated with the collision zone are manifest in the experimentally determined cross sections, and will now be discussed. First, the

absolute number density for hydrogen in the collision zone cannot be directly measured in the present apparatus, so the magnitude of the experimentally determined cross sections are normalized to previously measured cross sections for X^- + H_2 (i.e. with the hydrogen source off) or the calculated detachment cross section for Cl^- + H (see section IV.B.2). Errors associated with the cross sections used for normalization are therefore incorporated into the experimental results. Although the beam energy is set by the anode potential in the ion source, the actual beam energy will be offset from the anode voltage by a small amount which may change over the course of the experiment. Since the normalization cross sections are a function of energy, it is very important that the data points with the rf on are taken at the exact same energy as with the rf off.

Another concern is associated with the intersection volume of the incident anion beam and neutral target beam. The overlap of the anion beam with the hydrogen beam is periodically checked by moving hydrogen source in the x-y plane and noting the corresponding changes in the product electron and ion count rates and primary beam current. Even so, the focusing properties of certain lenses, as well as the relative detection efficiency between the ion and electron detectors, depend upon the beam energy; furthermore, certain lens voltages are often changed during the course of an experiment. All these properties can alter

the effective intersection volume between the crossed beams during the course of an experiment; therefore, it must be emphasized that, particularly when cross sections for $X^- + H$ are normalized to those of $Cl^- + H$ (discussed below), the focusing conditions at a given beam energy remain unchanged until all count rates for that data point are taken and the beam energy changed. This insures that the effective intersection volume, and hence target number density, is consistent for all measurements taken an a given data (energy) point.

III.D: Hydrogen Source

Atomic hydrogen is produced within a radio-frequency (rf) discharge of hydrogen gas. The so-called Slevin source is commercially available and the technical details are described in Ref. [53]; therefore, only a few of the relevant details of operation will be discussed here. The source operates at 36 MHz and uses about 30 Watts of rf power. The rf cavity is bounded by the innermost wall of two concentric pyrex tubes, coolant flows through a jacket formed by the region between the tubes. A 1:1 mixture of water and methanol is cycled though the coolant jacket to a chiller and then back to the jacket, thus maintaining the coolant between 2 and 10 $^{\circ}$C. Neutral hydrogen atoms and molecules exit the source through an S-shaped tube of 2-mm bore and 15 mm length, into a 1-mm bore capillary of 18 mm

length. The neutral beam exiting the source is described by a cosine curve with a density in the range of 10^{12} to 10^{14} cm^{-3} 2 mm from the exit aperature. The dissociation fraction, i.e. the fraction of H_2 dissociated to H, is measured to be in the range of 30-40% for all the experiments.

In order to prevent degradation of the dissociation fraction, the rf power is left continually on while the apparatus is under vacuum, and the rf is turned off and the hydrogen flow stopped only to make necessary background measurements. Often, after long periods of venting or if the hydrogen flow though the source is terminated for an extended period of time, the dissociation fraction can become quite small. However, it was found that running a discharge of He for one day brings the dissociation fraction within the range of 30-40%, where it will typically remain stable (to within about 5%) for several days. Turning the rf power on and off repeatedly (for durations of a few seconds to minutes) does not seem to affect the dissociation fraction. Hydrogen atoms are most likely to recombine on the walls of the Slevin source, therefore contamination of the pyrex surface within the source is the most probable cause of small dissociation fractions. The manufacturer recommends cleaning the tube with hydrofluoric acid along with washes of hot acetone and distilled water and claims a disassociation fraction of 95% can be obtained. During the

course of these experiments, using this cleaning procedure
did not yield better results than the He discharge and high
dissociation fractions were never obtained, but recent
reports [54] claim that a 90% dissociation fraction can be
obtained by cleaning the source with ortho-phosphoric acid.

The hydrogen source is minor source of background noise
in the particle detectors. Presumably, the noise signal
(with the anion beam terminated) is due to photoelectrons
liberated from surfaces near the collision zone by uv
photons which emerge from the rf discharge. This count rate
never exceeds about 10^3 s^{-1}, and is a slight function of
beam energy since the electric field in the collision zone
depends upon the incident beam energy. There is one
potential source of error which cannot be quantified,
however: If vibrationally excited H_2 molecules which are
produced within the rf discharge survive, free electrons
resulting from $X^- + H_2(v \neq 0) \rightarrow e + \ldots$ could be important.
The problem of contamination by vibrationally excited H_2
from a similar rf discharge source has been discussed by
Morgner and co-workers [55,56]. They found that at
least 1/3 of the electrons produced by $Ne^* + H_2 \rightarrow e + Ne +$
H_2^+ are due to vibrationally excited hydrogen when the
reaction chamber is connected to the rf discharge by a
teflon tube, but apparently quenching occurs when the teflon
tube is replaced by an aluminum tube (on which molecules
leaving the discharge frequently collide before reaching the

reaction chamber). In the present study, the hydrogen effuses through an S-shaped Pyrex tube maintained at a temperature between 2 and 10 $^\circ$C , as described above, and the effusing hydrogen must clearly make tens of collisions with the walls of the capillary tubes. In the discussions below, it is assumed that $H_2(v \neq 0)$ is not present in the "atomic hydrogen" beam when the rf discharge is on.

III.E: Data Analysis

The experimental quantities measured with the apparatus are the incident beam current, i_o (nA), and the count rates for electrons or ions, N (s^{-1}). From these two quantities it is useful to define two normalized count rates which take background noise into account:

$$I_{on} = \frac{N_{on} - N_{rf}}{i_o} - \frac{N_{beam}}{i_o} \qquad (III.2)$$

and

$$I_{off} = \frac{N_{off}}{i_o} - \frac{N_{beam}}{i_o}, \qquad (III.3)$$

where N_{on} and N_{off} are the count rates with the rf power on and off, N_{rf} represents the count rate measured with the rf power on and the incident beam directed away from the collision zone. N_{beam} is the count rate due to beam background, determined with the rf power off and the flow of H_2 to the source terminated. Except for N_{rf}, it is

understood that i_0 is the average primary beam current at the time the respective count rate is taken. With the rf power turned off the target beam is, of course, entirely H_2, so the normalized count rate is easily related to the cross section for electron detachment or ion production for the system $X^- + H_2$:

$$I_{off} = kT(E_{lab}) n_{H_2} \sigma (H_2, E_{lab}) ,\qquad \text{(III.4)}$$

where E_{lab} is the collision energy in the laboratory frame, $T(E_{lab})$ is a transmission function or detection efficiency of either of the detectors, n_{H2} is the number density of H_2, and k is a constant which incorporates units and the effective target length. With the rf turned on, the flux of atomic hydrogen emerging from the source is related to that for H_2 with the rf turned off by

$$\phi (H) = 2f\phi (H_2) ,\qquad \text{(III.5)}$$

where f is the dissociation fraction. The atomic hydrogen traverses the anion beam with a mean velocity v given by

$$v(H) = \sqrt{2}\, v(H_2) ,\qquad \text{(III.6)}$$

so that the atomic hydrogen density with the discharge on is related the H_2 density with the rf off by

$$n(H) = \sqrt{2}\, f n(H_2).\qquad\qquad\text{(III.7)}$$

Hence I_{on} can be related to the cross section for collisions of anions with H and H_2 by

$$I_{on} = k T(E_{lab})\, n_{H_2}\, [\,(1-f)\, \sigma(H_2, E_{lab}) + \sqrt{2}\, f \sigma(H, E_{lab})\,].\quad\text{(III.8)}$$

If we combine Eqs. (III.4) and (III.8) and solve for f,

$$f = \frac{\dfrac{I_{on}}{I_{off}} - 1}{\sqrt{2}\,\dfrac{\sigma(H, E_{lab})}{\sigma(H_2, E_{lab})} - 1},\qquad\qquad\text{(III.9)}$$

we can determine the dissociation fraction when $\sigma(H_2, E_{lab})$ and $\sigma(H, E_{lab})$ are known and $\sigma(H_2, E_{lab})$ is non-zero. Such is the case for Cl^-, where the electron detachment cross sections are known for the systems $Cl^- + H_2$ via Huq et al. [57] and $Cl^- + H$ via a calculation by Gauyacq [58]. This latter calculation has been experimentally verified in this laboratory, and is presented in section IV.B.1. Alternatively, the dissociation fraction can be determined using an O^- projectile since the cross section for $O^- + H_2 \rightarrow H^- + \ldots$ is known [59], e.g. it is about 2.3 $Å^2$ for a relative collision energy $E = 0.7$ eV, but the energetic threshold for $O^- + H \rightarrow O + H^-$ lies above 0.7 eV, i.e. $\sigma(H,E)$ is identically zero below 0.7 eV. Therefore, for collisions

of O⁻ + H and H_2 at relative collisions energies below 0.7

eV, Eq. (III.9) becomes

$$f = 1 - \frac{I_{on}}{I_{off}}.$$
(III.10)

This latter expression for f may also be used with the

system F⁻ + H: the system F⁻ + H_2 exhibits a peak in the

ion production cross section [57] at a relative collision

energy of about 2.1 eV, corresponding to E_{lab} = 22 eV, and

the energetic threshold for F⁻ + H → F + H⁻ lies around E_{lab}

= 52 eV. All these methods consistently determine the

dissociation fraction to lie between 30 and 40%, and is

reproducible to within 5%, e.g. 35 ±5%. Several methods of

data analysis are used to determine the cross sections for

the system X⁻ + H from the measured quantities;

nevertheless, all the measurements and data analysis methods

result from two distinct experimental techniques. The

simpler of the two is employed when $\sigma(H_2, E_{lab})$ is known for

a system, so that $\sigma(H, E_{lab})$ is normalized to $\sigma(H_2, E_{lab})$ by

measuring both I_{on} and I_{off}. If $\sigma(H_2, E_{lab})$ is not known or,

for some other reason, cannot be used to establish the

magnitude of the cross section for a system X⁻ + H, then

$\sigma(H, E_{lab})$ is determined by the normalization to the known

cross section for the Cl⁻ + H. In such a case, a Cl⁻ beam,

for which both $\sigma_e^{Cl}(H, E)$ and $\sigma_e^{Cl}(H_2, E)$ are known [57,58],

must be made simultaneously with the X^- beam such that one can switch between the two beams, taking data for both systems at a given laboratory energy. Hereafter this second technique will be referred to as a back-to-back measurement. For either technique, it must be emphasized that all count rates, except for N_{beam}, are taken at a given laboratory energy before changing the beam energy and taking the next data point, thus insuring identical $T(E_{lab})$ and n_{H2} between the measurements. After all these count rates are measured, the hydrogen flow is terminated and I_{beam} is measured over the entire laboratory energy range of the experiment. The various methods of data analysis for these techniques will now be discussed.

III.E.1: <u>Method 1; O^-, S^- (E>1 eV), Cl^-, F^-, Na^-,</u>

<u>and K^- + H → e + ...;O^-, S^-, Cl^-, F^- + H → H^- + ...</u>

Eq. (III.9) can be inverted and solved for $\sigma(H,E_{lab})$:

$$\sigma(H,E_{lab}) = \frac{\sigma(H_2,E_{lab})}{\sqrt{2}}\left(\frac{I_{on}/I_{off}-1}{f}+1\right). \qquad \text{(III.11)}$$

Thus the magnitude of $\sigma(H,E_{lab})$ can be established with Eq. (III.11) for systems where $\sigma(H_2,E_{lab})$ is known, but is most useful for those systems for which $\sigma(H_2,E_{lab})$ is fairly smooth and large in magnitude, i.e. $I_{off} \gg I_{beam}$. This method is employed to determine charge transfer and electron

detachment cross sections for the systems O^- + H and S^- + H

using the experimentally determined $\sigma(H_2,E)$ given in Huq *et*

al. [59]. For E < 1 eV a different method (method 3, below)

must be employed to determine the electron detachment cross

section for the system S^- + H because the present experiment

extends to energies below those for S^- + H_2 given in Ref.

[59]. The electron detachment cross section for collisions

of Na^- or K^- with atomic hydrogen were normalized to the

$\sigma_e(H_2,E)$ measured by Scott *et al.* [60]. Although

$\sigma_e(H_2,E_{lab})$ for the alkali anion systems are small, no other

experimental technique could be used since other methods

inevitably require two anion beams to be formed within the

same discharge, but no other negative ions could easily be

extracted from the same discharge as the alkali anions.

   The charge transfer cross sections for Cl^- and F^- were

also determined by the normalization to the known ion

production cross sections for Cl^- + H_2 or F^- + H_2 [57,61].

Charge transfer of alkali anions with atomic hydrogen

requires special consideration and is discussed in the

following section.

III.E.2: <u>Method 2; Na^-,K^- + H → H^- + ...</u>

   Although the cross sections for the process Na^- + H_2 →

H^- + ... are known [60], they are not used to normalize the

charge transfer cross section, as in method 1 above, since

H^- produced via $Na^- + H_2 \rightarrow H^- + NaH$ can have significant velocity in the direction of the incident anion beam and might not be collected and detected with the current crossed beam geometry. However, the charge transfer cross section can be normalized to the electron detachment cross section, $\sigma(H_2, E_{lab})$, by

$$\sigma_i(H, E_{lab}) = \frac{\sigma_e(H_2, E_{lab})}{\sqrt{2}} \left(\frac{I^i_{off}}{I^e_{off}} \right) \left(\frac{T_e(E_{lab})}{T_i(E_{lab})} \right)$$

$$X \left(\frac{I^i_{on}/I^i_{off} - 1}{f} + 1 \right)$$

(III.12)

The factor $(T_e(E_{lab})/T_i(E_{lab}))$ which appears on the right hand side of Eq. (III.12) is the ratio of the collection efficiencies for electron and ions, and can be determined from

$$\left(\frac{T_e(E_{lab})}{T_i(E_{lab})} \right) = \frac{\sigma^H_i(H, E_{lab})}{\sigma^H_e(H, E_{lab})} \left(\frac{I^e_{on} - (1-f) I^e_{off}}{I^i_{on} - (1-f) I^i_{off}} \right)$$

(III.13)

by performing experiments of $H^- + H$ since the electron detachment cross section, $\sigma_e^H(H, E_{lab})$, and charge transfer cross section, $\sigma_i^H(H, E_{lab})$, are both known [50]. In practice, $(T_e(E_{lab})/T_i(E_{lab}))$ is found to be 1.0 ± 0.1 over the entire range of laboratory energies, and is therefore taken to be unity for these experiments.

III.E.3: <u>Method 3; S⁻ + H → e + ..., E < 1 eV</u>

Since both $\sigma_e^{Cl}(H,E)$ and $\sigma_e^{Cl}(H_2,E)$ are known for the

system Cl⁻ + H, the transmission function can be found from

Eq. (III.8):

$$T(E_{lab}) = \frac{I_{on,Cl}}{(1-f)\,\sigma_e^{Cl}(H_2,E_{lab}) + \sqrt{2}\,f\sigma_e^{Cl}(H,E_{lab})}. \qquad \text{(III.14)}$$

Then, by using back-to-back S⁻ and Cl⁻ beams, $\sigma(H_2,E_{lab})$ is

determined from Eq. (III.4):

$$\sigma_e^{S^-}(H_2,E_{lab}) = \frac{I_{on,S^-}}{T(E_{lab})}. \qquad \text{(III.15)}$$

Having thus determined $\sigma(H_2,E_{lab})$ for S⁻ + H₂, Eq. (III.11)

may be used to obtain $\sigma(H,E_{lab})$ for S⁻ + H. This method has

the advantage of being able to obtain $\sigma(H_2,E_{lab})$ as well as

$\sigma(H,E_{lab})$; as will be discussed in Chapter IV, the S⁻ + H₂

results lead to an interesting consequence.

III.E.4: <u>Method 4; Cl⁻, F⁻, Br⁻, and I⁻ + H → e + ...</u>

In using the back-to-back technique, $\sigma(H,E_{lab})$ can be

expressed solely in terms of the calculated Cl⁻ + H electron

detachment cross section:

$$\sigma(H,E_{lab}) = \sigma_e^{Cl}(H,E_{lab})\,\frac{I_{on} - (1-f)\,I_{off}}{I_{on}^{Cl} - (1-f)\,I_{off}^{Cl}}. \qquad \text{(III.15)}$$

This method is used to obtain electron detachment cross

sections for F⁻, Br⁻, and I⁻ + H. For collisions of halogen

anions with H and H_2, $\sigma(H_2,E_{lab})$ is negligibly small compared to $\sigma(H,E_{lab})$. Consequently Eq. (III.16) is virtually independent of the dissociation fraction f, so the systematic error associated with this method is small compared to the other methods discussed above. In order to independently measure $\sigma(H,E)$ for $Cl^- + H$ and ascertain the validity of the normalization procedures described above, back-to-back measurements of $O^- + H$ and $Cl^- + H$ were made and Eq. (III.16) was used to normalize $\sigma(H,E_{lab})$ to the $O^- +$ H electron detachment cross section previously determined using method 1. This result will be discussed in Chapter IV.

CHAPTER IV

RESULTS AND DISCUSSION

In what follows, measurements of total cross sections

in collisions of negative ions with atomic hydrogen are

presented. Over the range of laboratory energies $2 < E_{lab} <$

500 eV, cross sections have been determined for electron

detachment, which results from associative detachment (AD),

$$X^- + H \rightarrow XH + e, \qquad (IV.1)$$

and direct detachment (DD),

$$X^- + H \rightarrow X + H + e, \qquad (IV.2)$$

and also for charge transfer (CT),

$$X^- + H \rightarrow X + H^-, \qquad (IV.3)$$

where X^- represents O^- or S^-, the halogen anions, or the

alkali anions Na^- or K^-. The experimental results for these

three groups of anions are presented in sections IV.A, IV.B,

and IV.C, respectively. Where possible, models and

calculations will be presented and discussed along with the

experimentally determined cross sections. A few remarks

unifying all the collision systems studied here is given in

section IV.D. Details of the experimental apparatus and

procedures can be found in Chapter III, and will not be

repeated here. The energetic thresholds for reactions

(IV.1)-(IV.3) are listed in Table IV.1 for the systems relevant to the present study.

IV.A: O^- and S^- + H

IV.A.1: Introduction; previous studies

The collision dynamics for O^- + H are somewhat complicated by the fact that $H(^2S)$ and $O^-(^2P)$ form four electronic molecular states which correlate to the ground states of the separated atoms. In what follows, the difference between the $^2P_{1/2}$ and $^2P_{3/2}$ states of O^- is neglected; that difference is 0.022 eV [62]. The intermolecular potentials for the ground state of OH and the four lowest for OH^-, based upon calculations by Huron and Tran Minh [63], are illustrated in Fig. IV.1.

The ground electronic state of OH^- is of $^1\Sigma$ symmetry, has a vertical electron affinity of 1.8 eV and has been well-characterized [64]. It does not cross the $^2\Pi$ state of OH and does not couple strongly to that state [65]. Hence collisions at low energies which are attributed to the $^1\Sigma$ state of OH^- should be essentially non-reactive. However, in a slow collision, the excited electronic states of the molecular anion must also be considered in the dynamics for reactions (IV.1)-(IV.3). In addition to the $^1\Sigma$ state of OH^-, there are the $^1\Pi$, $^3\Pi$ and $^3\Sigma$ states. As may be

Exothermicity (eV)

Anion	$X^-+H \rightarrow XH+e$	$X^-+H \rightarrow X+H+e$	$X^-+H \rightarrow X+H^-$
H^-	3.72	−0.75	————
O^-	2.39	−1.46	−0.71
S^-	1.4	−2.08	−1.33
F^-	2.47	−3.40	−2.65
Cl^-	0.82	−3.61	−2.86
Br^-	0.39	−3.37	−2.61
I^-	−0.003	−3.059	−2.31
Na^-	1.4	−0.55	0.21
K^-	1.3	−0.5	0.25

Table IV.1: The exothermicity of reactions (IV.1) - ((IV.3) for negative ions relevant to the present study.
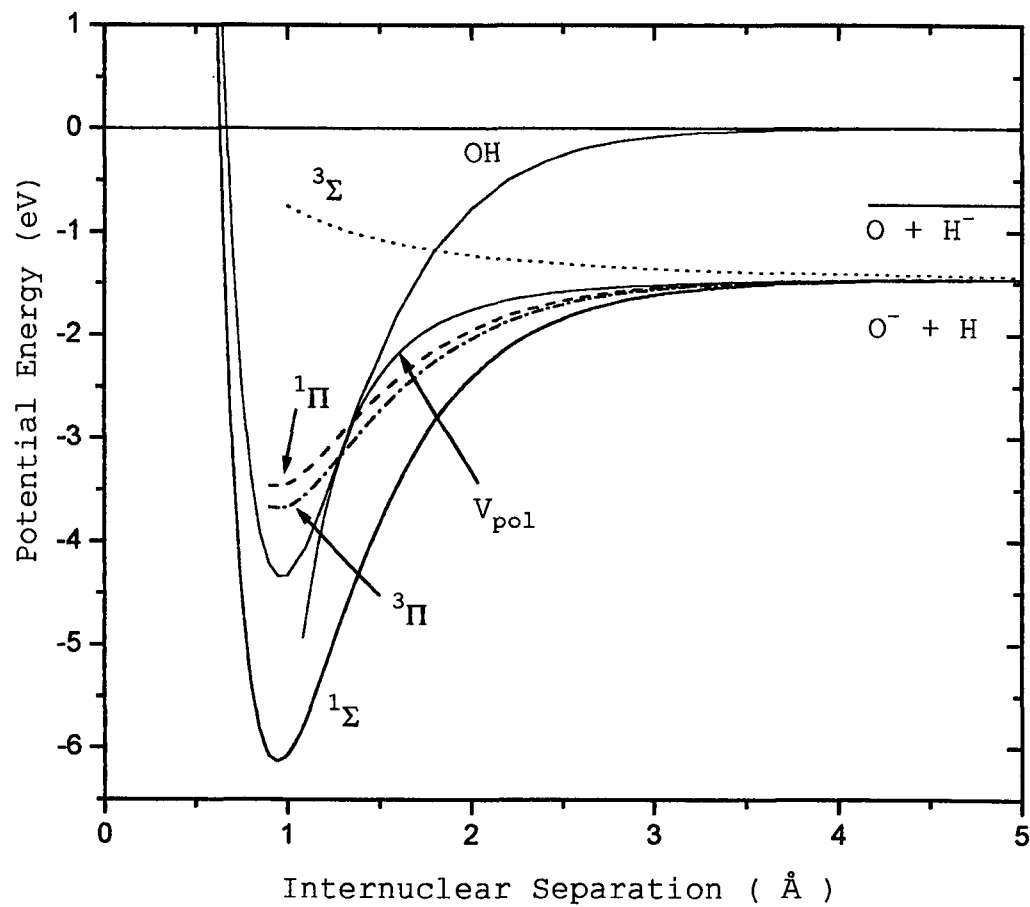
Figure IV.1: Intermolecular potentials for OH and OH⁻, taken from Ref. [63]. Also shown is the polarization potential V_{pol}.

seen in Fig. IV.1, the $^1\Pi$ and $^3\Pi$ states were calculated [63] to be attractive, intersecting the neutral OH ($^2\Pi$) curve at an internuclear separation of about 1.25 Å. The combined statistical weights of these two curves is 2/3 and their long range attractive behavior is somewhat similar to that given by the induced dipole potential, $V_{pol}(R) = -\alpha e^2/8\pi\epsilon_o R^4$ (where α is the polarizability of H, *viz.*, 0.7 $Å^3$), which is also shown in Fig. IV.1. The calculations for these Π-states do not exhibit a barrier, which implies there should be no barrier to associative detachment via the Π-states. Consequently, one might expect reaction channel (IV.1) to have a large rate constant, specifically one which is about 2/3 of that predicted by a simple Langevin orbiting model (see section II.C). At low collision energies the Σ states, with combined weights of 1/3, should not contribute to (IV.1). All of this discussion is, of course, predicated upon the validity of the intermolecular potentials as given in Fig. IV.1. It should be pointed out that, in contrast to the results of Huron and Tran Minh, the $^1\Pi$ state of OH⁻ was calculated to be repulsive by Tellinghuisen and Ewig [66], and also by Acharya, Kendall, and Simons [65]. These latter authors do not report any results for the triplet sates; nonetheless, they predicted that the rate for (IV.1) should be small. Tellinghuisen and Ewing calculate the $^3\Sigma$ state to be repulsive, whereas they find the $^3\Pi$ to be attractive and to cross the continuum at 1.75 Å.

No information is available for the intermolecular potentials which separate asymptotically to $H^- + O$. Hence a detailed description of charge transfer (IV.3) for these reactants is not possible. Detailed calculations for the molecular states of SH^- are, other than the stable $^1\Sigma$ configuration, likewise not available. Nevertheless, it is clear that, like $O^- + H$ there may be several routes to associative electron detachment for the reactants $S^-(^2P) + H(^2S)$. To date, it appears that there are no measurements of rate constants or low energy cross sections for the reactants $O^- + H$ or $S^- + H$.

IV.A.2: **Results: $O^- + H$**

The experimental results for the electron detachment cross sections are given in Fig. IV.2. For E < 1.46 eV (the electron affinity of O), only associative detachment [i.e., (IV.1)] is energetically possible. The increase in the cross section as E is lowered below the electron affinity of oxygen implies, unambiguously, that one or more of the intermolecular potentials which describe $O^- + H$ must be attractive and couple strongly to the $^2\Pi$ state of OH. Although the $^1\Sigma$ state of OH^- is attractive it probably does not lead to appreciable associative detachment [65] and, even if it did, it could not account for the observed cross section as its relative statistical weight is only 1/12.
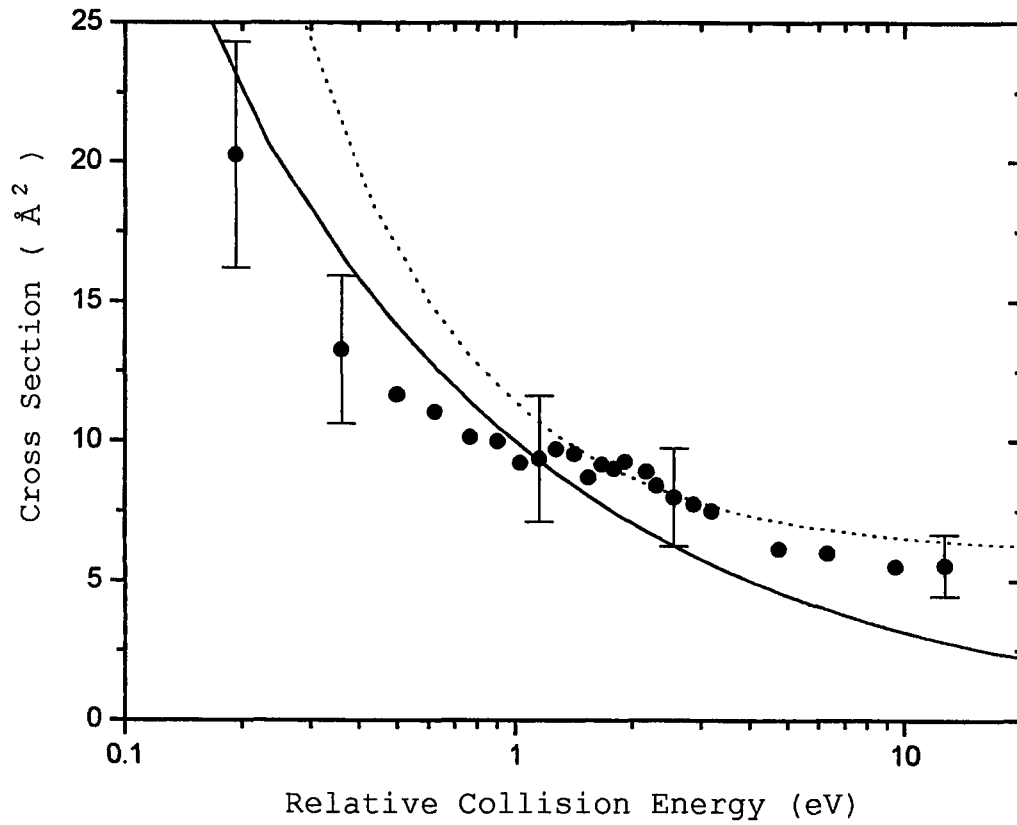
Figure IV.2: Cross section for electron detachment for O⁻ +

H as a function of relative collision energy: the solid

circles are the present experimental results, the solid line

represents two-thirds of the Langevin (orbiting) cross

section (see section II.C), and the dashed curve is the

result of Eq. (IV.4).

Hence one is led to conclude that other states, such as those depicted in Fig. IV.1, are attractive and lead to the low energy behavior observed in Fig. IV.2 for the detachment cross section.

One simple method to model the cross section for electron detachment is to assume that every trajectory which leads to a crossing of the anion potential with the $^2\Pi$ state of OH produces a free electron, as discussed in section II.C. This is an obvious oversimplification of the problem, neglects charge transfer, and can only suggest an upper limit to the detachment cross section. Neglecting the $^1\Sigma$ state of OH$^-$, this cross section is given by

$$\sigma(E) = \sum_{i=1}^{3} w_i \cdot \pi b_i^2(E) \qquad (IV.4)$$

where w_i are the statistical weights of the $^1\Pi$, $^3\Pi$ and $^3\Sigma$ states (2/12, 6/12, and 3/12) and $b_i(E)$ is given by

$$b_i(E) = R_i \left(1 - \frac{V_i(R_i)}{E}\right)^{1/2}. \qquad (IV.5)$$

The $V_i(R)$ are the intermolecular potentials for the electronically excited OH$^-$ molecular anion illustrated in Fig. IV.1 and R_i are their crossing radii. The results of Eq. (IV.4) using the potentials given in Fig. IV.1 are also presented in Fig. IV.2. The results of this simple model and our measurements are in excellent agreement at high

collision energies, but the calculation exceeds the experimental results at lower energies. Also shown in Fig. IV.2 is two-thirds of the Langevin (or orbiting) cross section for atomic hydrogen (see section II.C). This orbiting cross section will underestimate detachment at high energies when the critical orbiting impact parameter, b_{orb} = $\{\alpha e^2/2\pi\epsilon_o E\}^{1/4}$, falls below the impact parameter which leads to a classical turning point around 1.3 Å, i.e., the crossing radii shown in Fig. IV.1. For example, $b_{orb}(7eV)$ ≈ 1.3 Å for the polarizability of H.

The cross section for the charge transfer reaction (IV.3) is shown in Fig. IV.3, along with a previous result from Snow, Rundell and Geballe [67]. A reasonable extrapolation of the present results is in excellent agreement with this previous measurement. Unfortunately nothing is known about the intermolecular potentials for H⁻ + O; consequently it is premature to speculate about the dynamics for charge transfer of O⁻ + H.

IV.A.3: Results: S⁻+H, H₂

There are two motivations for measuring electron production cross sections for S⁻ + H₂. First, the analysis of the data for S⁻ + H requires a knowledge of the cross section for the molecular target for collision energies below those given by Huq et al. [68]. Second, it is not readily apparent that the results of Ref. [68] are
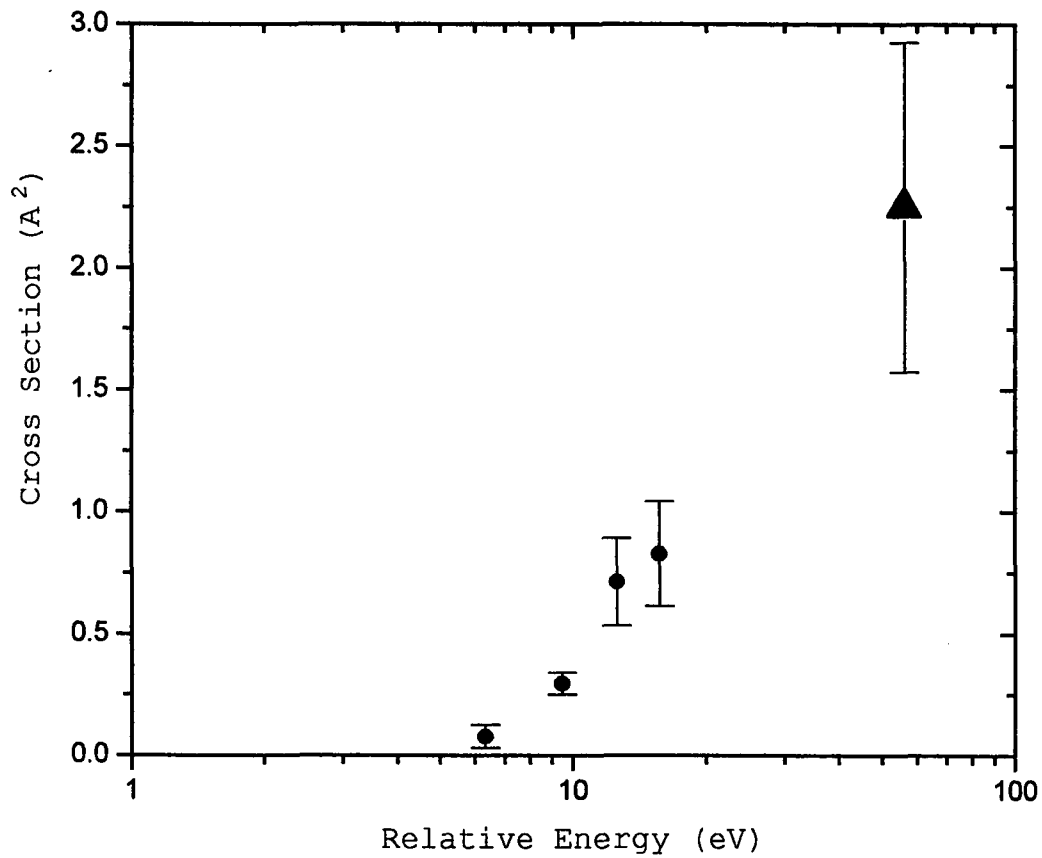
Figure IV.3: Cross section for charge transfer for O⁻ + H;
the solid circles are the present experimental results and
the triangle at an energy of 60 eV is taken from Ref. [67].

consistent with cross sections inferred from earlier rate constant measurements at lower collision energies [69]. Specifically, the cross sections for electron detachment as reported by Tellinghuisen et al. [69] for S^- + D_2 diminish with a reduction in energy, while those of Ref. [68] rise with decreasing energy, failing to connect with the results derived from the rate constant measurements. As can be seen in Fig. IV.4, the present results agree remarkably well with the previous measurements of Huq et al. at higher energies and will clearly extrapolate to the lower energy results of Ref. [69] if (and only if) the results are plotted as a function of collision velocity. These results imply the existence of a barrier to associative detachment, which is the only allowed channel for electron production for E < 2.08 eV, the electron affinity of S^-. What remains unclear, however, is why the measurements for the two different isotopes scale with the collision velocity rather than the relative collision energy.

The detachment cross sections for S^- + H are obtained via normalization to the present values of $\sigma(H_2, E_{lab})$ as well as those of Ref. [68]. The experimental results obtained by using the normalization procedure described above are shown in Fig. IV.5, along with a curve which represents 2/3 of the Langevin cross section. As can be seen, the detachment cross section corresponds very well with the Langevin limit below 1 eV, but levels off between 6
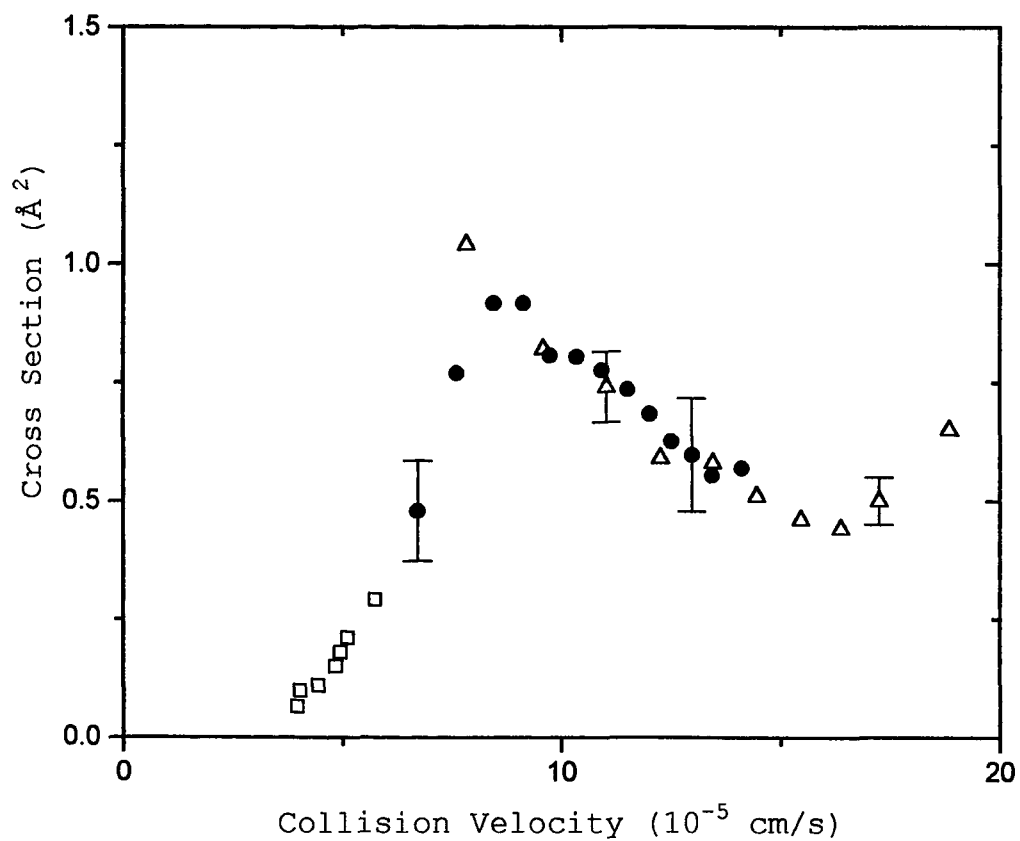
Figure IV.4: Associative electron detachment cross sections for S⁻ + H₂ (or D₂) as a function of the collision velocity: the triangles are from Ref. [68] and the solid circles are the present results, each for the H₂ target. The squares are the results for the D₂ target and are taken from Ref. [69].
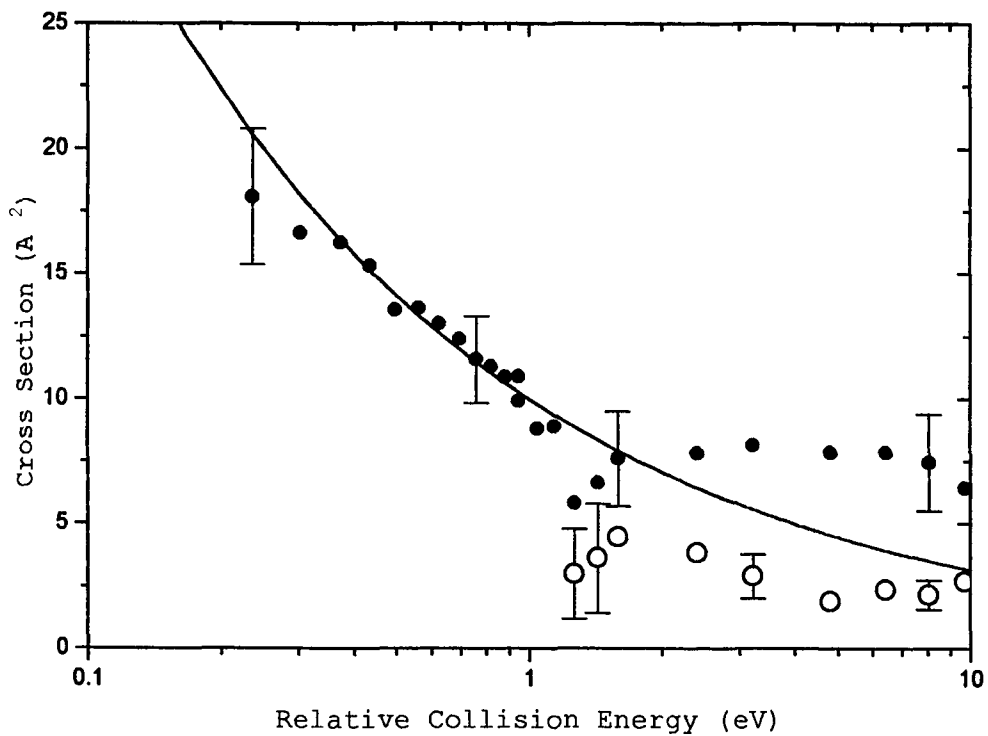
Figure IV.5: Cross sections for electron detachment and charge transfer for S⁻ + H: the solid circles are the present results for detachment and the open circles represent *four times* the cross section for charge transfer.

and 8 Å^2 above 1 eV. The fact that the curve steadily rises with decreasing energy suggests that there may be no barrier to associative detachment. Furthermore, the cross section resembles that for $O^- + H$, suggesting that the electronic molecular potentials may also be similar. The OH ($^2\Pi$) state has an equilibrium separation of 0.97 Å while that of SH ($^2\Pi$) is 1.34 Å [70], so one would expect, if the electronic structures are similar, the cross sections for S^- to be greater than those for O^-; this is observed to be the case.

Also shown in Fig. IV.5 is the small cross section for charge transfer. The magnitude of the signal used to infer this charge transfer cross section is such that the uncertainty in the measurements is as high as 60%. The energetic threshold for charge transfer appears to occur at the thermodynamic value, *viz.*, 1.3 eV.

IV.A.4: Summary: collisions of O^- and S^- with H

No barrier to associative detachment is observed in collisions of O^- or S^- with atomic hydrogen. This experimental result is consistent with the potential curves calculated by Huron and Tran Minh and by Tellinghuisen and Ewig: both collaborations calculate the $^3\Pi$ state to be attractive into the autodetaching region. Although the collision dynamics are complicated by the fact that at least

the $^3\Pi$, $^1\Pi$, and $^3\Sigma$ states, and possibly the state

corresponding to O + H⁻, participate in electron detachment,

the simple classical model presented in section II.C is

found to provide a reasonable estimate of the electron

detachment cross section. This is especially true for the

system S⁻ + H, and may indicate that a potential of the form

$(1/R^4)$ is a good approximation of the $^3\Pi$ state. For both O⁻

and S⁻ + H, the charge transfer cross sections never exceed

about 1 $\AA^2$ over the entire energy range investigated;

therefore charge transfer is not an important channel, as

compared to electron detachment, in regard to the

neutralization of O⁻ or S⁻ in collisions with atomic

hydrogen.

IV.B: F⁻, Cl⁻, Br⁻, and I⁻ + H

IV.B.1: Introduction; previous studies

Among the elements which form stable negative ions, the

halogens are characterized by their unusually high electron

affinities (EA), which range from 3.61 eV for chlorine to

3.06 eV for iodine [3]. Although the collision mechanisms

which govern the destruction of halogen anions has received

considerable attention in the past, only a few experimental

studies have involved atomic hydrogen targets, mainly due to

the difficulties of obtaining well-characterized beams of

atomic hydrogen at room temperature. Owing to the large

endothermicity for charge transfer, the cross section for (IV.3) is expected to be small at low collision energies and processes (IV.1) and (IV.2) are expected to dominate for E_{lab} < 500 eV when $X^- = F^-$, Cl^-, Br^-, and I^-.

Of all the halogen anion-hydride systems, F^- + H and Cl^- + H have received the most attention from a theoretical point of view, due in part to the number of experimental measurements which exist for these systems. The rate constant for AD in F^- + H has been reported previously [18] to be about 1.6×10^{-9} cm^3/s at 300 K, which agrees well with the more recent measurement of Smith and Adams [71] who found values of 1.5×10^{-9} cm^3/s and 8×10^{-10} cm^3/s at 300 K and 515 K respectively. For Cl^- + H the AD reaction rate has been measured at thermal energies by a number of authors [18,19]. In general, good agreement exists between the measurements and the calculations of Gauyacq [2,72] and Haywood and Delos [73], all yielding a value of about 9.5×10^{-10} cm^3/s. The calculation of Gauyacq, which is based on a zero range potential (ZRP) approximation, has also been used to determine the product vibrational distributions for AD in F^- and Cl^- + H at room temperature, and excellent agreement is found with the measurements of Zwier *et al.* [74,75]. The large measured reaction rates for AD indicate that the intermediate anion states formed in the collisions are attractive into the autodetaching region;

this has been verified in the case of HF⁻ by several *ab initio* calculations [76,77,78,79] and also for HCl⁻ by the calculations of Morgan *et al.* [80] and by Gorczyca and Norcross [79]. The quasimolecular intermediate ion states of HCl⁻ and HF⁻ have been investigated through various electron scattering experiments, such as those of Rohr and Linder [81], in which vibrational excitation was measured for e⁻ + HCl and HF. In both cases the integral cross sections for vibrational excitation exhibited sharp peaks at the energetic threshold and additional broad maxima were observed at collision energies of about 2-3 eV. These original experiments of Rohr and Linder showed the scattering to be isotropic in angle, indicating pure s-wave scattering. Experimental studies of dissociative attachment have also shown that the total cross section for this process varies stepwise as the electron energy is varied [82] and that the cross section increases substantially with the vibrational excitation of the target [83]. These observations prompted a series of theoretical studies of electron scattering by hydrogen halides and it was recognized rather early that neither the threshold peaks observed for vibrational excitation nor the above features observed for dissociative attachment could be explained by a collision model which utilizes a local resonance theory [84,85]. However, all of these observations were accounted for in either non-resonant [85,86,87] or in

non-local, resonant theories [88,89]. More recently, electron scattering experiments by Knoth *et al.* [90] with HF and HCl targets have been performed with higher resolution than those of Rohr and Linder. They also find sharp peaks at the energetic thresholds for vibrational excitation and, in the case of HCl but <u>not</u> HF, a broad maximum is seen for collision energies in the range of 2-3 eV. Unlike Rohr and Linder, however, Knoth and co-workers find the angular dependence of electron scattering to be non-isotropic and suggest that the scattering process requires the consideration of higher partial waves (i.e. s,p, and d). These considerations are taken into account in recent *ab initio* HCl⁻ and HF⁻ potential curve calculations [78,79,80]. These calculations all agree on the general shape of the ground state intermolecular potentials for the molecular anion HX⁻: it is attractive and crosses or merges with the intermolecular potential for HX in the vicinity of the HX equilibrium position. Table IV.2 contains a survey of calculations for these molecular anions which have appeared during the past fifteen years. The interested reader can find further theoretical considerations of electron scattering in the review article by Morrison [91].

In contrast to F⁻ and Cl⁻, few theoretical studies have concentrated on the collision systems formed by I⁻ or Br⁻ + H, and experimental work has focused on thermal energy

Survey of Potential Curve Calculations

for Halogen Hydride Molecules and Anions

Reference	Anion	R_c (Å)	α' (Å^3)	Comments
Gorzyca and Norcross [79]	HCl⁻	1.48	0.36	SEP results, close-coupling (C-C) approximation
	HCl⁻	1.7	——	SE results, C-C approximation. V(1.7 Å) lies above Cl⁻ + H at R = ∞
	HF⁻	1.01	0.15	SEP results, C-C approximation.
	HF⁻	1.05	0.39	SE results, C-C approximation.
Åstrand and Karlström [92]	HCl⁻	1.6	0.03	RASSCF calculation
Morgan, Burke, and Gillian [80]	HCl⁻	1.51	0.3	SEP model, R-matrix method
	HCl⁻	1.47	0.38	PSS model, R-matrix method
Morgan and Burke [78]	HF⁻	1.09	0.41	R-matrix method
Chapman, Balasubramanian, and Lin [93]	HBr⁻	1.72	-----	SOCI calculation; V(1.71 Å) lies above Br⁻ + H, R = ∞
	HBr⁻	1.69	-----	RCI calculation; V(1.69 Å) lies above Br⁻ + H, R = ∞
	HI⁻	1.85	-----	SOCI calculation
	HI⁻	1.88	-----	RCI calculation
O'Neil, Rosmus, and Norcross [93]	HCl⁻	1.6	0.03	MC-CI caluculation; the crossing point is an extrapolation of the calulation

Betten-dorff, Beunder, and Peyerim-hoff [77]	HCl⁻	1.69	-----	Multireference CI calculation; V(1.69 Å) lies above Cl⁻ + H, R = ∞
	HF⁻	1.38	0.1	Multireference CI calculation
Gauyacq [72]	HCl⁻	1.38	0.43	The HCl⁻ curve of Ref. [72] is not an *ab initio* calculation, but a fit to experimental data
Segal and Wolf [76]	HF⁻	1.06	0.4	CI and stabilization method
Goldstein, Segal and Wetmore [94]	HCl⁻	1.57	0.14	CI and stabilization method

Table IV.2: Survey of calculated potential curves for halogen hydride anions. R_c is taken from the corresponding reference. α' is inferred from R_c and $V(R_c)$, where $V(R)$ is the Morse potential of Ref. [70] (see section IV.B.3(a)). SEP denotes the static exchange plus polarization model; RASSCF denotes the restricted-active-space self-consistent-field model; PSS denotes the perturbed-stationary-states model; SOCI denotes the second-order configuration-interaction model; RCI and MC-CI are the relativistic and multiconfiguration models; and FOCI is the frozen-orbit CI model.

measurements. Smith and Adams [71] have measured the rate constant for AD in Br^- + H at 300 K and 515 K and found a constant value of $7x10^{-10}$ cm^3/s. For AD in I^- + H, they found a reaction rate of $3x10^{-10}$ cm^3/s at 300 K, and $6x10^{-10}$ cm^3/s at 515 K; the former value is about five times greater than the upper limit for this reaction as determined by Fehsenfeld [70]. Cross sections for DA in collisions of electrons with HI have been measured by Alajajian and Chutjian [95]; they report approximate potential curves for HI^- which are based upon their measurements. Chapman *et al.* [96] have calculated potential curves for several electronic states of HBr^- and HI^-, but no calculations exist for electron detachment cross sections.

IV.B.2: <u>Theoretical study: Cl^- + H</u>

As discussed in Chapter III, many of the electron detachment cross sections presented here are obtained by normalization to the collision system Cl^- + H; moreover, the dissociation fraction is most easily determined by performing Cl^- + H experiments. Since the results of this calculation are directly relevant to the present study, a synopsis of the calculation is given here.

The traditional view of the detachment process in collisions of X^- with Y invokes the formation of an unstable XY^- ion during the collision time. This ion subsequently

decays by electron emission, thus leading to electron detachment. Experiments with hydrogen-halide systems revealed features which could not be accounted for by a standard local complex potential approximation in which the decay of the intermediate negative ion is described via a local rate, $\Gamma(R)$, which depends only on the internuclear distance, R. Various different approaches were then developed and tested on the hydrogen halide systems (see e.g. [85,97]). These new theoretical models included non-local effects in the resonance approach or used a non-resonant approach. Among the latter, the effective range approximation [2,87] -an extension of the zero-range potential approximation discussed in section II.E- was shown to be very successful in describing direct detachment [98,99] as well as associative detachment [72,100] and electron-molecule collisions [87]. In the effective range approach, the electron-molecule interaction is represented by a local potential $V_{ext}(r)$ at large electron-molecule distances, say, $r > r_0$ and the short range interactions are described by a boundary condition at $r = r_0$ independent of the electron energy:

$$\frac{1}{\psi}\frac{d\psi}{dr}\Big|_{r=r_0} = f(R) , \qquad (IV.6)$$

The ZRP approach corresponds to the limit of vanishing r_0 and V_{ext}. This representation can be used in the treatment of the collision problem without any further

approximation and the heavy particle motion can be treated either quantally [72] or classically [98,99]. It is worth noting that in this approach, no resonant state is present. The HCl⁻ system, illustrated in Fig. IV.6, presents a bound state at large internuclear distances which disappears below a certain distance, R_c, where the ion potential energy curve merges with that of the neutral.

The cross section for associative detachment in Cl⁻ + H collisions has been previously calculated for energies below 0.6 eV [72] in the ZRP approximation with a quantal treatment of the nuclear motion. A study of direct detachment at higher energies was performed by using a semi-classical approximation which consists of determining the time evolution of the semiclassical wave packet [98,99]. The modeling for the e-HCl system, shown as the dotted line in Fig. IV.6, was taken from Teillet-Billy and Gauyacq [87]. This modeling was successful in reproducing the features observed for e + HCl; viz., the vibrational excitation and the dissociative attachment cross section. Fig. IV.7 presents results of this semiclassical calculation for the detachment probability $P_d(b)$ as a function of the impact parameter, b, for the two collision energies 4 and 20 eV. The detachment probability exhibits a very strong dependence on b: for $b < R_c$, the system enters the unstable region and $P_d(b)$ is almost equal to one, whereas for $b > R_c$ a bound state always exists and detachment can only occur via a

direct dynamic transition from the bound state to the continuum causing P_d to be very small. As a consequence, in the absence of trajectory effects, the detachment cross section is roughly equal to πR_c^2. Obviously, at low collision energies, trajectory effects appear due to the attractive ion potential and the detachment cross section increases as the energy decreases. The weak dependence of $P_d(b)$ on the collision energy can be understood by considering two opposing effects: (i) the probability for direct transitions from the bound state to the continuum increases with increasing collision velocity and (ii) the spreading of the electron wave packet in the unstable region causes the detachment probability to decrease with increasing collision velocity (see e.g. the discussion in [101]). The net result of these dynamic effects is a very weak energy dependence of the total detachment cross section for $4 < E < 20$ eV; these results, along with the previous calculations for $E < 0.6$ eV are shown in Fig. IV.8. A spline fit to these calculations is used for $\sigma_{Cl}(E_{lab})$ employed in Eq. (III.15) for the purpose of normalizing the results for F^-, Br^-, and I^- + H.

IV.B.3: Experimental Results and Discussion

IV.B.3(a): Cl^- + H

In low energy collisions of halogen anions with atomic
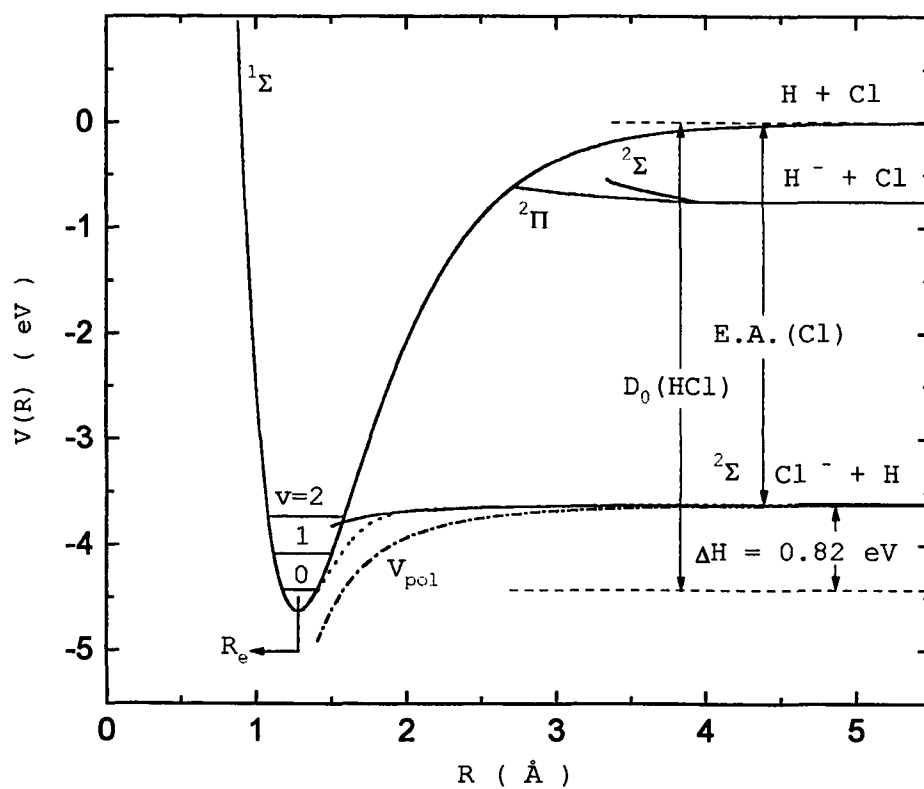
Figure IV.6:   Intermolecular potentials of HCl and CHl⁻: HCl
$^1\Sigma$ [70], solid line; HCl⁻ $2^2\Sigma$ and $^1\Pi$ [95] HCl⁻ $^2\Sigma$ [72],
dotted line; the dipole potential V_{pol} with $\alpha = 0.7$ Å³,
dash-dotted line; the dipole potential with $\alpha' = 0.14$ Å³,
solid line.
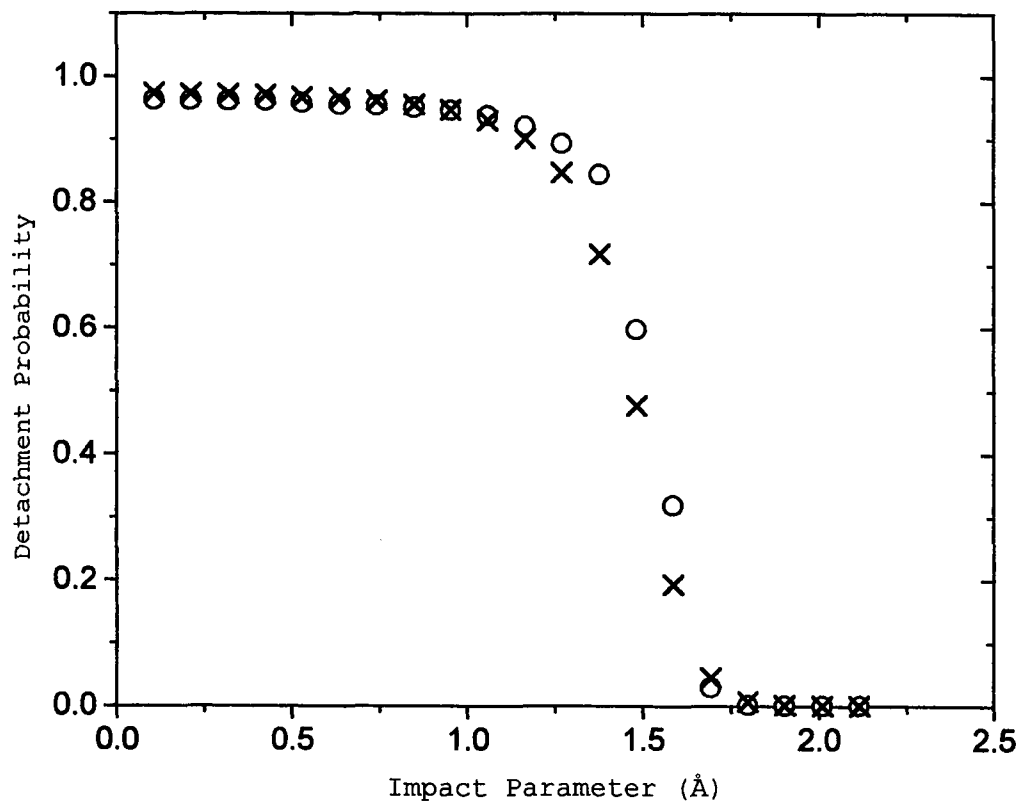
Figure IV.7: Detachment probability $P_d(b)$ as a function of the impact parameter b for the system $Cl^- + H$. Open circles are the results for 4 eV and crosses correspond to 20 eV.
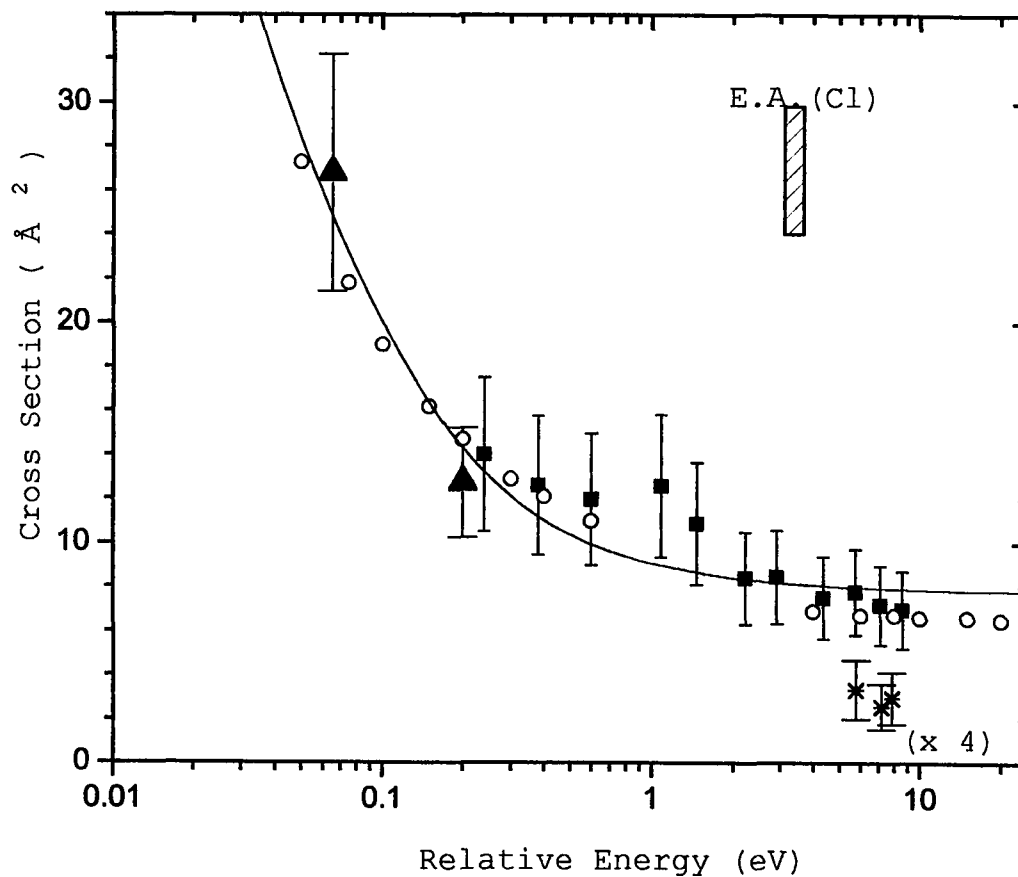
Figure IV.8: Electron detachment cross sections for Cl⁻ + H as a function of relative collision energy. The present measurements are given by the solid squares; cross sections inferred from the reaction rates of Refs. [18,19], solid triangles; the present calculation and that of Ref. [72], open circles; and the results of the classical model described in section IV.B.3(a), solid line. The asterisks represent *four times* the charge transfer cross section.

hydrogen, electron loss may occur via associative detachment (AD) or direct detachment (DD), i.e. reactions (IV.1) and (IV.2). The process of AD may be discussed with the aid of Fig. IV.6, which illustrates the potentials of the neutral ground state of HCl ($^1\Sigma$) [70] as well as the lowest states of the transient molecular anion HCl$^-$ representing Cl$^-$ + H ($^2\Sigma$) [72] and H$^-$ + Cl ($^2\Pi$, $2^2\Sigma$) [95]. For relative collision energies below the electron affinity (EA) of Cl, only AD is energetically allowed, and the system of Cl$^-$ + H evolves along the state indicated by $^2\Sigma$ in Fig. IV.6. This state lies above that of the neutral continuum for internuclear separations $R < R_c$, where R_c is the crossing or merging radius. The dissociation energy, D_0, of HCl is larger than the EA of Cl, and this exothermicity, ΔH, is partitioned among the reaction products; it has been demonstrated [2,72,74,102] that almost all the exothermicity (0.82 eV) is distributed in the internal degrees of freedom of the product HCl such that the detached electron carries away less than half a vibrational quantum of energy. For relative collision energies above the EA of Cl (3.61 eV), DD may occur. Since the $^2\Sigma$ state of HCl$^-$ is attractive into the autodetaching region, no energetic threshold for AD is expected, and, assuming near unit detachment probability for all $R < R_c$, an asymptotic (i.e. high energy) detachment cross section, $\sigma_e(E)$, of

approximately πR_c^2. Various estimates of R_c for HCl^- can be found in Table IV.2.

The experimentally determined total cross sections, $\sigma_e(E)$, for electron detachment in collisions of $Cl^- + H$ for relative collision energies between 0.2 and 12 eV are shown in Fig. IV.8; no distinction can be made between DD and AD in the present experiment. Also shown in Fig. IV.8 are cross sections derived from previous rate constant measurements [18,19]; these are in good agreement with the present results. The open circles represent the previously discussed ERP calculations which are in good agreement with the measurements over the entire energy range investigated, and, within the limits of the experimental uncertainties, correctly predict a detachment cross section of about 6.5 $\mathring{A}^2$ at the highest collision energy.

If the polarizability of hydrogen (0.7 $\mathring{A}^3$) is used in Eq. (II.12) for $V_{pol}(R)$, the resulting potential (denoted V_{pol} in Fig. IV.6) falls well below any reasonable estimate of the true interaction potential. Clearly if one is to take advantage of the analytic simplicity of the orbiting model discussed in section II.C, the static polarizability of hydrogen (0.7 $\mathring{A}^3$) must be replaced by a smaller "effective" polarizability, α', in order for (II.12) to mimic the molecular anion potential. In light of the above discussion, the following approach is taken in order to provide a simple model which describes the detachment

process: An interaction potential of the form given by Eq.
(II.12) is assumed, except that α is replaced by an
effective polarizability, α', which is determined by R_c from
the calculations of Goldstein et al. [96] (see Table IV.2),
and $V(R_c)$ from the Morse potential for the neutral molecule
[70]. In Fig. IV.6 the resulting potential is shown for α'
$= 0.14$ Å^3 ($R_c = 1.57$ Å, $E_o = 0.17$ eV) and, as mentioned
previously, the induced dipole potential with $\alpha = 0.7$ Å^3.
This particular value for R_c and hence α' is chosen because
the resulting detachment cross section determined by (II.14)
and (II.15), shown in Fig. IV.8, best matches the present
data as well as previous rate constant measurements.

It should be mentioned that certain problems arise in
determining $V(R_c)$ and hence α' from the calculations listed
in Table IV.2. Many of the anion potential curves from
Table IV.2 are presented in the literature as difference
potentials and are not accurate when referenced to a Morse
potential (for the neutral species) which has been inferred
from spectroscopic data. In most cases, this problem occurs
because the calculated neutral potential curves (of the same
species) differ considerably from the Morse potential.
Specifically, if the energy difference between the
calculated anion potential and neutral parent is subtracted
from the Morse potential, then the resulting anion
potentials display barriers not present in the original
representation. If, on the other hand, the calculated anion

curve is directly compared to the Morse potential for the neutral molecule then the crossings may not occur at the same point. In summary, the principal useful feature of almost all of the calculations listed in Table IV.2 is the merging, or crossing distances for the anion-neutral systems. This merging radius, R_c, and the known potential for the neutral molecule can be used to find α'. We will employ this procedure to model the interactions for F^- and $Br^- + H$ in the discussions that follow.

Finally a few words about charge transfer for collisions of $Cl^- + H$. Charge exchange leading to $H^- + Cl$ is endothermic by 2.85 eV and hence cannot occur for laboratory energies below 100 eV. From Fig. IV.6 it may be seen that the two lowest states of $H^- + Cl$ are repulsive outside the autodetaching region, and do not approach the $^2\Sigma$ state of $Cl^- + H$. Since the lifetime of HCl^- inside the autodetaching region is very short, charge transfer would have to occur before either of the curves cross into the HCl continuum. The charge transfer probability is roughly proportional to $\exp(-\Delta E(R)b/hv)$ (as in Eq. (II.26)), where v is the collision velocity and $\Delta E(R)$ represents the energy difference between, e.g., the $^2\Sigma$ state of $Cl^- + H$ and the $^2\Pi$ state of $H^- + Cl$. From Fig. IV.6, $\Delta E(R) \geq 2.85$ eV for all R; thus the charge transfer probability is expected to be very small for the range of laboratory energies sampled in

this study. The notion that the $^2\Pi$ and $2^2\Sigma$ states of H$^-$ +
Cl are repulsive is supported by the observation that in
electron scattering experiments on HCl, the H$^-$ production
cross section suggests the presence of two dissociative
anion resonances of HCl$^-$, located at about 7 and 9 eV in the
Franck-Condon region of the HCl(v=0) molecule [103]; this
implies that the two lowest states of H$^-$ + Cl are repulsive.
In the present measurements, the charge transfer cross
section is indeed found to be small; the results are
presented in Fig. IV.8.

In conclusion it may be stated that the electron
detachment cross section for Cl$^-$ + H is fairly well
characterized for laboratory energies below 500 eV. We will
advantage of this by using Cl$^-$ + H to normalize the results
(i.e. via method 4 and Eq. (III.15), discussed in section
III.E.4) for the reactants F$^-$, Br$^-$, and I$^-$. In particular,
the calculation of $\sigma_e(E)$ discussed in section IV.B.2 will be
used for the simple normalization procedure described by Eq.
(III.15).

IV.B.3(b): F$^-$ and Br$^-$ + H

The total electron detachment cross sections for F$^-$ + H
are presented in Fig. IV.9 as a function of relative
collision energy. For collision energies below 3.4 eV, i.e.
the electron affinity of F, only associative detachment is

energetically allowed. Also shown in Fig. IV.9 is the associative detachment cross section inferred from the thermal reaction rate measurement of Fehsenfeld [18], specifically k_{AD} = 1.6 x 10^{-9} cm^3/s at 300 K (or about 0.04 eV), which is about 0.82 k_L, where k_L is the Langevin reaction rate discussed in section II.C. This is comparable to k_{AD} = 1.5 x 10^{-9} cm^3/s reported by Smith and Adams [71] for the same reactants at 300 K. These latter authors, however, report that the AD reaction rate is diminished by a factor of two at 500 K (or 0.067 eV). Also shown in Fig. IV.9 are the results of the classical model discussed above. In this case, we use R_c = 1.06 Å from Segal and Wolf [76] with α' = 0.4 $Å^3$ and E_o = 2.26 eV. The model predicts a cross section which is in agreement with our results and the rate measurements at 300 K. The modified polarization potential with α' = 0.4 $Å^3$ presented in Fig. IV.10(a) clearly provides an excellent approximation to the $^2\Sigma$ potential for HF^- taken from Segal and Wolf. The rate measurement at 500 K does not seem to be compatible with the present results; the reason for this apparent discrepancy is not understood. The small charge transfer cross section for F^- + H is also shown in Fig. IV.9.

Total electron detachment cross sections for Br^- + H are shown in Fig. IV.11, along with cross sections determined from previous reaction rate measurements [71];

Figure IV.9:   Electron detachment cross section for F^- + H

as a function of relative collision energy.   Present

measurement, solid circles; cross section inferred from the

reaction rates of Ref. [18], solid square; and of Ref. [71],

solid triangles; and the results of the classical model

described section IV.B.3(a). with $\alpha' = 0.4$ Å^3, solid line.

The asterisks represent *ten times* the charge transfer cross

section.
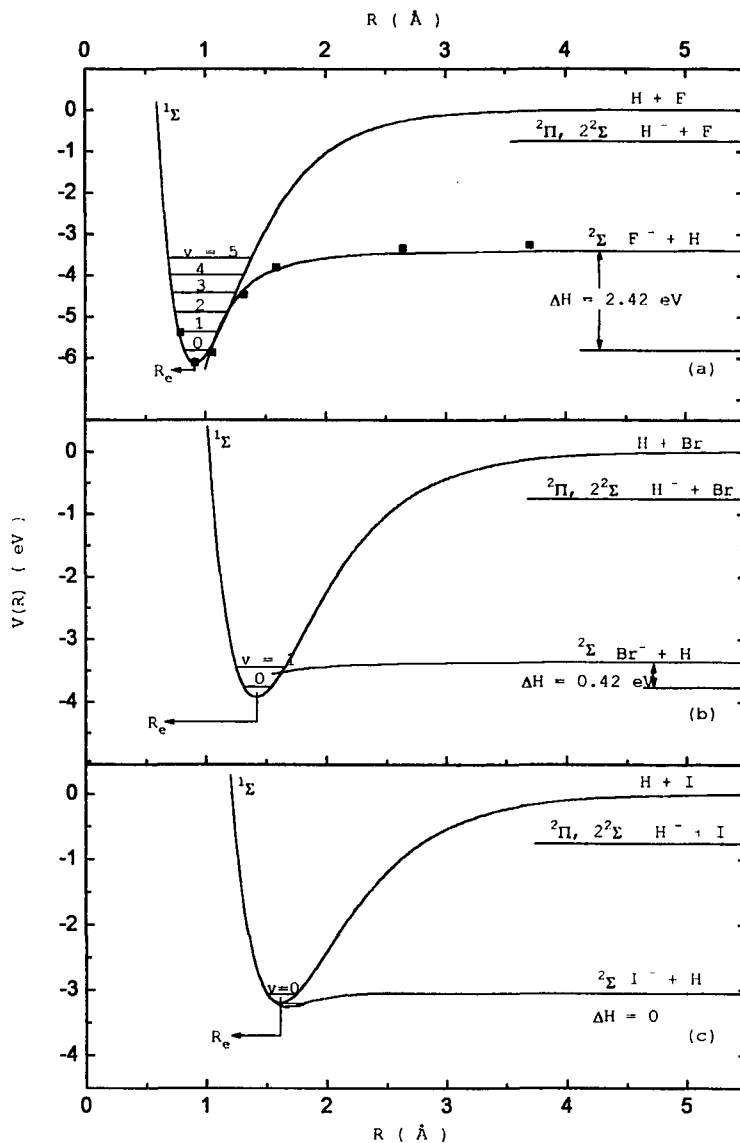
Figure IV.10: Intermolecular potentials for (a) HF $^1\Sigma$ [70], solid line; HF$^-$ $^2\Sigma$ [76], solid squares; dipole potential with $\alpha' = 0.4$ Å^3, solid line; (b) HBr $^1\Sigma$ [70], solid line; polarization potential with $\alpha' = 0.09$ Å^3, solid line; (c) HI $^1\Sigma$ [70], solid line; HI$^-$ $^2\Sigma$ schematic inferred from present results, solid line.
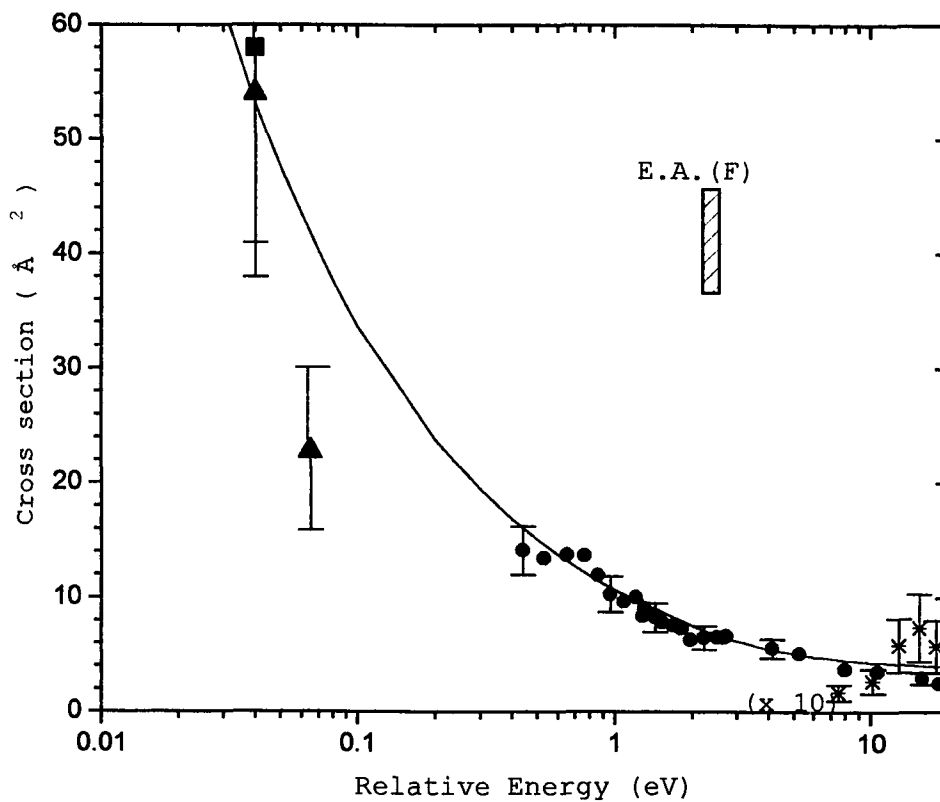
Figure IV.11: Electron detachment cross sections for Br⁻ +
H as a function of relative collision energy. Present
measurements, solid circles; cross sections inferred from
the reaction rates of Ref. [71], solid triangles; results of
the classical model described in section IV.C.3(a) with $\alpha' =$
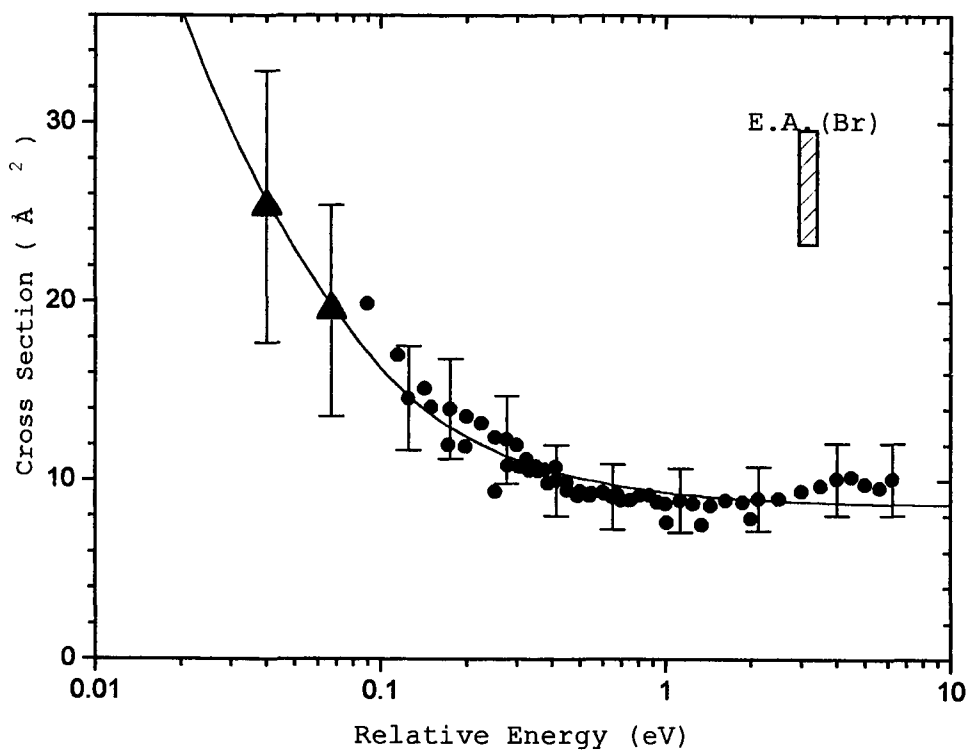0.09 $\text{\AA}^3$, solid line.

the present results are in good agreement with the reaction rates. The cross section which results from the classical model with R_c = 1.65 Å, α' = 0.09 Å^3, and E_0 = 0.09 eV is also shown in Fig. V.11. The particular value for R_c was chosen such that the resulting cross sections best matched the present measurements. This value (1.65 Å) is slightly smaller than the merging radius R_c = 1.72 Å calculated by Chapman et al. [93]. It should be noted that V(1.72 Å), where V(R) is the Morse potential for HBr, lies slightly above the asymptotic limit for Br$^-$ + H implying a barrier to AD. Fig. IV.10(b) depicts the Morse potential for HBr and the polarization potential with α' = 0.09 Å^3. A statistically significant charge transfer cross section for Br$^-$ + H could not be determined; however, the measurements indicate that the cross section should be less than about 1 Å^2 over the energy range investigated.

The similarity of $\sigma_e(E)$ for Br$^-$ + H at low energies to that for Cl$^-$ + H indicates that analogous detachment mechanisms are involved, and that the non-Born-Oppenheimer effects, indicated in the ERP model, play similar roles in both cases. Indeed the two systems are comparable in many respects; both have an exothermicity (for AD) which is small, 0.42 eV for Br$^-$ + H and 0.82 eV for Cl$^-$ + H, compared to the large ΔH of about 2.42 eV for F$^-$ + H. The number of accessible vibrational states for the AD products is two for

HCl and one for HBr, compared to five for the HF products. This, and the apparent similarity of the HF$^-$ $^2\Sigma$ state to the induced polarization potential with $\alpha' = 0.4$ Å^3, may explain why electron detachment in collisions of F$^-$ with H is adequately described by a simple orbiting model over the entire energy range investigated.

IV.B.3(c): I$^-$ + H

Presented in Fig. IV.12 are the detachment cross sections for I$^-$ + H as a function of relative collision energy. The EA of iodine is 3.059 eV [3] and the dissociation energy of HI ($^1\Sigma$) is 3.054 eV [70]. Thus associative detachment for I$^-$ + H is slightly endothermic. In this respect I$^-$ + H is different from the previous halogen-hydride systems investigated here. From Fig. IV.12 it is evident that the $\sigma_e(E)$ for I$^-$ + H displays a dramatically different behavior when compared to F$^-$, Cl$^-$ or Br$^-$ + H. The detachment cross section for I$^-$ + H is relatively constant between 0.09 and 1.2 eV, and then increases sharply with energy above the threshold for which direct detachment is energetically possible. The rate constants for associative detachment have been measured by Smith and Adams at about 300 K and 500 K [71], and the cross sections inferred from their measurements are also indicated in Fig. IV.12. These results appear to be incompatible with
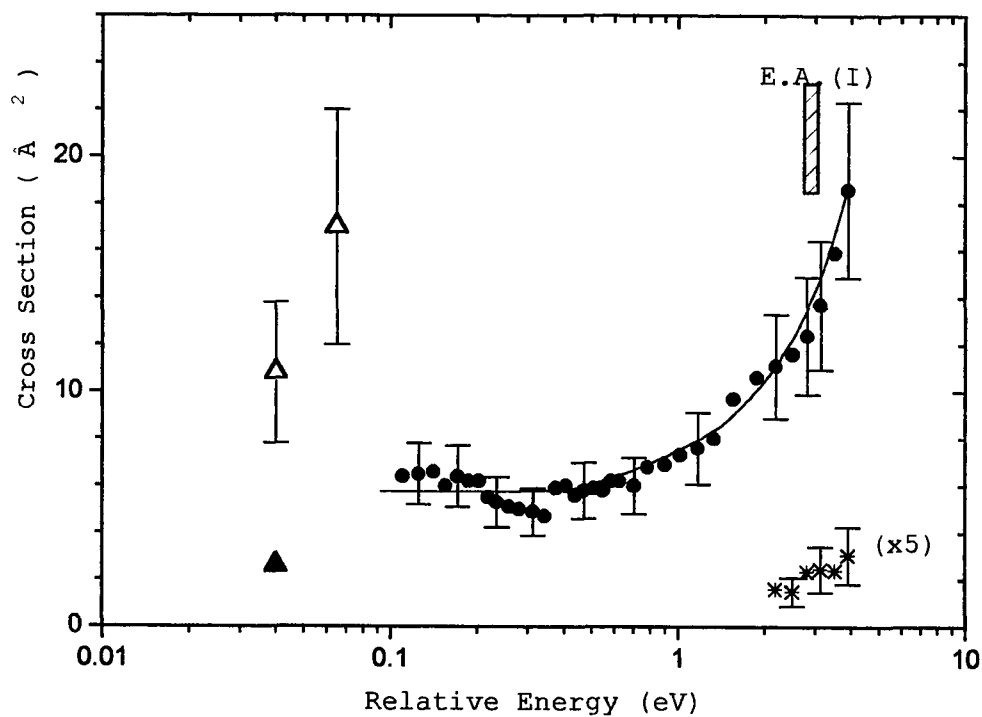
Figure IV.12: Cross sections for electron detachment and charge transfer for $I^- + H$. Present results for detachment, solid circles; *five times* the present results for charge transfer, asterisks; detachment cross sections inferred from the reaction rates of Ref. [71], open triangles; and of Ref. [18], solid triangle. The solid line is a guide to the eye.

the present measurements and that inferred from a 300 K rate
measurement by Fehsenfeld [18].

The charge transfer cross section, $\sigma_{ct}(E)$, for $I^- + H$
is observed to increase slowly with energy from about 0.3 to
0.6 Å^2 for relative collision energies between 2.2 and 4 eV.
Charge transfer in $I^- + H$ is endothermic by about 2.3 eV;
although an energetic threshold for $\sigma_{ct}(E)$ is not directly
apparent, the cross section extrapolates to an experimental
threshold of approximately 1.5 eV. The difference of 0.8 eV
from the energetically allowed threshold may be accounted
for by thermal broadening [104].

An additional aspect of HI, which sets it apart from
the previously discussed halogen hydrides, is that it forms
a stable negative ion [105]. Thus the $HI^-(^2\Sigma)$ potential
must support at least the lowest vibrational state, which
requires a well depth of about 0.15 to 0.2 eV based on the
vibrational ground state of HI. A few conclusions about the
$^2\Sigma$ state may be drawn from the measured detachment cross
sections. At the lowest collision energies, $\sigma_e(E)$ is
constant at about 6.3 ± 1.1 Å^2, and no evidence for a rapid
decrease with decreasing collision energy is observed. If
indeed an energetic threshold exists for
associative detachment, then, based on the present
measurements, it is expected to be less than or equal to
about 0.1 eV. This observation is compatible with the
calculations of Chapman et al. [93] who report an energetic

threshold of 0.1 eV for AD, and also with the experimental

results of Alajajian and Chutjian [92] who suggest a

threshold of less than 0.1 eV, based upon dissociative

attachment measurements. This threshold is also in

agreement with the rate measurements of Fehsenfeld [18] if

thermal broadening is considered.

If one assumes that the detachment cross section is

given simply by πR_c^2, then our present results would

indicate that R_c is slightly less than the HI equilibrium

separation of 1.6 Å. The results of dissociative attachment

experiments by Alajajian and Chutjian suggest a crossing

radius which is approximately equal to the equilibrium

separation of HI, whereas the calculations of Chapman *et al.*

give R_c = 1.9 Å. The present results tend to support the

observations of Alajajian and Chutjian if indeed the near-

threshold cross section is given by πR_c^2. An intermolecular

potential for HI⁻ with $R_c \approx 1.6$ Å and a well depth of about

0.2 eV is presented in Fig. IV.10(c).

Finally, the disagreement of the detachment cross

sections at the lowest energies reported here with previous

rate constant measurements of Smith and Adams is not

understood. Their experimental method used to obtain the

thermal reaction rates for AD in I⁻ + H (and Br⁻, F⁻ + H)

is self-consistent, and no systematic error is evident in

their measurements which might be specific to I⁻ + H that

would explain the discrepancy with the measured cross

sections reported here or the rate constant measurements of
Fehsenfeld [14]. It should be noted that if their result,
obtained at 300 K, is normalized to the measurement of
Fehsenfeld, then their high energy data point agrees
reasonably well with the lowest energy measurement presented
here.

IV.B.4: Summary: Collisions of halogen anions with H

The electron detachment cross sections, $\sigma_e(E)$, for
collisions of $Cl^- + H$ have been measured for relative
collision energies below 20 eV, and are in good agreement
with previous rate constant measurements and a ERP type
calculation. The detachment cross section for $Cl^- + H$ has
also been described by a classical orbiting model with a
target polarizability modified to represent the principal
feature of the anion-neutral interaction, *viz.*, the distance
at which the potentials for each are approximately equal.
Subsequently, the system of $Cl^- + H$ has been used as a model
system to normalize the experimental results for other
reactants.

The total electron detachment cross sections for
collisions of F^-, Br^- and I^- with H have also been measured.
The experimental results of $\sigma_e(E)$ for F^- and $Br^- + H$ are
well described by the simple model mentioned above. For F^-,
Cl^-, and $Br^- + H$, the measured detachment cross sections at
the lowest collision energies are in good agreement with

thermal rate constant measurements, and no barriers to AD are observed. This implies that the $^2\Sigma$ states of HF^-, HCl^-, and HBr^- are attractive into the autodetaching region. The modified polarizabilities which can be used to model the anion potential and hence the detachment cross section are all smaller than the known static polarizability of H. It must be emphasized that the form of the potential given by (II.12), along with the effective polarizability, is used only because of its analytic simplicity in the orbiting model presented in section II.C. The analytic form given by (II.12) is thus used to approximate the intermolecular potential near R_c, and the value of R_c used to calculate α' is chosen such that the resulting detachment cross section fits the present measurements. It should be emphasized that this form does not mimic other important features of the intermolecular potential and results from a semi-empirical fit to the experimental observations.

The system of $I^- + H$ is found to display a quite different detachment cross section compared to those of the above halogen-hydride systems. The detachment cross section for $I^- + H$ is relatively constant for collision energies below about 1 eV. Above 1 eV, $\sigma_e(E)$ increases with increasing energy. These observations and the existence of stable HI^- underscore the difference of the $I^- + H$ collisional system from the previously discussed halogen-hydrides. Indeed, the low energy detachment cross sections

suggest a crossing radius of the HI^- $^2\Sigma$ state with the $^1\Sigma$ HI

continuum which is approximately equal to the equilibrium

radius, R_e, of the neutral HI molecule. This is in contrast

to the other halogen-hydride systems studied, all of which

have $R_c > R_e$.

IV.C: Na^- and K^- + H

IV.C.1: Introduction; previous studies

The alkali hydrides, especially LiH, and their ions

have been the subject of several theoretical and

experimental studies, and their properties are reviewed in

detail by Stwalley *et al.* [106,107]. The alkali

hydrides are well known for their large dipole moments and

ability to bind an electron, forming a stable negative ion

and, in the extreme limit of the Born-Oppenheimer

approximation, an infinite number of bound excited states.

However, when the normal rotational motion of the molecule

is considered, most of the bound excited states vanish

[108]. A detailed multiconfigurational calculation of

the properties of LiH^- has been presented by Adamowitz and

Bartlett [109] and they conclude that the first excited

state of that molecular anion (of $A^2\Sigma^+$ symmetry) is bound,

lying about 2.8 meV below the ground state of LiH.   One

would expect the same type of behavior for the NaH and KH

molecular anions as they have larger dipole moments than

LiH. However, the intermolecular potentials associated with these "barely-bound" states are probably not relevant to the collision dynamics for the collision energies discussed in the present experiments: the electron wave functions simply can not adjust fast enough to the subtle configurational mixing required for stabilizing the excited $A^2\Sigma$ molecular anion at small internuclear separations. In some sense then, *less* sophisticated calculations of the excited anion states provide a more accurate description of the collision dynamics in the present studies. Under any circumstances, there are as yet no calculations for the $A^2\Sigma$ state of NaH⁻ or KH⁻ which display a bound state.

Several experiments have examined the structure of NaH⁻ via collisions of H⁻ with Na (see Stwalley et *al.* [106] and references cited therein, and Gauyacq et *al.* [99]), and potential energy curves for NaH and NaH⁻ have been calculated by Olson and Liu [110] and by Stevens et *al.* [111]. The latter authors calculated the ground state of NaH⁻, $X^2\Sigma$, while the former reported results for both the $X^2\Sigma$ and $A^2\Sigma$ states which are relevant to the present study; these are seen for NaH⁻ in Fig. IV.13. The KH and KH⁻ ground state potentials have been calculated by Stevens et *al.* [111] with results that are similar to those for the NaH⁻ system, implying that the collisional dynamics for K⁻ + H should be similar to those for Na⁻ + H. No cross section

measurement or calculation for collisions of Na^- or K^- with atomic hydrogen appears to exist.

IV.C.2: Electron Detachment: Na^- and K^- + H

The cross sections for electron detachment, $\sigma_e(E)$, for Na^- and K^- + H are presented in Fig. IV.14 as a function of the relative collision energy, E. The collisional dynamics for detachment can be described with the aid of Fig. IV.13; these potentials are based on the results of Olson and Liu [110] with the energy of the anion states shifted slightly downward to correspond to the correct energy separation between the anion states and the continuum at infinity, i.e. the electron affinities of H and Na. This places the crossing of the $A^2\Sigma$ state with the continuum at $R_1 = 3.6$ Å, while the $X^2\Sigma$ state crosses the continuum at $R_2 = 1.4$ Å. An initial estimate of the detachment cross section based simply on the intermolecular potentials of Fig. IV.13 would suggest that the detachment cross section for Na^- + H should be governed primarily by the internuclear separation, R_1, at which the $A^2\Sigma$ state of NaH^- crosses or merges with the $X^1\Sigma$ state of NaH. If the detachment probability, $P_d(b)$, is unity for impact parameters $b < R_1$ then, in the absence of trajectory effects and charge transfer, the detachment cross section should be $\pi R_1^2 \approx 41Å^2$ and independent of energy. The assumption of straight line trajectories is indeed a
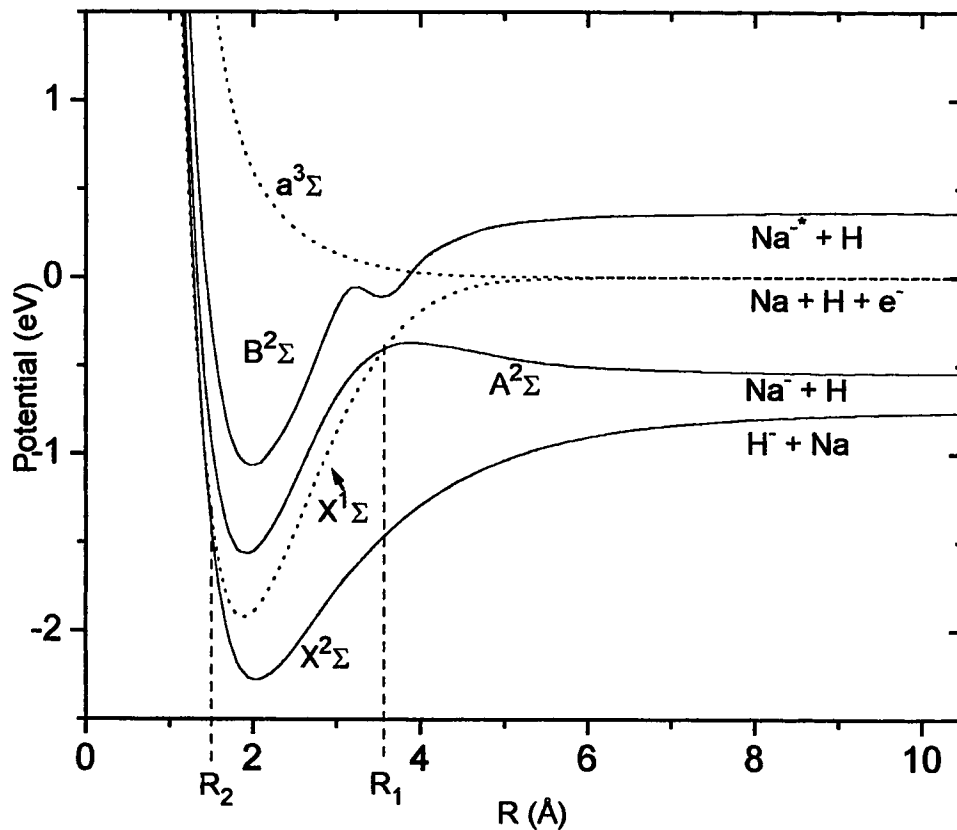
Figure IV.13: Intermolecular potentials for NaH⁻ take from Olson and Liu [110]. The $X^2\Sigma$ and $A^2\Sigma$ states are shifted to correspond to the electron affinities of hydrogen and sodium at infinite internuclear separations.
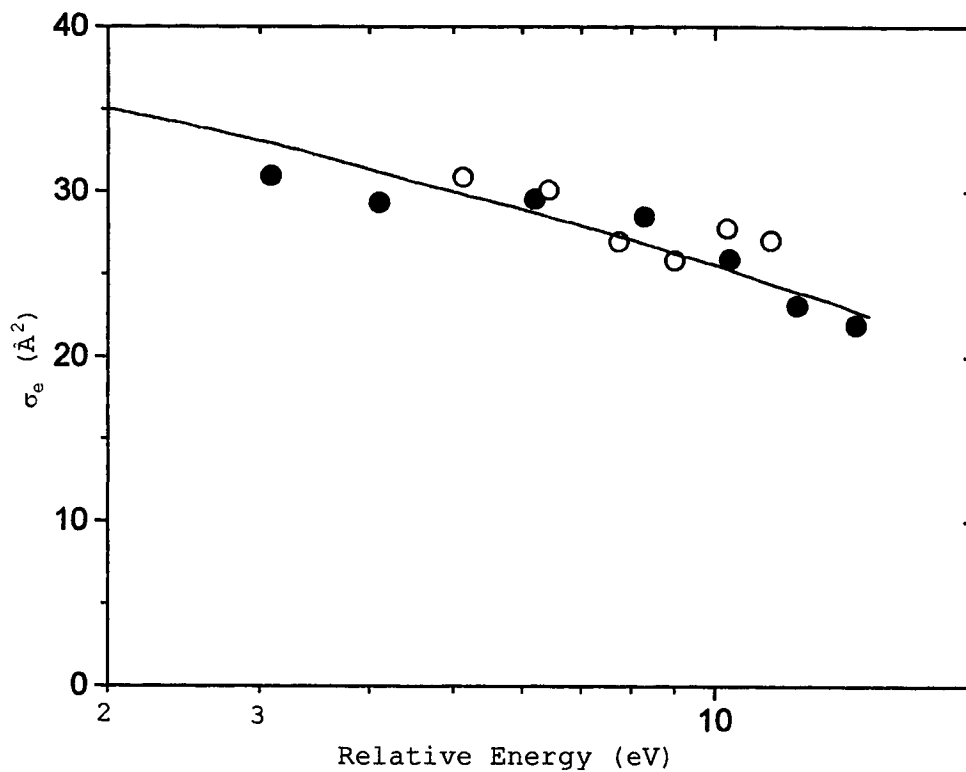
Figure IV.14: Electron detachment cross section for collisions of Na$^-$ + H (solid circles and K$^-$ + H (open circles). The solid line represents the detachment cross section obtained from Eq.(IV.8), in which NaH$^-$ is assumed to have an average width of 65 meV for R < R$_1$.

reasonable approximation for the energy range of the experiments discussed herein. We will show later that the charge transfer cross section is quite small.

As may be seen in Fig. IV.14, the measured detachment cross sections are substantially less than this value of πR_1^2 and *decrease* with increasing energy. One way to account for the magnitude and behavior of the observed cross section is to assign the "unstable" NaH^- an average lifetime or, alternately, a width, Γ, to describe its decay in the region $R < R_1$. In particular, the survival probability, $P_s(b)$, will then be given by:

$$P_s(b) = \exp-\frac{\Gamma \times \Delta X(b)}{v} , \qquad \text{(IV.7)}$$

where $\Delta X(b)/v$ is the time that Na^- spends within the circle $R < R_1$, as depicted in Fig. IV.15, and v is the collision velocity which is approximated to be independent of R. In this case the detachment cross section $\sigma_e(E)$ is simply:

$$\sigma_e(E) = \pi R_1^2 \times \left[1 - 2\frac{(1 - (\alpha + 1)\exp-\alpha)}{\alpha^2} \right] , \qquad \text{(IV.8)}$$
$$\text{where} \quad \alpha = 2\Gamma\frac{R_1}{v}$$

The average width which provides a reasonable fit to the experimental results for $Na^- + H$ is $\Gamma = 65$ meV; the results of Eq. IV.8 for this width are also shown in Fig. IV.14.
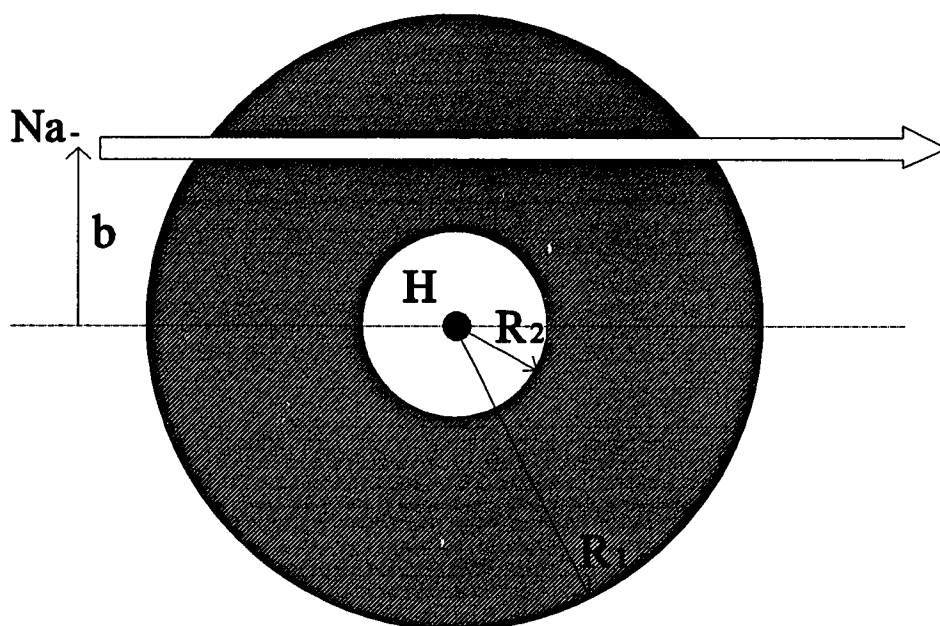
Figure IV.15: Diagram representing rectilinear collisions of Na⁻ + H in the laboratory frame of H. R_1 is the internuclear separation at which the $A^2\Sigma$ anion state crosses into the $X^2\Sigma$ continuum. R_2 corresponds to the crossing of the $X^2\Sigma$ anion state with that of the neutral continuum.

This width is much narrower than that for most resonance states of negative molecular ions and may be due to the spin rearrangement in $A^2\Sigma \rightarrow X^1\Sigma$ transitions. Na^- has total electron spin zero and the electron in H is deeply bound (compared to the outer two electrons on Na^-) and the perturbation to its wave function is small during a slow collision of Na^- with H, especially for large impact parameters. One of the outermost electrons of Na^- is more likely ejected in a detachment collision. In order for the dynamics to be governed completely by the $X^1\Sigma$ state of NaH the spin of the detached electron must be the same as that of the reactant hydrogen atom and this may necessitate spin exchange between the outermost electrons of Na^- and the electron on H. Alternately, we may think of the NaH^- as interacting with a superposition of the triplet and singlet states of NaH and, in the absence of any spin exchange, a statistically weighted superposition. The actual degree of singlet-triplet mixing is difficult to predict but is clearly needed to understand the interplay between spin exchange and electron detachment.

It is interesting to point out that experiments by Tuan and Esaulov [112] revealed that the auto-ionizing state Na^{-*} is an important detachment channel in collisions of H^- + Na for collision energies in the range 100-500 eV. For H^- + Na, long range coupling leads to H + Na^- which apparently

survives the $A^2\Sigma - X^1\Sigma$ crossing at $R = R_1$ and subsequently

couples to H + Na^-* at the $A^2\Sigma - B^2\Sigma$ avoided crossing very

near that for the $A^2\Sigma - X^1\Sigma$ crossing, as is illustrated in

Fig. IV.13. Such a process will produce Na^-* which will

then autodetach. Although no quantitative comparison

between the two experiments is possible, the present

observation of a narrow width (long lifetime) for the

negative ion in the unstable region is compatible with the

observations of Taun and Esaulov.

As may be seen in Fig. IV.14, the results for the

detachment of K^- by H are essentially indistinguishable from

those for Na^- + H. To our knowledge, no potential

calculations other than for the ground state exist for the

KH^- molecular anion.

IV.C.3: <u>Charge Transfer: Na^- and K^- + H</u>

The experimental results for charge transfer are given

in Fig. IV.16 along with the measurements of Wang *et al.*

[113] at higher relative collision energies for H^- + Na.

The collision dynamics for charge transfer can be described

by referring to the intermolecular potentials for NaH and

NaH^- shown in Fig. IV.13.

The PSS formalism which will be used to calculate the

charge transfer cross section closely follows that reviewed

by Delos [47] and presented in Chapter II. In the PSS

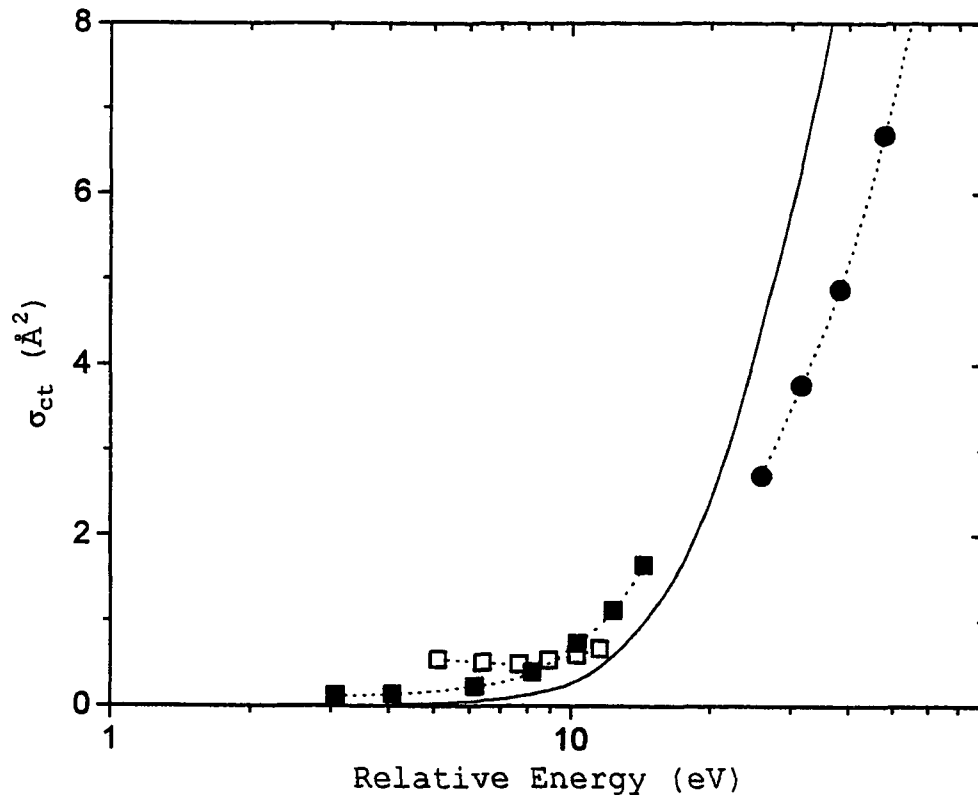Figure IV.16: Charge transfer cross section for $Na^- + H$ (solid squares), $K^- + H$ (open squares), and for $H^- + Na$ [113] (solid circles). The solid line is the result of the PSS calculation discussed in section IV.C.3 and obtained from Eq. (IV.15).

approximation, it is assumed that the electron wave function can only imperfectly adjust to the nuclear motion, thus giving rise to coupling between the $A^2\Sigma$ and $X^2\Sigma$ states, which subsequently leads to charge transfer. In the present approach, depicted in Fig. IV.15, the trajectories are approximated by straight lines such that the internuclear separation is given by $R = b + v \times t$, where b is the impact parameter and v is the velocity. Initially the system resides in the $A^2\Sigma$ state, corresponding to $Na^- + H$ at $t = -\infty$. It is assumed that charge transfer can occur in three distinct ways. First, if $b > R_1$, one can neglect electron detachment and simply calculate the probability that the system resides in the $X^2\Sigma$ state at $t = +\infty$. Second, for $R_2 < b < R_1$, one can calculate the probability that the system resides in the $X^2\Sigma$ state when the trajectory first reaches R_1 and assume that the system remains in this state as the trajectory passes through the region $R_2 < R < R_1$ (the shaded region in Fig. IV.15). This seems reasonable as the $X^2\Sigma$ and $A^2\Sigma$ states are widely separated in this zone. However, one must account for a subsequent return to the $A^2\Sigma$ state (and loss of charge transfer product) as the systems separates for $R > R_1$, $t \to \infty$. The contribution to charge transfer is small for $b < R_2$ as electron detachment will be the dominant inelastic process for small impact parameters.

Finally, we must consider the possibility of the negative ion surviving the region $R < R_1$ and subsequently undergoing charge transfer.

The wave function descriptive of the collision is determined by a linear combination of two states, whose time evolution is given by (see section II.F):

$$i\hbar \frac{d}{dt} \underline{C} = \underline{V}\underline{C},$$
(IV.9)

where $\underline{C} = \begin{pmatrix} C_1(t) \\ C_2(t) \end{pmatrix}$ and $|C_1(t)|^2$ and $|C_2(t)|^2$ are probabilities that the system be found in a state corresponding to $Na^- + H$ or $Na + H^-$, respectively. For this problem, $\underline{V}$ is assumed to contain two terms: an electronic Hamiltonian, $\underline{H}$, which is diagonal if the basis is chosen to be adiabatic, i.e. the potentials of Fig. IV.13; and a part representing the total change of the basis functions with R, $v \cdot \underline{P}$, which has off-diagonal terms in an adiabatic representation. Alternatively, the collision may be described by a "diabatic" basis with the property that $v \cdot \underline{P}$ is negligibly small, and $\underline{H}$ non-diagonal. If potentials of the form $\frac{\alpha e^2}{(8\pi \epsilon_0 R^4)}$ where α is the polarizability, are assumed for the diabatic diagonal matrix elements, then a unitary transformation between the two representations yields the off-diagonal elements. In

the diabatic representation, the off-diagonal element is approximated by the form:

$$H_{12} = \beta\, e^{-\gamma R} , \qquad (IV.10)$$

where $\beta = 0.873$ eV and $\gamma = .328$ Å^{-1}. These values are close to those obtained by Olson and Liu [110], who report $\beta = 0.754$ eV and $\gamma = .323$ Å^{-1}.

With the phase transformation

$$C_n(t) = B_n(t) \exp\left(-i \int_{-\infty}^{t} \frac{V_{nn}}{\hbar}\, dt'\right) , \qquad (IV.11)$$

the coupled equations (IV.9) can be written in the following form:

$$\frac{dB_1}{dx} = \frac{B_2}{i\hbar v}\, V_{12} \exp\left(-i\theta(x,v,b)\right) , \qquad (IV.12)$$

$$\frac{dB_2}{dx} = \frac{B_1}{i\hbar v}\, V_{12} \exp i\theta(x,b,v) , \qquad (IV.13)$$

where

$$\frac{d\theta}{dx} = \frac{V_{22} - V_{11}}{\hbar v} . \qquad (IV.14)$$

These equations were solved numerically in the adiabatic representation, so the charge transfer cross section is then given by:

$$\sigma_{ct}(E) = 2\pi \times [\int_{R_1}^{\infty} |B_2(x=\infty)|^2 b\,db$$

$$+ \int_{R_2}^{R_1} |B_2(x=R_1)|^2 (1-|B_2(x=R_1)|^2) \; b\,db \qquad (IV.15)$$

$$+ \int_{0}^{R_1} (1-|B_2(x=R_1)|^2) \; P_s(b) \; |B_2(x=R_1)|^2 b\,db].$$

The results of Eq. (IV.15) with $\delta = 0.873$ eV, $\gamma = 0.328$ $\text{\AA}^{-1}$, and $P_s(b)$ given by (6) with $\Gamma = 65$ meV are presented in Fig. IV.16 as the solid line; the integrands for each of the integrals in Eq. (IV.7) are plotted in Figs. IV.17 - IV.19 for a few energies. The calculation underestimates the measured values for $Na^- + H$ at low collision energies and is somewhat larger than the results reported by Wang *et al.* [113] for $H^- + Na$ at higher collision energies. In the absence of detachment, the principle of detailed balance would require the two results, $H^- + Na \rightleftharpoons Na^- + H$, to be identical. [The difference between relative collision energy and *total* energy for considerations of detailed balance is trivial for these energies and systems. The expression used by Wang *et al.* to calculate the charge transfer cross section did not include the third term of Eq. (IV.15). They assumed that $P_s(b) = 0$ for $b < R_1$; we have seen from the
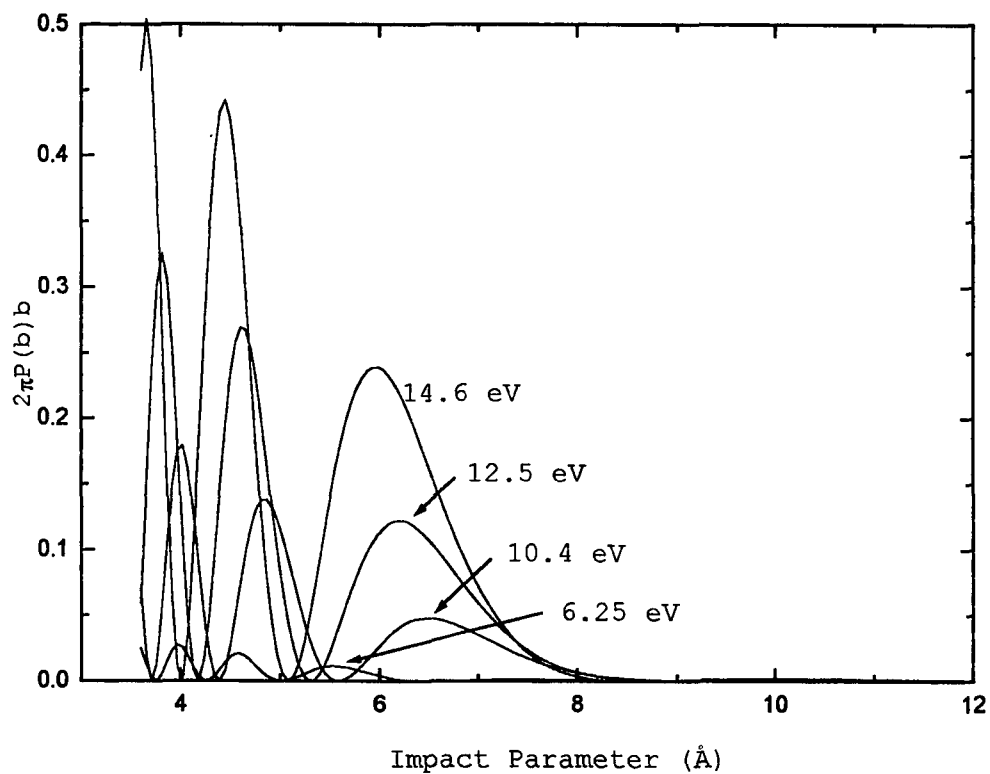
Figure IV.17: $2\pi \times |B_2(x=\infty)|^2$ b(see Eq. (IV.15)) plotted as

a function of the impact parameter b, for values of b

ranging from R_1 to infinity. $|B_2(x=\infty)|^2$ is the probability

that the system resides in the state corresponding to Na +

H^- at $x = \infty$.
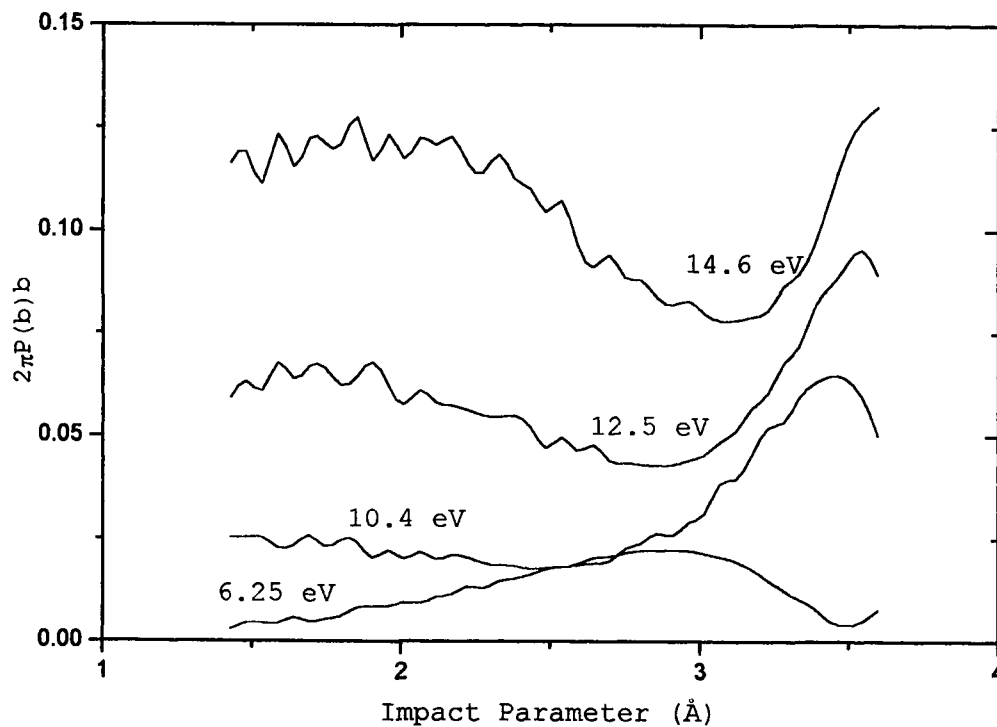
Figure IV.18: $2\pi \times |B_2(x=R_1)|^2 (1 - |B_2(x=R_1)|^2)b$ plotted as a function of impact parameter b, for b ranging from R_1 to R_2. $|B_2(x=R_1)|^2$ is the probability that the system resides in the state corresponding to $Na + H^-$ at R_1, whereas $1 - |B_2(x=R_1)|^2$ is the probability corresponding to $Na^- + H$.
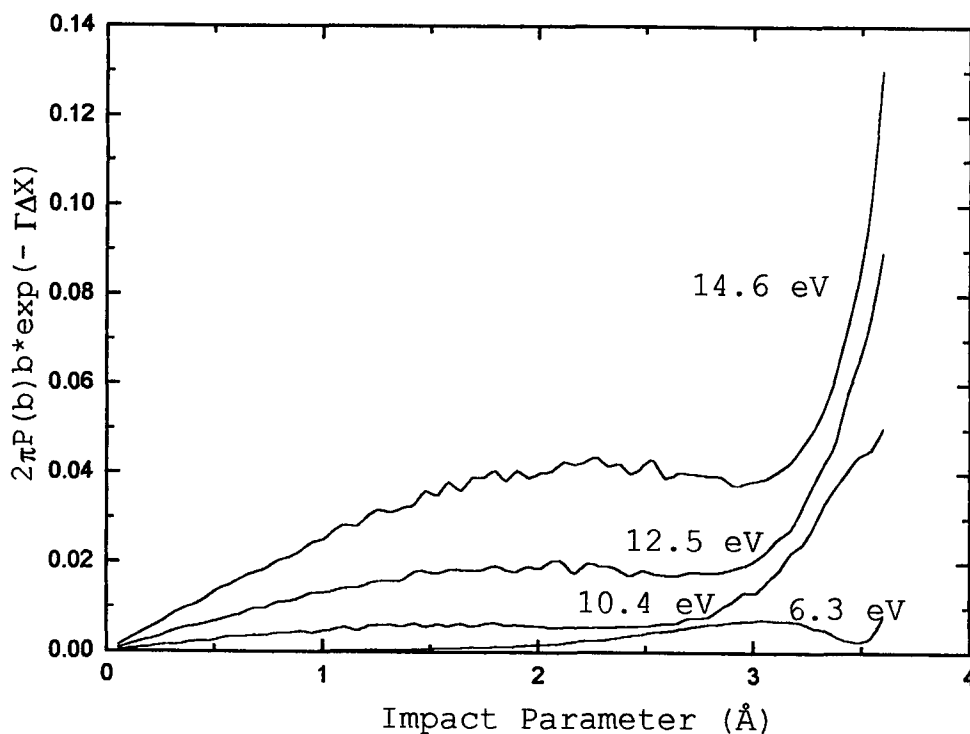
Figure IV.19: 2π x $(1 - |B_2(x=R_1)|^2)P_s(b)|B_2(x=R_1)|^2$ b

plotted as a function of impact parameter b, for b ranging

from 0 to R_1. $(1 - |B_2(x=R_1)|^2)$ is the probability that the

system is in the $A^2\Sigma$ at x = R_1, $P_s(b)$ is the probability

that the system survives (i.e. no electron detachment)

through the autodetaching region, and $|B_2(x=R_1)|^2$ is the

probability that the system subsequently transfers to the

$X^2\Sigma$ state.

previous discussion for electron detachment that this is not the case. One way to bring the PSS calculation into closer agreement with the experimental results for E < 15 eV is to increase both β and γ by a substantial amount. Doubling β and increasing γ by 50%, for example, yields a 34% increase in the calculated σ_{ct}(10 eV) while lowering the cross section for E > 25 eV. However, such a drastic change in $H_{12}(R)$ is not justifiable within the framework that Eq. (IV.10) was derived. Our results for both electron detachment and charge transfer indicate that the collision dynamics for R < R_1 cannot be described using intermolecular potentials of Fig. IV.13 alone. Although the survival probability given by Eq. (IV.7) adequately models the detachment cross section, its inclusion in Eq. (IV.15) has only a minor effect on the charge transfer cross section. A more sophisticated PSS calculation for charge transfer must also include couplings in the unstable region R < R_1 which have been completely neglected in Eq. (IV.15); the present measurements suggest that the collision dynamics in this unstable region are of importance in collisions of Na$^-$ with H. The charge transfer measurements for K$^-$ + H are also presented in Fig. IV.16. The magnitude of the cross section is very similar to that for the Na$^-$ projectile but the

energy range of the experiment for which statistically

significant data could be obtained is too small to make any

generalizations for these reactants.

IV.C.4: <u>Summary: Collisions of alkali anions with H</u>

Unlike most of the other collision systems studied

here, electron detachment in collisions of Na^- and K^- with

atomic hydrogen is not well described by the simple orbiting

model presented in section II.C; the detachment results are

about 30% below that given by πR_1^2. However, the detachment

results can be described in context of a phenomenological

model in which the incoming state is assigned a narrow width

and assumed to decay exponentially with the width. Previous

experiments by Tuan and Esaulov lend support this

description: In collisions of H^- + Na, it was observed that

H + Na^- formed by charge transfer can survive into the

autodetaching region to produce the autoionizing state Na^{-*}.

Charge transfer cross sections are measured to be less than

2 Å over the entire energy range investigated, and are not a

significant loss of probability in the detachment channel.

A PSS approximation which incorporates the survival

probability inferred from the detachment results is used to

calculate the charge transfer. The calculation does not

take into consideration coupling in the unstable region and

underestimates the charge transfer cross section; this

result and the detachment results are clear indications that

couplings between the molecular states at small internuclear

separations must be taken into account in collisions of Na^-

+ H.

IV.D: Grand Summary: Collisions of atomic anions with H

It is now appropriate to make a few general comments on

collisions of negative ions with atomic hydrogen. With the

exception of the alkali anions and I^-, electron detachment

seems to be well described by the simple classical model

presented in section II.C; indeed the Langevin orbiting

model can be modified to adequetely describe detachment for

most of the projectiles in the present study. That electron

detachment in collisions of alkali and iodide negative ions

with atomic hydrogen is not well described by the classical

model is probably due to the fact that the adiabatic

intermolecular potentials for these systems are not well

approximated by a $1/R^4$ potential. Moreover, the measured

electron detachment cross section suggests that simple semi-

classical models cannot alone describe the collision.

In all the systems studied here, charge transfer is a small neutralization channal as compared to electron detachment; this is in contrast to the system $H^- + H$, where resonant charge transfer is the dominant channel over the range of laboratory energies $2 < E_{lab} < 500$ [50]. The PSS calculation presented in section IV.C.3 reflects the difficulties in theoretically assesing non-symmetric charge transfer. It would seem that accurate calculations of the intermolecular potentials are required to perform a satisfactory calculation of the charge transfer cross section; but these are all but lacking for states corresponding to the channel $X^- + H$. Nevertheless, the present measurements would seem to indicate that, in general, non-symmetric charge transfer is not a very likely reaction channel in low energy collisions, whereas associative detachment must be considered in low energy collisions of negative ions with atomic hydrogen.

REFERENCES

1. H. S. W. Massey, *Negative Ions* (Cambridge University Press, London, 1976).

2. J. P. Gauyacq, *Dynamics of Negative Ions* (World Scientific, Singapore, 1987)

3. H. Hotop and W. C. Lineberger, J. Phys. Chem. Ref. Data **14**, 731 (1985); the EA for iodine is take from D. Hanstrop and M. Gustafsson, J. Phys. B **25**, 1773 (1992).

4. T. M. Miller, in *CRC Handbook of Chemistry and Physics, 74th edition,* edited by D. R. Lide (CRC Press, Boca Raton, Florida, 1993)

5. E. E. Ferguson, in *Kinetics of Ion-Molecule Reactions,* edited by Pierre J. Ausloos (Plenum, New York, 1978), p. 377.

6. R. P. Wayne, *Chemistry of atmospheres: an introduction to the chemistry of the atmospheres of earth, the planets, and their satellites* (Oxford University Press, New York, 1991).

7. E. E. Ferguson, in *Interaction Between Ions and Molecules,* edited by Pierre J. Ausloos (Plenum, New York, 1975), p.313.

8. E.E. Ferguson, F. C. Fehsenfeld, and D. L. Albritton, in *Gas Phase Ion Chemistry,* edited by Michael T. Bowers (Academic Press, New York, 1979), Vol. 1, p. 45ff.

9. H. S. W. Massey, in *Applied Atomic Collision Physics,* edited by H. S. W. Massey and D. R. Bates (Academic Press, New York, 1982), Vol. 1, p. 105ff.

10. S. M. Radicella and V. Restbergs, J. Atmospheric and Terr. Phys. **43**, 1 (1981).

11. A. R. Ravishankara, S. Solomon, A. A. Turnipseed, and R. F. Warren, Science **259**, 194 (1993)

12. M. J. Prather and R. T. Watson, Nature **344**, 729 (1990).

13. J. A. Rutherford, B. R. Turner, and D. A. Vroom, J. Chem. Phys. **58**, 5267 (1973).

14. R. P. Turco, J. Geophys. Res. **82**, 3585 (1977).

15. A. Y. Wang, R. F. Wuerker, J. Sabutis, R. Suchannek, C. D. Hendricks, and R. Gotilieb, in *Nonlinear and Relativistic Effects in Plasmas,* edited by V. Stefan (AIP, New York, 1992), 586ff.

16. A. Y. Wong, J. Steinhauer, R. Close, T. Fukuchi, and G. M. Milikh, Comments Plasma Phys. Controlled Fusion **12**, 223 (1989).

17. S. S. Prasad, J. Geophys. Res. **98**, 18597 (1993).

18. F. C. Fehsenfeld, in *Interactions between Ions and Molecules,* edited by Pierre J. Ausloos (Plenum, New York, 1975), p. 387ff.

19. C. J. Howard, F. C. Fehsenfeld, and M. McFarland, J. Chem. Phys. **60**, 5086 (1974).

20. H. F. Calcote, in *Ion-Molecule Reactions,* edited by J. L. Franklin (Plenum, New York, 1972), Vol. 2, p. 673ff.

21. P. K. Bohme, in *Kinetics of Ion-Molecule Reactions,* edited by Pierre Ausloos (Plenum, New York, 1978), p. 323ff.

22. A. N. Hayhurst and T. M. Sugden, Proc. Roy. Soc. A **293**, 36 (1966).

23. W. J. Miller, J. Chem. Phys. **57**, 2354 (1972).

24. P. T. Gilbert, in *Analytical Flame Spectroscopy,* edited by R. Mavrdineanu (Springer-Verlag, New York, 1970), p. 181ff.

25. R. Wildt, Atrophys. J. **93**, 47 (1941).

26. A. J. Deutsch, Rev. Mod. Phys. **20**, 388 (1948).

27. A. Dalgarno and R. A. McCray, Astrophys. J. **181**, 95 (1973).

28. K. Takayanagi, Publ. Astron. Soc. Japan **25**, 327 (1973).

29. F. Chaizy, H. Reme, J. A. Saraoud, C. d'uston, R. P. Lin, D. E. Larson, D. L. Mitchell, K. A. Anderson, C. W. Carlson, A. Korth, and D. A. Mendis, Nature **349**, 397 (1991).

30. P. J. Chantry, in *Applied atomic collision physics,* edited by E. W. McDaniel and W. L. Nighan (Academic Press, New York, 1982), Vol. 3, p. 35ff.

31. W. L. Nigham, in *Applied atomic collision physics,* edited by E. W. McDaniel and W. L. Nighan (Academic Press, New York, 1982), Vol. 3, p. 319ff.

32. Yu. Belchenko, Rev. Sci. Instrum. **64**, 1385 (1993).

33. L. M. Lea, A. J. T. Holmes, M. F. Thorton and G. O. R. Naylor, Rev. Sci. Instrum. **61**, 409 (1990).

34. Yu. Belchenko and A. S. Kuproyanov, Rev. Sci. Instrum. **61** 484 (1990).

35. J. R. Hiskes, A. Karo, and M. Gardner, J. Appl. Phys. **47**, 3888 (1976).

36. Hiroshi Tsuji, Junzo Ishikowa, Takeshi Maekawa, and Toshinori Takagi, Rev. Sci. Instrum. **61**, 427 (1990).

37. H. H. Michaels and J. M. Wadehra, in *Production and Neutralization of Negative Ions and Beams, Fifth International Symposium,* AIP Conf. Proc. No. **210**, edited by Ady Hershcovitch (AIP, Brookhaven, 1990), p. 142ff.

38. M. A. Huels, L. Parenteau, and L. Sanche, J. Chem. Phys. **100**, 3940 (1994).

39. E. W. McDaniel, J. B. A. Mitchell, and M. E. Rudd, *Atomic Collisions: heavy particle projectiles* (John Wiley & Sons, New York, 1993).

40. A. Herzenberg, Phys. Rev. **160**, 80 (1967).

41. H. Goldstein, *Classical Mechanics, Second Edition* (Addison-Wesley, Reading, MA, 1980), p. 90)

42. S. K. Lam, J. B. Delos, R. L. Champion, and L. D. Doverspike, Phys. Rev. A **9**, 1828 (1974).

43. R. L. Champion, L. D. Doverspike, and S. K. Lam, Phys. Rev. A **13**, 617 (1976).

44. Yu N. Demkov, Sov. Phys. JETP **19**, 762 (1964).

45. J. P. Gauyacq, J. Phys. B **13**, L501 (1980).

46. R. Taylor and J. B. Delos, Proc. Roy. Soc. A **379**, 179 (1982).

47. J. B. Delos, Rev. Mod. Phys. **53**, 277 (1981).

48. R. Taylor and J. B. Delos, Proc. Roy. Soc. **379**, 209 (1982).

49. T. S. Wang and J. B. Delos, J. Chem. Phys. **79**, 4306 (1983).

50. M. A. Huels, R. L. Champion, L. D. Doverspike, and Yicheng Wang, PHys. Rev. A **41**, 4809 (1990).

51. S. R. Walther, E. C. Morse, and K. N. Leung, J. Appl. Phys. **66**, 2930 (1989).

52. J. H. Moore, C. C. Davis, and M. A. Coplan, *Building Scientific Apparatus* (Addison Welsey, London, 1983).

53. J. Slevin and W. Sterling, Rev. Sci. Instrum. **52**, 1780 (1981).

54. R. W. McCullough, J. Geddes, A. Donnelly, M. Liehr, and H. D. Gilbody, Nucl. Instrum. and Methods is Phys. Res. B **79**, 708 (1993).

55. S. Lorenzen, H. Morgner, W. Bussert, M. -W. Ruf, and H. Hotop, Z. Phys. A **310**, 141 (1983).

56. H. Morgner and A. Niehaus, J. Phys. B **12**, 1805 (1979).

57. M. S. Huq, D. S. Fraedrich, L. D. Doverspike, R. L. Champion, and V. A. Esaulov, J. Chem. Phys. **76**, 4952 (1982).

58. J. P. Gauyacq, J. Phys. B **15**, 2721 (1982); also see section IV.B.2 of the present work.

59. M. S. Huq, D. Scott, R. L. Champion, and L. D. Doverspike, J. Chem. Phys. **82**, 3118 (1985).

60. D. Scott, M. S. Huq, R. L. Champion, and L. D. Doverspike, Phys. Rev. A **33**, 170 (1986).

61. L. D. Doverspike, B. T. Smith, and R. L. Champion, Phys. Rev. A **22**, 393 (1980).

62. D. M. Neumark, K. R. Lykke, T. Andersen, and W. C. Lineberger, Phys. Rev. A **32**, 1890 (1985).

63. B. Huron and Tran Minh, Astron. and Astrophys. **38**, 165 (1975).

64. H. Hotop, T. A. Patterson, and W. C. Lineberger, J. Chem. Phys. **60**, 1806 (1974).

65. P. K. Acharya, R. A. Kendall, and J. Simons, J. Chem. Phys. **83**, 3888 (1985).

66. J. Tellinghuisen and C. S. Ewig, Chem. Phys. Lett. **165**, 355 (1990).

67. W. R. Snow, R. D. Rundell, and R. Geballe, Phys. Rev. **178**, 228 (1969).

68. M. S. Huq. D. Scott, R. L. Chpamion, and L. D. Doverspike, J. Chem. PHYS. **82**, 3118 (1985).

69. The results of J. Tellinghuisen, M. McFarland, D. L. Albritton, F. C. Fehsenfeld, and W. Lindinger have been reported by F. C. Fehsenfeld, *Interactions between Ions and Molecules,* Vol. 6 of *NATO Advanced Study Institute, Series B: Physics,* edited by Pierre Ausloos (Plenum, New York, 1974), p. 387.

70. K. P. Huber and G. Herzberg, *Molecular Spectra and Molecular Structure IV, Constants of Diatomic Molecules* (Van Nostrand and Reinhold, New York, 1979).

71. D. Smith and N. G. Adams, J. Phys. B **20**, 4903 (1987).

72. J. P. Gauyacq, J. Phys. B **15**, 2721 (1982).

73. S. E. Haywood and J. B. Delos, Chem. Phys. **145**, 253 (1990).

74. T. S. Zwier, M. Matti Maricq, C. J. S. M. Simpson, Veronica M. Bierbaum, G. Barney Ellison, and S. R. Leone, Phys. Rev. Lett. **44**, 1051 (1980).

75. T. S. Zwier, J. C. Weisshaur, and S. R. Leone, J. Chem. Phys. **75**, 4873 (1981).

76. G. A. Segal and K. Wolf, J. Phys. B **14**, 2291 (1981).

77. M. Bettendorff, R. J. Buenker, and S. D. Peyerimhoff, Mol. Phys. **50**, 1363 (1983).

78. L. A. Morgan and P. G. Burke, J. Phys. B **21**, 2091 (1988).

79. T. Gorzyca and D. W. Norcross, Phys. Rev. A **45**, 140 (1992).

80. L. A. Morgan, P. G. Burke, and C. J. Gillian, J. Phys. B **23**, 99 (1990).

81. K. Rohr and F. Linder, J. Phys. B **9**, 2521 (1976).

82. R. Abouaf and D. Teillet-Billy, J. Phys. B **10**, 2261, (1977).

83. R. Allan and S. F. Wong, J. Chem. Phys. **74**, 1687 (1981).

84. L. Dube and A. Herzenberg, Phys. Rev. Lett. **38**, 820 (1977).

85. *Aspects of Electron-Molecule Scattering and Photoionization,* AIP Conf. Proceedings <u>204</u>, edited by A. Herzenberg (New Haven, 1989).

86. J. P. Gauyacq and A. Herzenberg. Phys. Rev. A **25**, 2959 (1982).

87. D. Teillet-Billy and J. P. Gauyacq, J. Phys. B **17**, 4041 (1984).

88. W. Domcke and C. Mundel, J. Phys. B **18**, 4491 (1985).

89. I. I. Fabrikant, S. A. Kalin, and A. K. Kazansky, J. Chem. Phys. **95**, (1991), and J. Phys. B **25**, 2885 (1992).

90. G. Knoth, M. Rädle, H. Ehrhardt and K. Jung, Europhys. Lett. **4**, 805 (1987); G. Knoth, M. Rädle, M. Gote, H. Ehrhardt, and K. Jung, J. Phys. B **23**, 299 (1989); M. Rädle, G. Knoth, K. Jung, and H. Ehrhardt, J. Phys. B **22**, 1455 (1989).

91. M. A. Morrison, Adv. At. Mol. Phys. **24**, 51 (1988).

92. P. -O. Åstrand and G. Karlström, Chem. Phys. Lett. **28**, 624 (1990).

93. S. V. O'Neil, P. Rosmus, and D. W. Norcross, J. Chem. Phys. **68**, 271 (1974).

94. E. Goldstein, G. A. Segal, and R. W. Wetmore, J. Chem. Phys. **68**, 271 (1978).

95. S. H. Alajajian and A. Chutjian, Phys. Rev. A **37**, 3680 (1988).

96. D. A. Chapman, K. Balasbramanian, and S. H. Lin, Phys. Rev. A **38**, 6098 (1988).

97. J. P. Gauyacq and D. Teilly-Billy, in *Negative Ions,* edited by V. Esaoulov (Cambridge University Press, Cambridge, England, 1994).

98. J. P. Gauyacq, J. Phys B **13**, 4417 (1980).

99. J. P. Gauyacq, Yicheng Wang, R. L. Champion, L. D. Doverspike, Phys. Rev. A **38**, 2284 (1988).

100. J. P. Gauyacq, J. Phys. B **16**, 4049 (1983).

101. J. P. Gauyacq, Comments At. Mol. Phys. **10**, 171 (1981).

102. M. A. Smith and S. R. Leone, J. Chem. PHYS. **78**, 1325 (1983).

103. R. Azria. L. Roussier, R. Paineau, and M. Tronc, Rve. Phys. **9**, 469 (1974).

104. P. J. Chantry, J. Chem. Phys. **55**, 2746 (1971).

105. D. Spence, W. A. Chupka, and C. M. Stevens, J. Chem. Phys. **76**, 2759 (1982).

106. W. C. Stwalley, W. T. Zemke, and Sze Cheng Yang, J. Chem. Ref. Data **20**, 153 (1990).

107. W. C. Stwalley and W. T. Zemke, J. Phys. Chem. Ref. Data **22**, 87 (1993).

108. O. H. Crawford and W. R. Garrett, J. Chem. Phys. **66**, 4968 (1977).

109. L. Adamowicz and R. J. Bartlett, J. Chem. Phys. **83**, 6268 (1985).

110. R. E. Olson and B. Liu, J. Chem. Phys. 2817 (1980).

111. W. J. Stevens, A. M. Karo, and J. R. Hiskes, J. Chem. Phys. **74**, 3989 (1981).

112. V. N. Tuan and V. A. Esaulov, Phys. Rev. A **32**, 883 (1985).

113. Yicheng Wang, R. L. Champion, and L. D. Doverspike, Phys. Rev. A **35**, 1503 (1987).

VITA

James Anthony Fedchak was born in St. Louis, Missouri, on the third of August, 1967. There he was raised and educated, receiving a Bachelor of Science in Physics from the University of Missouri in St. Louis in the year of 1989. During July of that year he moved to Williamsburg, where he subsequently began graduate work in the Department of Physics at The College of William and Mary in Virginia. He completed the requirements for a Doctor of Philosophy degree on June 7, 1994. Today his whereabouts are unknown, but it is rumored that he is living in South America, learning the secrets of time from a Mayan priest.